TRACER DIFFUSION OF OXYGEN IN $YBa_2Cu_3O_{7-x}$ FROM MONTE CARLO SIMULATIONS OF AN ISING-TYPE MODEL

by

STEPHEN NAPOLIAN ZIBUSISO GUMEDE

Submitted in partial fulfilment of the requirements for the degree of
Master of Science
in the

Department of Physics,
University of Natal

Pietermaritzburg
May 1998

Preface

I declare that this thesis represents original work by the author, and where the work of others has been used it is duly acknowledged in the text. This study has not been submitted for any degree or diploma to any educational institute.

The research on which this thesis is based was done in the Department of Physics, University of Natal, Pietermaritzburg, from April 1996 till February 1998, under the supervision of Dr. Assen Ilchev.

Acknowledgements

I wish to express my gratitude to the following:

Dr. A. Ilchev for invaluable help with computation and useful discussions.

Prof. O.L. de Lange for financial assistance for my studies through his grant from the South African Foundation for Research Development, and for useful discussions.

Dr. N. Chetty for assistance with the use of the computing facility.

Prof. R.E. Raab for useful discussions.

The staff of the Physics Department for providing a conducive atmosphere for learning, in particular the Head of Department, Prof. C. Graham.

My mother for her invaluable motherly support.

God for keeping me strong.

Abstract

In the research reported here, a two-dimensional Ising-type model was used to study the tracer diffusion coefficients of oxygen ions in $YBa_2Cu_3O_{7-x}$(YBCO) for various values of oxygen concentration and temperature.

The first chapter provides a brief introduction to the problem considered in this thesis. This is followed by a short review of superconductivity, with particular reference to the experimental and theoretical aspects of high-temperature superconductivity and its applications. The structure of YBCO is then presented, with emphasis on its behaviour for various values of oxygen concentration and temperature. The model used in the simulations and the results for tracer diffusion coefficients and related quantities obtained by previous workers concludes the chapter. Results from other theoretical models are also included.

In the second chapter a theoretical background for the Monte Carlo simulations employed in the present investigation is discussed. This chapter includes a short account on how these numerical methods evolved. The Monte Carlo approach to numerical evaluation of integrals is described. Then the idea of Markov sampling for obtaining members of the canonical ensemble is presented, and the Metropolis algorithm is described. In particular, convergence and the detailed balance condition are

discussed. The consequence of starting from an arbitrary initial state when evaluating an observable of interest, and the effect on the reliability of the values of observables, are analysed. The chapter closes with a discussion of Monte Carlo methods applied to a lattice model in statistical mechanics.

In chapter three results for the oxygen distribution produced by the diffusion of oxygen in YBCO are presented. These results were obtained from Monte Carlo simulations of the anti-symmetric next-to-nearest neighbour Ising (ASYNNNI) model. In addition to the uniform equilibrium distributions obtained by previous workers, it is found that this model also possesses nonuniform equilibrium oxygen distributions. The nonuniform distributions show a rich phase structure, and some preliminary results for this structure are presented.

Results for the tracer diffusion coefficients in the nonuniform equilibrium distributions are given in the last chapter. Both local and global tracer diffusion coefficients for nonuniform equilibrium configurations are presented. Results obtained for uniform and nonuniform equilibrium configurations are compared.

CONTENTS

Chapter 4: Tracer Diffusion Coefficient from Uniform and Nonuniform Equilibrium Configurations

CHAPTER 1

Introduction, Review of Superconductivity, and the ASYNNNI model

1.1 Introduction

The fact that a satisfactory theory of high-temperature superconductivity is still unavailable, is partly due to a lack of entirely reliable experimental data on high-temperature superconductors. It took about 46 years after the discovery of superconductivity before a successful formulation of the BCS microscopic theory of conventional superconductors. A substantial amount of experimental work and phenomenological theories developed immediately after the discovery of superconductivity contributed immensely in the formulation of the BCS theory of superconductivity. A similar amount of experimental and phenomenological work may be necessary before a satisfactory theory of high-temperature superconductivity is obtained.

One area of interest concerns the oxygen distribution in nonstoichiometric cuprates such as $YBa_2Cu_3O_{7-x}$ (YBCO). In particular, a two-dimensional lattice gas model, the anti-symmetric next-to-nearest neighbour Ising (ASYNNNI) model is used to simulate the oxygen distribution and to obtain the oxygen tracer diffusion coefficients D^* in the CuO plane (the plane with the chains or the basal plane). This study was presented in the 5^{th} International Workshop on "High-Temperature Superconductors and Novel Inorganic Materials Engineering" held at Moscow State

University, March 24-29, 1998, and has produced two papers to be published in the proceedings of the Nato Science Series, Volume [1,2]. The YBCO compound has been selected for its illustrative character of all cuprates and for the fact that more detailed experimental work is available on it compared with other high-temperature superconductors.

Experiments have shown that in YBCO, oxygen diffusion perpendicular to the basal plane is negligible as compared to diffusion parallel to the basal planes, and that varying oxygen content in the Cu-O chains affects the state of oxidation in the CuO_2 planes (the conduction planes). The maximum superconducting transition temperature T_c corresponds to maximum oxygenation in the Cu-O chains [3-8]. A change in the oxygen content in YBCO is almost entirely due to oxygen loss/gain in the Cu-O chains. Unfortunately, the exact mechanism of oxygen diffusion in the basal plane is not known, and consequently it is not easy to control the oxygen content. Better knowledge of the details of oxygen diffusion will help elucidate a relationship between the oxygen content and the superconducting properties. It will also help in maximising the oxygen content, since it is difficult to obtain a stoichiometric $YBa_2Cu_3O_7$ compound. Oxygenation is an important phenomenon in the processing of the YBCO compound. As a result, the studies of oxygen diffusion in the basal plane will contribute to standardising the manufacturing procedure of this compound. Moreover, experiments have shown that D^* does not depend on the oxygen concentration [5,9]. The aim of this thesis was to study the diffusion of oxygen in YBCO, using Monte Carlo(MC) simulations to evaluate the observables of interest.

This study yielded an unexpected result, namely the fact that the ASYNNNI model possesses nonuniform equilibrium distributions of oxygen in the basal plane. Furthermore, these distributions exhibit a rich phase structure (Chapter three). In addition, the

tracer diffusion coefficients of oxygen for these nonuniform distributions have been evaluated to determine whether the results resolve the well-known disagreement between measured and calculated values of D^* [5,9], in particular the concentration dependence of the evaluated D^*. We found that this disagreement remains for our results. The fact the ASYNNNI model does not give results in agreement with experiments, suggests that either the ASYNNNI model is not suitable for this purpose, or that it has not been fully applied to the system under investigation, eg comparisons of results within the canonical and micro-canonical ensembles have not been made.

1.2 Brief Review of Superconductivity

Since the discovery of superconductivity in 1911 by Onnes in the Netherlands, the highest known superconducting transition temperature T_c has risen from ≈4K to ≈150K [10,11]. In 1973 the highest T_c was 18K (Nb_3Sn) and by 1986 it had increased to 23K (Nb_3Ge). Then occurred the historical discovery of a new class of superconducting materials, the high-temperature superconductors, which opened up a new field in condensed matter physics, and for which there is no generally accepted theoretical explanation as yet. Between 1986 and 1988, T_c was increased to 125K (Tl-Ba-Ca-Cu-O), and in 1993 it was further improved to 153K (Hg-Ba-Ca-Cu-O). Superconductivity occurs in a variety of materials, most notably in alloys and compounds, and is found more frequently in non-magnetic metals. Alkaline and noble metals are not known to be superconducting [12-15] down to the lowest temperatures yet achieved (currently 1.8×10^{-7}K [16]).

A successful microscopic treatment of superconductivity was formulated in 1957 in the form of the BCS theory, and which was based on an electron-phonon mechanism (a mechanism induced by

lattice vibrations) and on the concept of Cooper pairs (paired electrons). Before then, phenomenological theories of superconductivity, such as the two-fluid model, the London and the Ginzburg-Landau formulations, explained some of superconducting properties, but were not complete and could not explain in detail how this unusual phenomena originates at microscopic level [12,14,17-20]. Nevertheless, some concepts of these theories were, even after the formulation of the BCS theory, found to be useful in understanding and conceptualising superconductivity. In its original form, the BCS theory was restricted to a weak-coupling limit, that is, to superconductors for which the electron-phonon coupling constant $\Lambda \ll 1$. It does not give accurate results for superconductors with $\Lambda \geq 1$(eg Pb with $\Lambda = 1.55$) [13]. For these a strong-coupling version of the theory had to be developed [13,21].

After the formulation of the BCS theory the search for materials with higher T_c continued. Since $T_c \propto \Lambda$ and because initially it was thought that the maximum value for Λ would be 0.5, which corresponds to a low T_c, superconductivity was seen as a low-temperature phenomena. This erroneous belief triggered the notion of a non-phonon mechanism for producing a Cooper pair, since it would be impossible to obtain a high T_c through a phonon-mechanism, for which $\Lambda_{max}=0.5$. A number of non-phonon mechanisms of superconductivity have been proposed [13,21]. Some were partially successful and some have never been developed enough to be compared quantitatively with experiment. In principle, phonon and non-phonon mechanisms can coexist. There is some experimental evidence for the existence of a non-phonon mechanism [13,21].

The new high-temperature superconductors (cuprates) were discovered experimentally. In general, these cuprates are divided

into three classes; the La-Ba-Cu-O and related compounds (214 compounds); YBCO and related compounds (123 compounds) and the Bi- and Tl- based copper oxides. Since cuprates dominate high-temperature superconductors, considerable attention has been paid to them. However, their complicated nature (the composition, the structure and the unusual properties) is one major stumbling block in trying to fully understand their behaviour, both analytically and experimentally. The main structural feature of cuprates is their layered nature. The CuO_2 planes are parallel to one another. The anisotropy in the structure is reflected in some of the properties. For instance, conduction of current seems to be confined to the CuO_2 planes [21,22]. In general, superconducting properties of cuprates depend on the stoichiometry. The superconducting properties of YBCO (the only cuprate which has Cu-O chains in addition to CuO_2 planes (see section 1.3)) are strongly dependent on the degree of oxidation in the CuO_2 planes. The formation of oxygen chains removes electrons from the CuO_2 planes (to form holes as charge carries) and highest T_c in these CuO_2 planes correspond to maximum oxygen content and maximum ordering of oxygen ions into chains. For Bi- and Tl- compounds the oxidation of the CuO_2 planes by oxygen atoms is not in such a direct way as for the 214 and 123 compounds [22].

Cooper pairs have also been identified in the cuprates, however, some measurements on such pairs are not yet reliable [13,21]. The coherence length in the superconducting state appears to be smaller for cuprates than for conventional superconductors. Some experiments indicate s-wave symmetry for the Cooper pairs, some a mixture of s- and d- wave symmetries, and most a d-wave symmetry [10,23]. Since some proposed theories produce a distinct symmetry of a Cooper pair, an experimental confirmation of the symmetry may help refine the theories. There is now some theoretical understanding of how it could be possible to obtain

high values of Λ (and hence of T_c) without any instabilities due to phonon-induced structural transitions [21]. A number of pairing intermediates other than the phonons have also been proposed. These include magnons, excitons, plasmons and other mixed-coupling mechanisms [10,13,21,23]. The fact that the properties of these materials depend on the defects (caused by missing O atoms, in particular) brings more complication both analytically and experimentally since such materials are open systems and as such are difficult to treat either experimentally or theoretically.

The discovery of Type II superconductivity (which was predicted by Ginzburg-Landau theory) in the sixties made several applications of superconductivity a reality, because this class of superconductors can have high critical currents (and hence produce high magnetic fields without any energy losses) and high critical fields (and hence stay superconducting even under the influence of high magnetic field strenghts). Commercialization of superconducting magnets (which are used in among other places, high-energy physics and in Magnetic Resonace Imaging) became possible. The discovery of Josephson effects (also in the sixties) and the successful fabrication of Josephson junctions opened up a new field of precision measurements such as SQUID (Superconducting Quantum Interference Device) magnetometry [22]. A number of applications in digital electronic devices are based on the properties of Josephson junctions. Other exapmles include energy storage and magnetic levitation [10,13,16,21,22]. However some applications, such as the transmission of electrical energy over long distances by lossless power lines, cannot be realized because it would require expensive mass coolants; the maximum value of T_c (153K) is still well below room temperature(300K) [10,21,22].

The discovery of high-T_c materials has not changed the status of applications of superconductivity as much as was expected. One reason is the unexpectedly low critical current density J_c in cuprates in particular. Low values of J_c are due to the vortices that are difficult to pin as well as to the inductility of the cuprates. In most conventional superconductors the grain boundaries, and other defects, tend to pin flux quanta, a phenomenon that results in higher J_c values. But in cuprates, the situation is much more complicated: Because of the very short coherence lengths, grain boundaries act like 'weak links', thereby strongly attenuating the maximum supercurrent that can be transported across the boundary. Decreasing the number of grain boundaries in the direction of the current gives higher J_c values [22]. More problems arise because in some instances pinning vortices can only be possible in one CuO_2 plane and not in adjacent planes in a given sample [24]. Also, the lack of mechanical strength, ductility and low processing cost are stumbling blocks to a large-scale commercialization of high-T_c materials.

1.3 The Structure of Yttrium Barium Copper Oxide

The structure of $YBa_2Cu_3O_{7-x}$ (YBCO) has been determined by a variety of techniques, namely, X-ray, neutron, and electron diffraction; microscopy; and thermogravimetry [25-27]. The main structure is well understood, but some disagreement still remains concerning the exact number of stable structures existing in this compound.

The YBCO compound is an open system. Its oxygen content is variable ($0 \leq x \leq 1$) and depends on the outside oxygen partial pressure (Po_2) and temperature. The structure and the electronic properties depend only on the oxygen stoichiometry and the state

of order of oxygen once the cation ratio Y:Ba:Cu=1:2:3 is fixed. The YBCO compound has two main distinct structural phases. The superconducting ordered orthorhombic (OrthoI) phase ($0.5>x\geq 0$) and the non-superconducting disordered tetragonal (T) phase ($1\geq x>0.5$). The superconducting transition temperature T_c decreases continuously with increasing x from ≈90K when x=0, to zero when x=0.5. Just before x=0.5, another ordered distinct phase, the double-cell phase (OrthoII), has been observed with $T_c \approx 60K$.

The optimization of oxygen (x=0) is difficult to achieve, possibly due to the fact that the equilibrium temperature for a stoichiometric $YBa_2Cu_3O_7$ crystal under an oxygen environment is too low (< 250°C) for the long-range oxygen diffusion to achieve complete occupation of oxygen sites [3]. The optimal value of oxygen stoichiometry so far obtained varies from 6.997 (Po_2=1atm, 300°C) to 6.91 [4,28,29]. (However an ideal value of 7 has once been reported [25]). The unit cell for an ideal $YBa_2Cu_3O_7$ compound is shown in Figure 1.

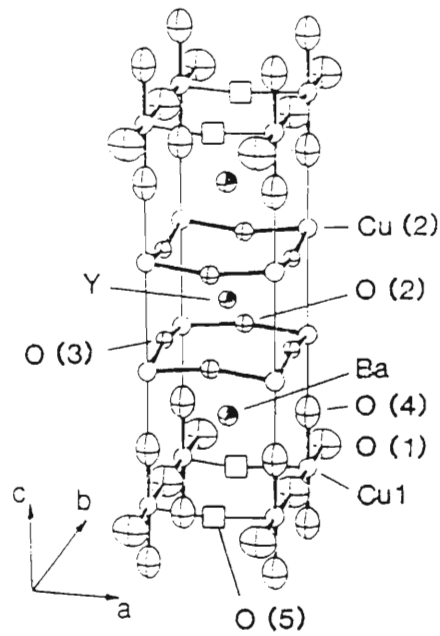

Figure 1.The ideal, perfectly ordered orthorhombic structure (OrthoI) of YBCO [28]. Only half of the oxygen sites in the basal plane are occupied when x=0 and all O(5) sites are empty.

In Figure 1, there are one-dimensional CuO_3 chains consisting of Cu(1), O(1), and O(4) ions, parallel to the b-direction (denoted as Cu-O chains). These chains are weakly coupled through the highly asymmetric Cu(1)-O(4)-Cu(2) bonds to two-dimensional CuO_2 planes consisting of O(2), O(3), and Cu(2) ions. The Cu(1) ions are four-fold coordinated to oxygens in both CuO_2 planes and chain environments. In the chain environments, each Cu ion is coordinated to two adjacent O(1) sites along the b-direction and two O(4) sites out of the chain plane (the basal plane). There are no oxygen ions in the Y plane, whereas there are O(4) ions

in the Ba plane. The O(2) and O(3) sites are crystallographically distinct in this OrthoI ordered structure. The O(1) and O(5) sites are also crystallographically inequivalent. The large anisotropy is evident as, for instance, the structure of the Cu-O basal plane (the chain plane) differs markedly from that of the other planes in the crystal. The O(5) sites are higher in potential energy than the O(1) sites. Under thermal equilibrium, the oxygen atoms in the basal plane are distributed among the two types of sites according to Boltzmann law: $C_{O(5)}/C_{O(1)} = \exp(-\Delta E/kT)$, where $C_{O(5)}$ and $C_{O(1)}$ are oxygen occupancies in sites O(5) and O(1) respectively and ΔE is the potential energy difference between these sites [3]. The ordered OrthoI structure occurs at low temperatures (<300°C) and high Po_2 ($\approx 10^5$Pa). In the OrthoI structure, O(1) sites are fully occupied and O(5) sites are empty. It is the concentration and ordering of oxygen ions/vacancies in the basal plane that differentiate between various structural phases in YBCO.

As x increases, due to increasing temperature (at constant Po_2) or decreasing Po_2 (at constant temperature) , ions on O(1) sites begin to disorder: some move onto O(5) sites and some leave the compound. The OrthoI phase is therefore not fully ordered into chains at higher temperatures (≈600°C). As the temperature is increased the site occupancy at O(5) sites increases, while the occupancy at O(1) sites decreases until both occupancies are equal to each other at the orthorhombic-tetragonal (O-T) structural phase transformation temperature, ≈700°C ($Po_2=10^5$ Pa), when x≈0.5. This is a order-disorder transition which destroys the chains, and at the same time the superconducting state is destroyed completely. Within the resolution of the diffraction measurements, the O-T transition appears to be continuous and second-order [29,30].

As the temperature is increased in the T-phase, the combined occupancy of the O(1) and O(5) sites, which are now equivalent, continues to decrease (Figure 2). The O(2) and O(3) sites are also equivalent in this disordered phase. The oxygen vacancies occur almost exclusively on the Cu-O chains (but excluding O(4) sites), however at higher temperatures there are a few vacancies on O(4) sites as well (about 10% of total vacancies)[28]. There is an indication that in the T-phase the atoms on the O(5) sites are not randomly located, but are arranged in shorter chains [30]. Nevertheless, in the T-phase, just above the O-T transition temperature, oxygen ions also line up in shorter chains, but the chains occur with equal probability along either a or b-directions [5].

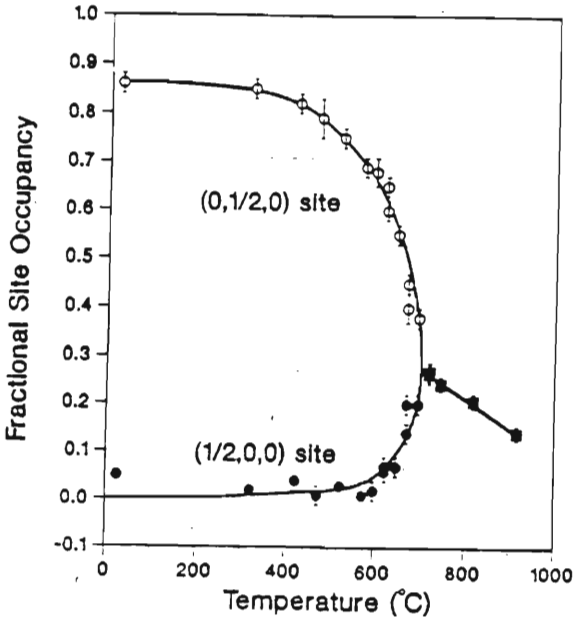

Figure 2. A typical behaviour of the fractional site occupancy of O(1) and O(5) sites versus temperature [29]. Here (0,1/2,0) and (1/2,0,0) are O(1) and O(5) sites respectively.

In the YBCO compound and those related to it by various cation substitution, the CuO_2 planes and the Cu-O chains both seem responsible for superconductivity, whereas in the two other classes of high-T_c oxides (the La compounds and the Bi-containing compounds) superconductivity appears to originate only from the CuO_2 planes [31]. The Cu^{3+} ions occupy the Cu(1) site in the chains, and the highest oxygen concentration at which simple charge balance considerations require an average charge state of 2+ for the atoms is 6.5. At the O-T transition the stoichiometry $\approx$ 6.5 and simultaneously the ordering disappears. Hence it is not possible to uniquely conclude whether the reason for the depression of superconductivity in the tetragonal phase is due to loss of Cu^{3+} or loss of the ordering in the one-dimensional chains. However, it is clear that the chains do affect the mechanism of superconductivity, either through mixed-valent copper ions or a dimensional enhancement [29].

The unit cell of the structure in the T-phase is shown in Figure 3(a). The two diagrams, Figures 3(b) and (c), show the basal plane in the OrthoI and T-phases respectively.

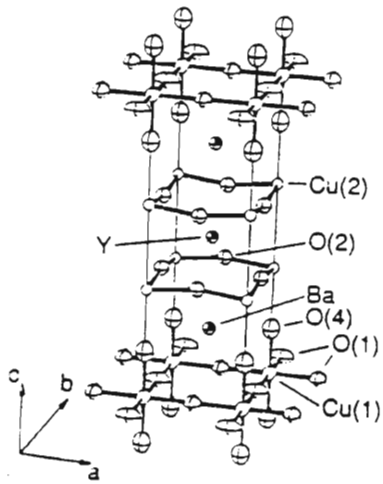

(a)

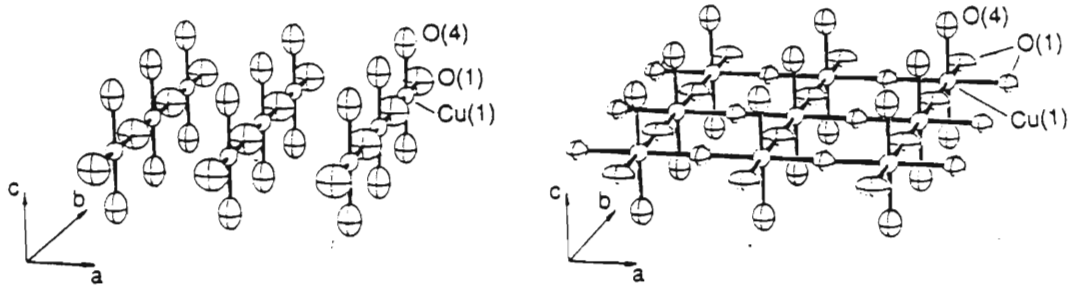

(b) (c)

Figure 3. (a) The T-phase in which the one-dimensional chains have been transformed into a two-dimensional structure. (b) The basal plane (z=0) showing one-dimensional Cu-O chains clearly. (c) The two-dimensional disordered T structure (z=0) in which the chains have been destroyed completely [29].

As the structure changes with temperature, the lattices constants, a_o, b_o, and c in the OrthoI phase and a_T and c in the T- phase, also change [25]. In general, the unit cell volume increases with temperature. In the OrthoI phase, the lattice constant in the b-direction is slightly greater than in the a-direction (b/a=1.016) and c≈3a [25,30,32]. When the temperature is increased both a_o and b_o increase until they are equal at the (O-T) transition. Towards the transition b_o decreases to a_T and a_o increases to a_T, whereas, c increases with increasing temperature until just above the transition, as shown in Figure 4.

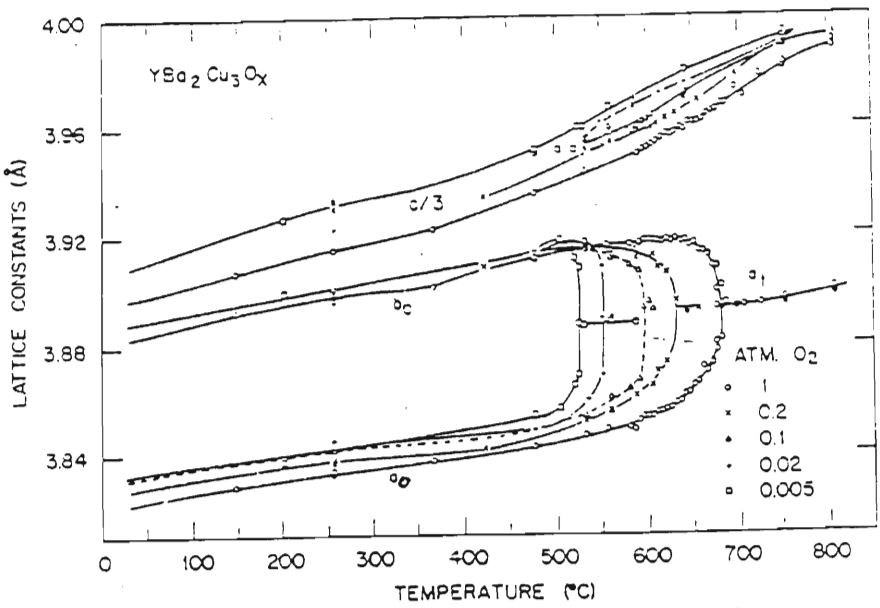

Figure 4. The lattice constants a, b, c/3 versus temperature at different oxygen atmospheres [25].

A trend towards larger lattice constants particularly in the c-direction, is observed as Po_2 is reduced. The oxygen partial pressure affects the lattice in the a-direction more than in the b-direction [25,29]. The transition always occurs near a stoichiometry of 6.5, thus lower-oxygen partial pressures result in lower structural transition temperatures [25,29,33] as shown in Figure 5. The latter figure also shows the relationship between oxygen concentration, temperature and Po_2. As expected, higher oxygen pressures and lower temperatures are required for maximum oxygen content.

Through the assumption that all oxygen gain and loss is due to oxygen changes in the basal plane (ie at the O(1) and O(5) sites but not the O(4) sites), it is possible to relate the stoichiometry index 7-x to the planar concentration c: $7-x = 2(c+3)$, where $0.5 \geq c \geq 0$. However since vacancies occur even on the O(4) sites at higher temperatures (»700°C) and since the YBCO compound is an open thermodynamic system, oxygen content cannot be controlled/measured exactly. As a result, controversy concerning the exact oxygen concentrations at which various phenomena take place, such as the O-T transition still exist.

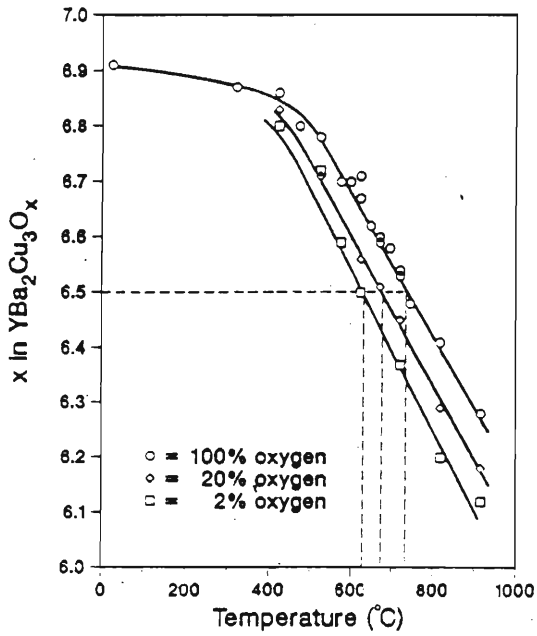

Figure 5. A plot of total oxygen content in YBCO against temperature for various oxygen pressures, showing that the O-T transition always occurs near x=0.5 [29].

An additional distinct ordered phase (OrthoII, the cell-doubling structure) at lower values of x has been found experimentally, as well as from phase diagram calculations [8,28,31]. A cell-quadrupling structure has also been predicted from the Ising model [31]. In general, for all values of x in the OrthoI phase, the oxygen ions are ordered into chains, and the spacing between the chains depends on the stoichiometry. For instance, for x=0.5, every second row of the O(1) sites is occupied, and for x=0.33, the sequence is two rows occupied, and one row empty, etc [28]. It seems as if the arrangement of oxygen ions into rows is preserved. The OrthoII phase shown in Figure 6(a) has a stoichiometry of x≈6.5. Only the basal plane is shown. The OrthoI phase is shown in Figure *6*(b) for comparison.

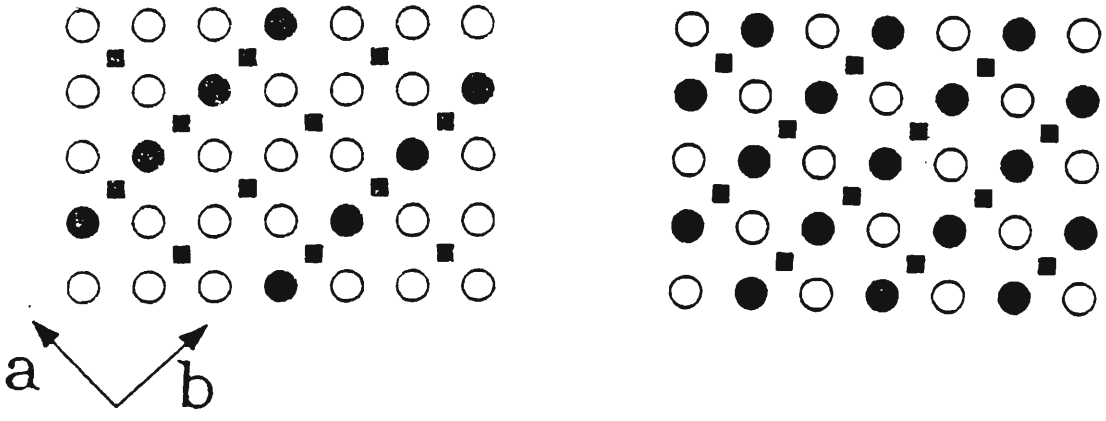

(a) (b)

Figure 6. The lattice for oxygen ions in the basal plane. Filled circles are oxygen ions, open circles are empty oxygen sites and solid squares are Cu ions.(a) The OrthoII phase. (b) The OrthoI phase [32].

In Figure 6(a), the unit cell is doubled in the a-direction and chains along the b-direction are alternatively occupied and unoccupied by oxygen ions.

More structures have been observed at finite temperatures (x=0.125,0.375) [7,26]. However, it is still unclear whether these are stable configurations and not metastable configurations (bearing in mind also the slow kinetics at low temperatures). There is a suggestion that the OrthoII phase is metastable [31]. A determination of the sign of interaction between oxygen atoms in the chains separated by Cu atoms from electron structure calculations may tell whether a double-cell phase is metastable (positive interaction) or a true ground state (negative interaction)[7].

1.4 The Asymmetric Next-to-Nearest-Neighbour Ising (ASYNNNI) model

The Ising model was originally proposed as a model for the structure of a ferromagnet [34]. The idea was that the field due to the magnetic dipoles of atoms or molecules decreases so rapidly that to a good approximation, only interaction between nearest neighbours need be taken into account. This can be extended to include the next-to-nearest neighbours, etc. The basic concept of this model is applicable in many areas of study, especially in cooperative phenomena (gas-liquid transitions, magnetic Curie points, order-disorder transition in alloys, phase transition in liquid mixtures, etc).

The geometry and notation for the two-dimensional lattice gas ASYNNNI model is shown in Figure 7, where the completely ordered OrthoI structure (x=0) of the basal plane (the chain plane) is depicted. It consists of a lattice of size n_x, n_y , where n_x, and

n_y is the number of oxygen sites in the x'- and y-directions respectively. The Cu sites are in between next-to-nearest O(1) sites, in the b-direction along the Cu-O chains. There are three sublattices, a fully occupied O(1) sublattice (denoted by O), an empty O(5) sublattice (denoted by □), and a Cu sublattice (denoted by •). The O(1) and O(5) sites are alternating. The Cu ions play no role in the ordering and mobility of oxygens in the basal plane other than modifying the effective pair interactions (EPI) between the two next-to-nearest oxygens adjacent to it. The model involves three EPI's, a symmetric nearest neighbour (NN) potential between any two nearest oxygen ions (V_1), a next-to-nearest neighbour (NNN) potential between any two next-to-nearest oxygen ions separated by a Cu ion (V_2), and an NNN potential between any two next-to-nearest neighbour oxygen ions not separated by Cu (V_3). The last two potentials are asymmetric.

● - Cu(1) site

O - 0(1) or α site

□ - 0(5) or β site

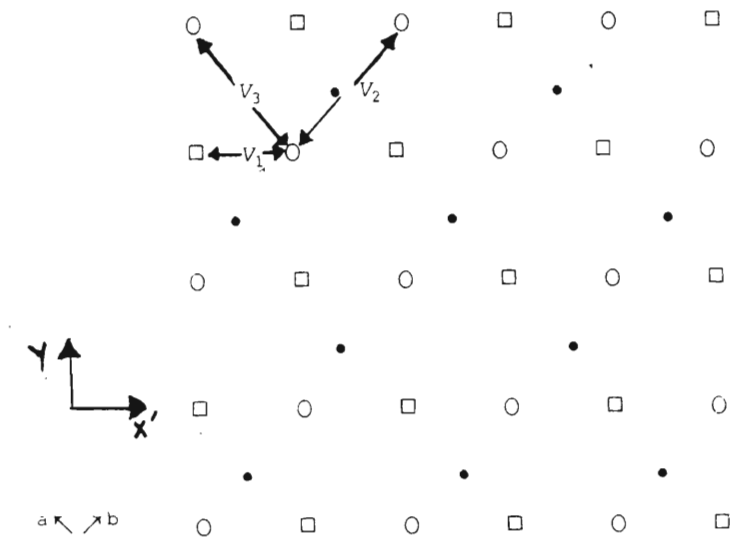

Figure 7. Schematic representation of the chain plane.

It is assumed that the EPI's do not depend on oxygen concentration [7,8,31] or temperature [8]. The EPI's represents ordering energies, and their magnitude is small compared to the cohesive energy of the compound. It is also assumed that other interactions in the system do not change the configurational energy of the system [30]. The total energy of a crystalline solid does not consist of a sum of EPI's [7,31]. The EPI's are

electronic in origin. It has been shown that EPI's form a rapidly convergent set in a variety of systems and so are short-range effective interactions (it has been found that the long-range part of the interactions cancel out in calculations and hence are neglected). The exact values of the EPI's can, in principle, be obtained from the electronic structure calculations for the completely disordered compound. Based on the stable OrthoI and OrthoII phases, a ground-state analysis has shown that the EPI's should satisfy the conditions, $V_2 < 0$ and $V_3 < V_1$ [7,8,26,35]. Sterne obtained EPI's values with similar order of magnitude to those predicted by the ground-state analysis by using orbital calculations [36]. There is a wide variety of the choices of the values of the interaction parameters depending on how the model is used. For instance, neglecting asymmetry in the next-to-nearest potentials (ie assuming $V_2=V_3$), may highlight other features, but it misses the OrthoII phase [7,8]. The ASYNNNI model has reproduced a number of experimentally observed features in the basal plane, including structural phase diagrams and the exact ordering of the atoms at various structural phases especially the ground states (T=0) [7,31,37].

1.5 Review of Tracer Diffusion Coefficients and Related Quantities in the YBCO compound

There has been a substantial amount of theoretical and experimental research on the diffusion of oxygen ions in the basal plane of YBCO. To date, none of the existing theoretical models account for all the features of diffusion in YBCO, and some experimental results are in conflict with each other. Much effort has been put into the investigation of the basic features of oxygen diffusion crucial to an understanding of the effect of oxygen and its ordering on the superconducting properties of cuprates, namely, independence of D^* on oxygen concentration, the

activation energy E_A of the individual jump (between any two sites) in the various phases, behaviour of the Arrhenius plot ($\ln(D^*)$ vs T^{-1}), and the exact diffusion mechanism of the oxygen ions. The theories of diffusion in YBCO are either based on the statistical mechanics of correlated motion of single vacancies in the basal plane or on the interstitial motion of oxygen along Cu-O chains. (It should be noted that the tracer correlation factor is due both to a configurational or geometrical factor and non-randomness of the atom (and defect) distribution [38].) A variety of the models based on the former motion have been suggested.

The Monte Carlo (MC) simulations of an ASYNNNI model (without NNN jumps) resulted in values of D^* that depend strongly on c, and anisotropy in the basal plane [35]. Relatively less dependence of D^* on c was found using the same ASYNNNI model but a different algorithm [39]. Also, a less dependence of D^* on c was predicted by the same model and an algorithm from Ref.39 [9]. The extension of this model to include NNN jumps reduced the c dependency on D^* only slightly [9]. There are several other Ising-like models that have been studied using different statistical and theoretical treatments to the MC methods [5,7,8,26,31,36,37,40-50]. A thermodynamic model for an open system predicted a slight Po_2 dependence (hence slight concentration dependence) and a break at the O-T transition with E_A in the range 1.3-2.1eV [40]. The pair approximation of the cluster variation method and the path probability method yielded a concentration-dependent D^* and a break in the Arrhenius plot at the O-T transition. The activation energies of oxygen ions were calculated as 0.8 and 1.2 eV in the T-phase and OrthoI phase respectively [41]. The oxygen ordering in the basal plane may be important for studying the diffusion mechanism, since the ordering mechanism could be related to an atomic diffusion mechanism [5,49,50]. Phase diagram calculations also indicate ordering [7,8,26,31,36,37,42-44]. The

experimentally observed dependence of oxygen nonstoichiometry on Po_2 and T have been predicted in a defect model chiefly for high values of x [46]. An order-disorder model for an open system using a quasichemical approximation and a mean-field theory, for the O-T transition, predicted the oxygen site occupancy in good agreement with the experimental data [47,48]. Other non Ising-like models have also been studied [51, 52]. An activation energy of 0.3 eV has been obtained from a shell model and associated two- and three-body short-range potentials [51]. A molecular-dynamics study of the oxygen diffusion at high temperatures yielded E_A=0.98 eV [52].

In their theoretical models, various workers have proposed somewhat different atomic mechanisms for diffusion [3,4,6,28,52,53]. Vacancy diffusion via the O(1)-O(4)-O(1) path was found to be energetically most favourable [5]. A calculation based on the energy minimization procedures, attributed diffusion to a vacancy migration between O(1) sites via O(5) or O(4) sites, and obtained $E_A \approx 1$eV. Ronay and Nordlander developed a model in which an oxygen ion could move interstitially over O(5) sites, parallel to the b-direction, and in which only ions at the end of the chains are mobile. Their mean field calculations predicted $E_A \approx 1.7$eV for D^* in both the a- and c- directions and $E_A \approx 0$eV for the b-direction [4,5,28]. In such a mechanism D^* may show a weak dependence on c, since the number of chains is less sensitive to stoichiometry than is the number of oxygen vacancies. Ausloos and Pekalski [9] concluded that at higher concentrations diffusion is taking place along Cu-O chains, ie, O(5)-O(5) or O(1)-O(1), whereas at lower concentrations vacancy diffusion O(1)-O(5) is also important. However a molecular-dynamics study has suggested that the correct path is O(1)-O(4)-O(1) and O(1)-O(5)-O(1) at lower and higher temperatures respectively [52]. In this mechanism, $D_b^* > D_a^*$ at low temperatures. No O(5)-O(5) jumps occur. A mechanism that moves an oxygen ion from an O(1) site to

an O(5) site first before moving it to the next O(1) site has been supported from a model by Tu *et. al.* [6]. A diffusion mechanism based on whether a particular oxygen jump is overcrowding a particular supercell has also been proposed [3]. Such a mechanism may not allow a jump even if there is a vacancy available. Correlations were not indicated in the mechanism . A mechanism that uses an O(4)-O(5) path has been deduced from elastic energy dissipation measurements [53].

In general, it is thought that diffusion can either take place from one O(1) site to the other via an O(5) site (O(1)-O(5)-O(1) or an O(4) site (O(1)-O(4)-O(1)) or directly in one jump (O(1)-O(1)) . At low temperatures either an O(1)-O(5)-O(1) path or O(1)-O(4)-O(1) is followed by an individual ion and at high temperatures the O(1)-O(5) path is also important.

Experimental investigations of D^* have been performed on single and polycrystal YBCO. On single crystals, measurements have shown that diffusion is highly anisotropic in the ab plane ($D_b^* \gg D_a^*$) at lower temperatures, and that in the c-direction it is much lower ($D_c^* \ll D_a^*$). The activation energy for diffusion in the c-direction is much larger than in the ab plane, but various researchers have found different values for E_A on polycrystalline YBCO. A value of $E_A \approx 1.5$ eV has been obtained in the temperature range 377-812°C from the oxygen ion conductivity measurements, whereas, $E_A \approx 2$eV was found following the investigation of the exchange of ^{18}O in the atmosphere with ^{16}O in YBCO powder with a microbalance [5]. A secondary ion mass spectrometry (SIMS) technique yielded $E_A = 0.97$eV over the temperature range 300-850°C, with no break at the O-T transition and a slight dependence of D^* on Po_2 [4]. *In situ* resistivity experiments have yielded $E_A \approx 0.5$eV at x=0.38 and $E_A \approx 1.3$eV at x=0 in the temperature range 200-550°C [6]. Resistivity measurements also gave $E_A = 0.4$eV in

the tetragonal phase [52]. Ion conductivity studies gave E_A=2.2eV and thermogravimetric studies E_A=1.38eV at x=0. Activation energies of 1.03eV [3] and 1.07eV [54] have been found from internal friction experiments. In Ref.54, E_A decreases above x=0.25, and hence the Arrhenius plot deviates from a straight line at high temperatures. An increasing D^* with c has been reported [55] and the simulations have suggested that this behaviour happens in the ordered OrthoI phase at high concentrations [9]. This could be due to the interstitial motion of oxygen ions along the Cu-O chains. Using ^{18}O as a tracer, a tracer diffusion coefficient that increases with c was obtained [56]. This unusual behaviour was attributed to the ordering in the system at low values of x. An activation energy of 33±4meV was found from the quadrupole relaxation measurements [57]. Elastic-energy measurements gave $E_A \approx 1$eV above room temperature [53]. The significant scatter in the results may partly be attributed to differences in the experimental conditions. Nevertheless a value of $E_A \approx 1$eV seems most probable.

There are some trends, however, in the experimental observations that any diffusion mechanism must be consistent with. First, the tracer diffusion coefficient is virtually independent of the oxygen concentration (or Po_2 independent), and hence independent of the oxygen ion vacancies and the interstitials. Second, the Arrhenius plot for $Po_2 = 10^5$ Pa is a straight line over the entire temperature range, with no break at the O-T transition, implying that the same jump is responsible for the OrthoI and T-phases; hence the motion of oxygen ions is not correlated. Third, the anisotropy in the ab plane decreases with the increasing temperature and the decreasing number of chains. This suggests that diffusion takes place parallel to the chains in the ab plane, be it a simple vacancy mechanism or any other type. Fourth, diffusion in the c-direction is much lower than in ab

plane [4,5,39,52]. However there is not much agreement on the details of the diffusion path, nor on the measurements of D^* and E_A, and the behaviour of the Arrhenius plot [28,39,52]. In some cases, there are arguments about how certain measurements were obtained [5]. It is evident that much is still desired both theoretically and experimentally before a clearer picture of D^* is realized. In particular, the failure of computer simulations to explain all the experimental features of D^* in YBCO is disappointing [5].

CHAPTER 2

Monte Carlo Simulations: A Steady-State Problem

2.1 Introduction

Monte Carlo (MC) methods are numerical methods that use random numbers and well-formulated algorithms to provide approximate solutions to a variety of mathematical problems. They are applicable in various fields of study, such as physics, chemistry, geology, life sciences, engineering, operations research, statistics, mathematics, and computer science. In physics, they are used to approximate large summations, evaluate integrals, solve ordinary differential equations and partial differential equations, thereby allowing one to study stochastic process (eg diffusion or radioactive decay of a particle), percolation processes, spin models, fluids, polymers, disordered materials, lattice gauge theories, lattice structure and equilibrium statistical mechanics problems, etc. The MC methods were developed in the 1940s. In about 1948 Fermi, Metropolis, and Ulam obtained MC estimates for eigenvalues of the Schrödinger equation [58].

In their evolution MC methods underwent three distinct but related historical developments in the mathematical sciences [59]. First, when it was realized in the 17^{th} century that the outcomes of successive games of chance formed a sequence of random events, and then in later centuries that the mean of a function of random variables took the form of an integral, it became apparent that, in principle, one could use random numbers to obtain an approximate solution to an integral. Second, from the turn of the present century until the early 1930s, a growing body of evidence suggested that 1- and 2- dimensional random

walk approaches could provide approximate solutions to boundary value problems for ordinary and partial differential equations. It was also discovered that a random walk could provide solutions to elliptic partial differential equations, and that there is a relationship between Markov stochastic processes and certain integro-differential equations. This showed a relationship between a random walk approach and the stochastic processes, because solutions to problems encountered in stochastic processes often corresponded to solutions that arose in the study of partial differential equations. Third, during the development of atomic energy in the late 1940s, scientists needed to solve problems of neutron diffusion and/or transport through an isotropic medium. These multidimensional problems could not be solved by conventional methods at the time. However, based on the realization that partial differential and integral equations resulting from these diffusion problems all had parallels in stochastic processes, John von Neumann and Stanislaw Ulam successfully suggested random walk models as means of obtaining approximate solutions to such stochastic problems, and even to integro-differential equations which did not necessarily have a probabilistic basis themselves. For example [58], a problem in electromagnetic theory, may require the solution of Laplace's equation subject to certain boundary conditions. Since Laplace's equation occurs also in the study of particles which diffuse randomly in a region bounded by absorbing barriers, one can then solve the electromagnetic problem by performing an experiment in which one guides particles by means of random numbers until they are absorbed on the barriers specifically chosen to represent the prescribed boundary conditions.

All numerical methods that rely on n-point evaluations in g-dimensional space to produce an approximate solution, have absolute errors that decrease as $n^{-1/g}$ at best in the absence of exploitable special structure, whereas the MC method has absolute

error of estimate that decreases as $n^{-1/2}$ [59]. This property gives the MC method an advantage over other methods in computational efficiency as g the size of the problem increases. In addition, the MC approach frequently provides an estimated solution with tolerable error at a computational cost that increases slower (no faster than as a polynomial in g) than that of solving a problem exactly (often increasing exponentially or superexponentially with g). A number of techniques for increasing efficiency of the MC approach for a particular class of problems have been developed [58]. A particular aspect of the MC approach, the generation of random numbers, is a huge topic by itself [59]. Actually, what is generated in practice are pseudorandom numbers, since such numbers are not entirely independent of one another; the sequence repeats itself after a certain interval. Here it will be assumed that the use of pseudorandom numbers involves negligible error in the final estimate of a particular solution.

In this chapter some elementary principles of MC methods for evaluating integrals are presented as an introduction to a random tour/walk approach. Markov sampling and the Metropolis algorithm are then introduced. Last, a lattice model is discussed which illustrates a case in which Markov sampling is used to approximate expectation values in statistical mechanics.

2.2 A General MC Approach to Evaluating Integrals

From the mean value theorem, the value of the integral I_{ab} can be estimated as follows,

$$I_{ab} = \int_a^b \psi(h)\,dh \approx (b-a).\ \psi(\beta),$$

where β is a point in (a,b).

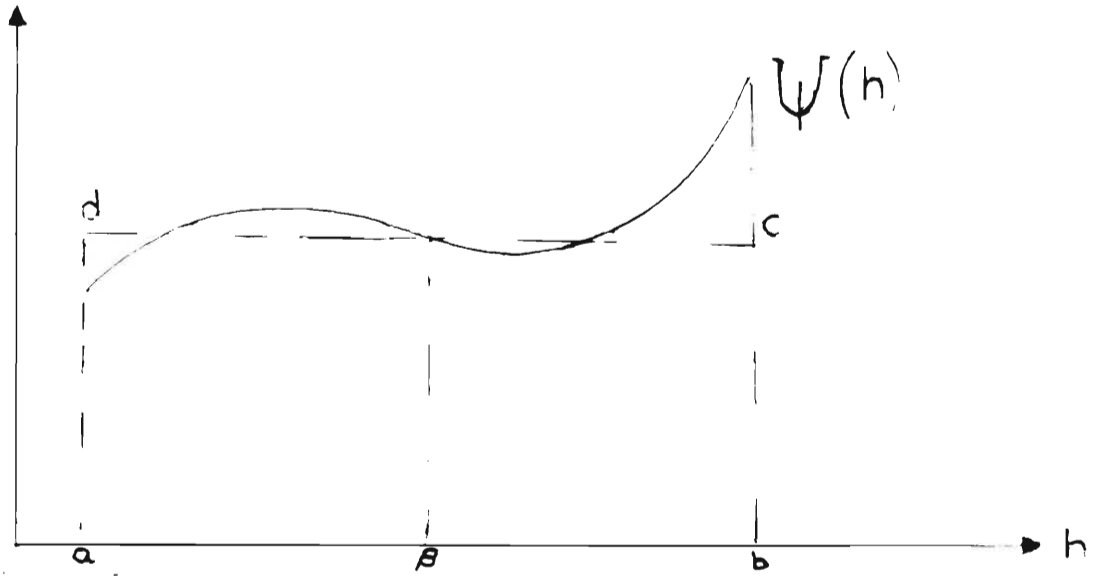

Figure 1. The area of rectangle abcd ≈ the area under the curve ψ(h).

Generalized for multiple integrals, one has

$$I_{Dg} = \int_D \psi(\mathbf{h})\,d\mathbf{h} \approx V(D_g).\psi(\beta), \qquad (2.2\text{-}1)$$

where $\{\beta = (\beta_1,\ldots,\beta_g)$ and $\mathbf{h}=(h_1,\ldots,h_g)$, all $\in D\}$, and $V(D_g)$ is the volume enclosed by D in a *g*-dimensional space. The standard MC strategy for evaluating integrals uses a sequence of *n* independent random points $\{\mathbf{H}^{(r)}=(H_1^{(r)},\ldots,H_g^{(r)});\ r=1,\ldots,n\}$ each drawn from a uniform distribution on the *g*-dimensional hypercube. The estimate of expression (2.1-1) then becomes

$$I_{Dg} \approx n^{-1} \sum_{\text{all } r} V(D_g).\psi(\mathbf{H}^{(r)}), \qquad (2.2\text{-}2)$$

where each r is an independent replication and n is the sample size. If $\{\mathbf{H} = (H_1,\ldots,H_g)\}$ is one of the n random points then H_f (where $f = 1,\ldots,g$) has a probability density function (PDF)

$$P(L) = \begin{cases} 1 & 0 \le L < 1, \\ 0 & \text{Otherwise,} \end{cases}$$

and $\mathbf{H}$ has PDF,

$$P(\mathbf{L}) = \begin{cases} 1 & 0 \le L_f \le 1, \\ 0 & \text{Otherwise,} \end{cases}$$

The H_f are drawn independently of one another. A sequence of independent random numbers is produced by a standard random number (SRN) generator. Suppose RAN is a generator of independent random numbers which are uniformly distributed in (0,1), then a sequence of n independent random points in D_g with a uniform distribution is

$$\mathbf{H}^{(r)} = (RAN_1^{(r)},\ldots,RAN_g^{(r)}),$$

where $r = 1,\ldots,n$. In general, for $V(D_g)$ in the interval $|\mathbf{a} - \mathbf{b}|$,

$$\mathbf{H}^{(r)} = \mathbf{a} + |\mathbf{b} - \mathbf{a}|.\mathbf{RAN}^{(r)}$$

where $\{\mathbf{a} = (a_1,\ldots,a_g)$, $\mathbf{b} = (b_1,\ldots,b_g)$ and $\mathbf{H}$; all $\in D_g\}$ and $\mathbf{RAN}^{(r)} = (RAN_1^{(r)},\ldots,RAN_g^{(r)})$. Procedures exist for sampling from many commonly encountered distributions, other than a uniform distribution. A uniform random sample of limited length can give an unreliable estimate for I_{Dg} in a function $\psi(\mathbf{h})$ that varies over many orders of magnitude in $V(D_g)$.

Consider a canonical system in equilibrium at a temperature *T*. A typical curve for the probability that the system has energy E is a sharp curve centred around the most probable energy, the minimum energy of the system, ⟨E⟩, as shown in Figure 2.

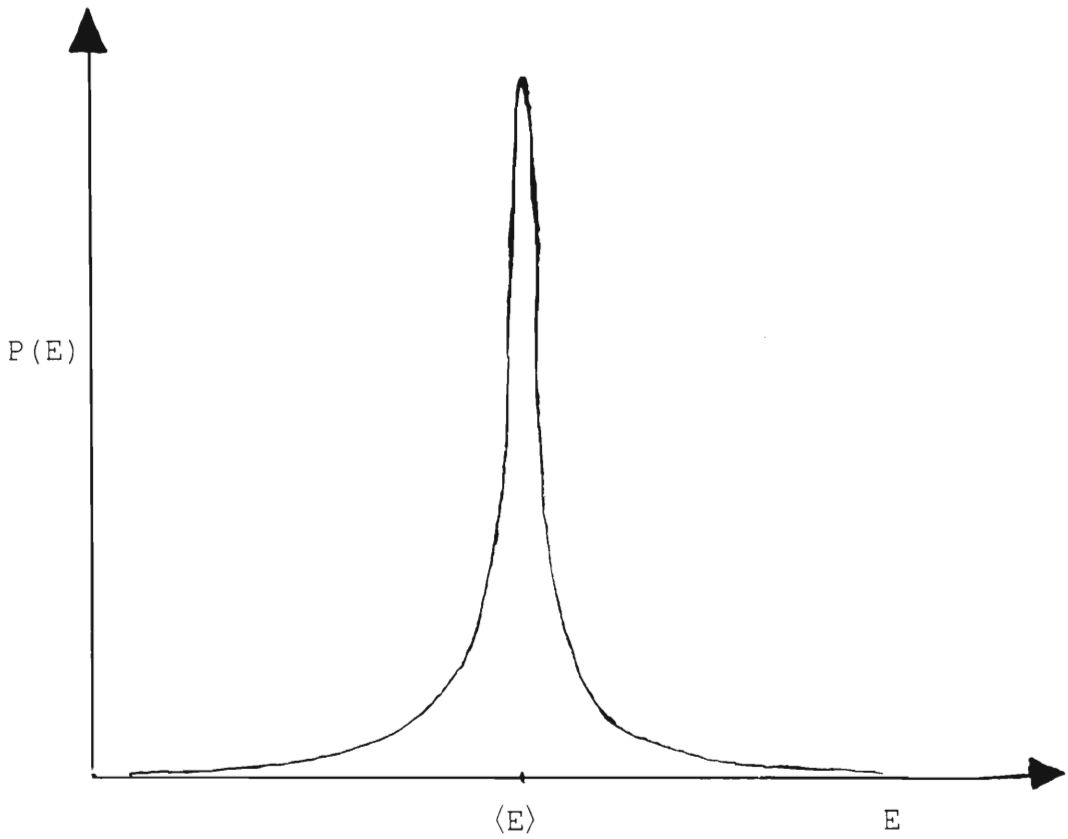

Figure 2. A typical probability curve for a canonical system in equilibrium and a temperature *T*.

Many points will fall in the sub-intervals where the probability is almost zero. So to get a reliable estimate one needs a sampling plan that samples the points distributed according to a particular distribution function F(**h**). In such a case, there would be more points in the region where the probability is large. However, the methods for sampling from commonly encountered distributions rely on the availability of F(**h**) for a particular problem. Techniques that use a smaller sample size

than that in the standard MC approach are available. One such technique is called *Importance Sampling*. It also modifies the interval (**a**,**b**) when necessary. This minimizes the variance of the integrand and improves the efficiency of the MC method.

There is a variety of sampling techniques for different problems. Some of the properties of F(**h**) are that it must be ≥ 0; it must not decrease with **h**; and F(-∞)=0 while F(+∞)=1. F(**h**) is a probability that the next random number will be generated in the interval (-∞,**h**) {ie it is a cumulative probability density} [60]. The probability density function P(**h**) is related to F(**h**) by

$$F(\mathbf{h}) = \int_{-\infty}^{\mathbf{h}} P(\mathbf{h})\, d\mathbf{h}.$$

Virtually all methods that generate samples according to a particular F(**h**) do so directly from F(**h**). However, finding F(**h**),(so that one knows which distribution to sample from),is not always possible. Moreover, to allow for direct sampling, F(**h**) must have certain mathematical properties such as separability, which it may rarely have. The approach of random tour/walk removes this limitation on generating samples directly from F(**h**)by producing a sample through a well-formulated random walk.

2.3 Random Tour/Walk: Markov Sampling

Suppose the objective is to evaluate

$$B = \int_D m(\mathbf{h})\, dF(\mathbf{h}). \qquad (2.3\text{-}1)$$

To approximate B one must generate samples $\mathbf{V}_z$ with distribution F(**h**) and then find the average over such samples. For an arbitrarily selected $\mathbf{v}_0 \in D$, let $\mathbf{V}_o = \mathbf{v}_o$ be the initial state.

Suppose for each $z \geq 1$ that one samples $\mathbf{V}_z$ from a sequence of the distributions conditionally dependent on $\mathbf{V}_{z-1}$, where each generation of $\mathbf{V}_z$ constitutes a MC step. If a conditional distribution depends on D and F(**h**) in a prescribed way, then $\mathbf{V}_z$ converges to a random vector **V** with distribution F(**h**) as $z \to \infty$. So, as $z \to \infty$ (n fixed), $\mathbf{V}_1^{(1)},\ldots,\mathbf{V}_z^{(n)}$, converges in distribution to n independent random vectors from F(**h**) and as $n \to \infty$ (z fixed) $\mathbf{V}_z^{(n)}$ converges in distribution to a random vector **V** with distribution F(**h**). The estimate of expression (2.2-1), for large n and s will then be

$$B \approx n^{-1} \sum_{r=1}^{n} m(\mathbf{V}_z^{(r)}) \equiv s^{-1} \sum_{z=1}^{s} m(\mathbf{V}_z). \qquad (2.3\text{-}2)$$

Many different procedures exist for sampling $\mathbf{V}_z$. In effect, a conditional distribution governs local behaviour at a particular step on the random tour, and F(**h**) governs the global behaviour. Sampling $\mathbf{V}_z$ randomly, starting from an arbitrarily selected state $\mathbf{V}_0$ and guided by the conditional distributions and F(**h**) in question, is called Markov sampling. The resulting sample is known as the Markov chain. If the probabilistic behaviour of each member of the chain $\mathbf{V}_z$ depends on the past history of the sequence only through $\mathbf{V}_{z-1}$, being independent of the preceding values, $\mathbf{V}_0,\mathbf{V}_1,\ldots,\mathbf{V}_{z-2}$, the chain is said to have the *Markov property*.

2.3.1 Metropolis Sampling

The Metropolis algorithm is one technique that ensures a particular tour, $\mathbf{V}_0,\mathbf{V}_1,\ldots,\mathbf{V}_z$, converges to a desired target distribution F(**h**) as $z \to \infty$. Given a weight function Γ (= the probability density up to a normalization constant)

$$\Gamma(\mathbf{h}) = \Gamma(h_1, \ldots, h_g),$$

then n points $,\mathbf{V}^{(1)},\mathbf{V}^{(2)},\ldots,\mathbf{V}^{(n)}$, distributed according to Γ, ie $\Gamma(\mathbf{h}) \approx \Gamma(\mathbf{V})$, can be generated in a random tour in which each step of the tour is driven by the Metropolis algorithm. The idea behind the algorithm is that as $z \to \infty$, $\mathbf{V}_z$ will certainly be one of the points of the required sample of $\Gamma(\mathbf{V})$. Once the initial point or state $\mathbf{V}_0 = \mathbf{v}_0$ (which could represent a particular configuration of a particular lattice) has been chosen, a random walk begins. Suppose that the walk has reached point $\mathbf{V}_z$. To generate the next point $\mathbf{V}_{z+1}$, the algorithm makes a trial step $\mathbf{V}_T$ chosen uniformly from the points in a small hypercube around $\mathbf{V}_z$. The trial step is accepted as the next step of the process according to the value of the ratio

$$[\Gamma(\mathbf{V}_T)].[\Gamma(\mathbf{V}_z)]^{-1} = \mu. \qquad (2.3\text{-}3)$$

If $\mu > 1$, then $\mathbf{V}_T$ is accepted as $\mathbf{V}_{z+1}$; if $\mu < 1$, $\mathbf{V}_T$ is accepted only if $\mu > \sigma$, where σ is a SRN. If $\mathbf{V}_T$ is rejected completely then another trial point is used. The Metropolis algorithm specifies the transition probability between the states through expression (2.2-3).

2.3.2 Convergence of the Metropolis Algorithm

Let Ξ represent a space of "configurations" $\mathbf{V}$ and $,\mathbf{V}^{(1)},\mathbf{V}^{(2)},\ldots,\mathbf{V}^{(n)},\ldots,$ be an infinite walk organised according to the Metropolis algorithm in Ξ. To prove convergence one must show that:

* the walk converges for every choice of the initial configuration. (ie for every $\mathbf{v}_0 \in \Xi$)

* the probability for having $\mathbf{V}^{(*)}$ as the limit of the walk is $\Gamma(\mathbf{V}^{(*)})$ {ie $\Gamma_{eq}(\mathbf{V}^*) = \Gamma(\mathbf{V})$, where $\Gamma_{eq}(\mathbf{V}^*)$ is the equilibrium PDF}.

According to the last statement, if a large number of random walks is organised in this way, their end-points $(\mathbf{V}^{*(1)}, \mathbf{V}^{*(2)}, ..)$ will provide a sample distributed according to $\Gamma(\mathbf{V})$. In the Metropolis algorithm the transition probability $P(\mathbf{V}_i, \mathbf{V}_j)$ for taking configuration $\mathbf{V}_i$ to $\mathbf{V}_j$ must be symmetric in $\mathbf{V}_i$ and $\mathbf{V}_j$ {ie $P(\mathbf{V}_i, \mathbf{V}_j) = P(\mathbf{V}_j, \mathbf{V}_i)$} and be ergodic. The latter implies that, $P(\mathbf{V}_i, \mathbf{V}_j)$ must allow accessibility to all the configurational states of the system. The transition probability must leave an equilibrium ensemble in equilibrium [61],

$$P(\mathbf{V}_i, \mathbf{V}_j)\ \Gamma(\mathbf{V}_i) = \Gamma(\mathbf{V}_j). \qquad (2.3\text{-}4)$$

(So if $\mathbf{V}_i$ is in equilibrium then $\mathbf{V}_j$ must also be in equilibrium) The ergodic property ensures that the distribution of $\mathbf{V}_z$ as $z \rightarrow \infty$ sampled by the Metropolis algorithm, converges to a equilibrium distribution $\Gamma_{eq}(\mathbf{V}^*)$ [59]. Treating $\mathbf{V}_z$ as having the equilibrium distribution for finite z will induce some error in the final estimate. If

$$P(\mathbf{V}_j, \mathbf{V}_i)\Gamma(\mathbf{V}_i) = P(\mathbf{V}_i, \mathbf{V}_j)\Gamma(\mathbf{V}_j), \qquad (2.3\text{-}5)$$

then the chain is said to be reversible. Expression (2.3-5) is referred to as the *detailed balance condition* and implies expression (2.3-4). The latter expression is a sufficient condition for approach to equilibrium (if $\mathbf{V}_i$ and $\mathbf{V}_j$ are not in equilibrium). If P is not ergodic, samples may converge to different equilibrium distributions, when the chain starts in

different initial states because of the nonuniqueness of the solutions to expression (2.3-4). If

$$\lim_{z\to\infty} P(\mathbf{V}_i,\mathbf{V}_j)^z = \Gamma(\mathbf{V}_j),$$

where $P(\mathbf{V}_i,\mathbf{V}_j)^z$ is the ergodic transition probability of moving state $\mathbf{V}_i$ to state $\mathbf{V}_j$ in z steps, then $\Gamma(\mathbf{V}_j)$ is said to be the equilibrium, limiting or steady-state distribution of the chain.

2.3.3 Some Consequences of Starting from an Arbitrary Initial State

For a more detailed analysis of this topic and the related issues see Ref.[59]. Here, only the basic ideas underlying the consequences of starting from an arbitrary state will be discussed. However, these ideas are generally applicable to a variety of random tour problems.

Consider expression (2.3-1) written as

$$B = \sum_{h \in \mathcal{F}} m(h)\Gamma_h \ , \qquad (2.3\text{-}6)$$

where $\mathcal{F}$ is a discrete-state space, and Γ_h (>0) is the equilibrium PDF for each $h \in \mathcal{F}$. To obtain an estimate for expression (2.3-6), the ergodic Markov chains $\{\mathbf{V}_z^{(r)},\ z\geq 0\}$, $r=1,..,n$ are generated. Ideally a MC sampling experiment should be composed of n independent ergodic Markov chains (i.e n independent replications). Each of the latter chains begins in the initial state ($\mathbf{V}_0^{(r)} = \mathbf{v}_0^{(r)}$) drawn from the nonequilibrium distribution Γ_0. Since the initial state $\mathbf{V}_0^{(r)}$ is chosen from Γ_0, it may be far from the equilibrium distribution. Hence $m(\mathbf{V}_0^{(r)})$

may be quite different from $m(\mathbf{V}_{eq}^{(r)})$, where $\mathbf{V}_{eq}$ is the equilibrium point/state. So, a "thermalising" interval of q MC steps on each replication r, is necessary to ensure that $\mathbf{V}_z^{(r)} \approx \mathbf{V}_{eq}^{(r)}$ for $z=q$. After thermalising, sampling continues for y additional steps, and one uses n independent shortened sample chains, each of length y, to estimate expression (2.3-6) as follows,

$$B \approx B_{\Gamma zny} = n^{-1} \sum_{r=1}^{n} y^{-1} \sum_{z=q}^{q+y-1} m(\mathbf{V}_z^{(r)}). \qquad (2.3\text{-}7)$$

The choices of q, n, y, and Γ_0 affect the computational and statistical efficiency, and especially the accuracy of B. Whereas the n-sample Markov chains are statistically independent, the random variables, $\mathbf{V}_o, \mathbf{V}_1, \ldots$, within a particular chain rarely have this property. Dependence among the observations on a single chain requires more subtle methods for assessing the statistical accuracy than n independent observations require. Though data from an independent replication can considerably simplify the problem of evaluating the statistical accuracy of a sample mean, in practice cost (in computer time) , limit this option. In particular, the need to account for the initial conditions on each replication can prove more costly that necessary to achieve a specified error bound. In many problems, a sample mean taken along a single sample chain (n=1) satisfies an error bound for a particular solution at a smaller cost than the multiple replications. Moreover, a single chain data can provide all the data needed to estimate a particular solution. However, the multiple replications assist greatly in determining an 'adequate' thermalising interval q. So in a way one is encouraged to lengthen a single replication chain to improve the accuracy in the estimate of a particular solution, once q has been found based on the multiple replications. Except in special cases, no complete analysis exists for finite q, n, and y . It turns out that all the techniques that approximate for finite q, n, and

y, induce errors that diminish as these parameters increases. A preliminary sampling experiment usually provides data for estimating a q that significantly weakens the influence of the initial conditions. Generally, such an experiment shows how the choices of q,n,y and the initial state affect the approach to equilibrium. It also shows how well an increasing q or y dissipates the influence of the initial states. The experiment consist of $n'(<n)$ independent replications each of length $y'(<y)$, each starting in the states drawn from Γ_0. Once q is estimated, data can also provide a basis for choosing values of n and y that yield parameter estimates which meet absolute or relative error criteria, while accounting for cost considerations. The graphical analysis and the alternative choices of Γ_0 offer a convenient although not foolproof method of identifying an 'adequate' q. There are at least three principal strategies for choosing the initial state in a random tour. The first uses the same state for each value of n, the second assigns an initial state in each replication drawn uniquely, and the third assigns the states drawn randomly and independently from a non-degenerate distribution for each value of n.

Consider the following data array:

z(step) →	0	1	q-1	q	y′	Row Averages
r(Replication) ↓						
1	$\mathbf{L}_0^{(1)}$,	$\mathbf{L}_1^{(1)}$,..,	$\mathbf{L}_{q-1}^{(1)}$,	$\mathbf{L}_q^{(1)}$,..,	$\mathbf{L}_{y'}^{(1)}$	$L_{q,y'-q+1}^{(1)}$
.	.	.	.	.	.	
.	.	.	.	.	.	
.	.	.	.	.	.	
n′	$\mathbf{L}_0^{(n)}$,	$\mathbf{L}_1^{(n)}$,..,	$\mathbf{L}_{q-1}^{(n)}$,	$\mathbf{L}_q^{(n)}$,..,	$\mathbf{L}_{y'}^{(n)}$	$L_{q,y'-q+1}^{(n)}$
Column Averages	$L_{0n'1}$,	$L_{1n'1}$,..,	$L_{q-1,n'1}$,	L_{qn1},..,	$L_{y'n1}$	$[L_{qn',y'-q+1}]$,

where $\mathbf{L}_z^{(r)} = m(\mathbf{V}_z^{(r)})$ for $1 \le z \le y'$; $1 \le r \le n'$. This data can serve as the basis for determining q. The quantity in brackets [] is an average of the row averages, which is also the average of the column averages. Each Figure below (3(a), 3(b) and 3(c)), shows graphs of the three quantities ($L_{zn'1}$; $L_{1n'z}$ and $L_{zn',y'-z+1}$), each versus z. Each n′ independent replication starts in the same state ie $\mathbf{V}_0^{(1)}=....=\mathbf{V}_0^{(n)}$. The first of these quantities is the column average (in which each point on the graph is an average over n replication for a particular value of z)

$$L_{zn'1} = (n')^{-1} \sum^{n'} \mathbf{L}_z^{(r)} , \qquad 1 \le z \le y'; \quad 1 \le r \le n'.$$

The second quantity, is an average over n, in which each value of n is an average over z steps including the influence of the initial conditions

$$L_{1n'z} = z^{-1} \sum_{s=1}^{z} L_{sn'1} = n'^{-1} \sum_{r=1}^{n'} L_{1z}^{(r)} , \qquad 1 \le z \le y'.$$

The third quantity is an average similar to $L_{1n'z}$, but without the influence of the initial conditions

$$L_{zn',y'-z+1} = [y'-z+1]^{-1} \sum_{s=z}^{y'} L_{sn'1} = n'^{-1} \sum_{r=1}^{n'} L_{z,y'-z+1}^{(r)} , \qquad 1 \le z \le y'.$$

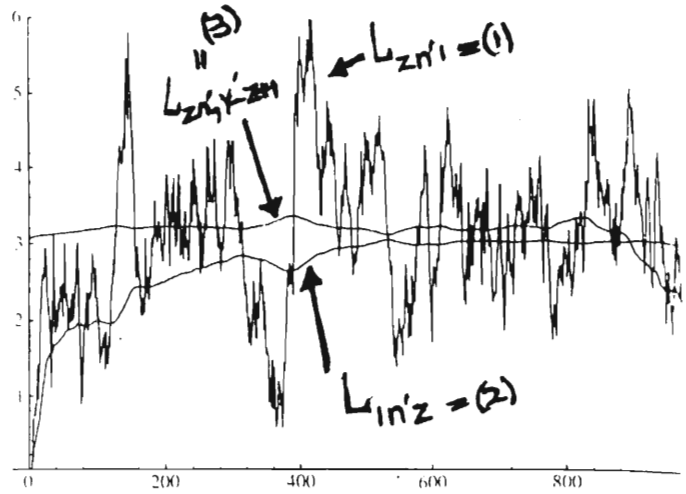

Figure 3(a). The graphs of $L_{zn'1}$; $L_{1n'z}$ and $L_{zn',y'-z+1}$ versus z (MC step) for n'=10 and y'=1000 [59].

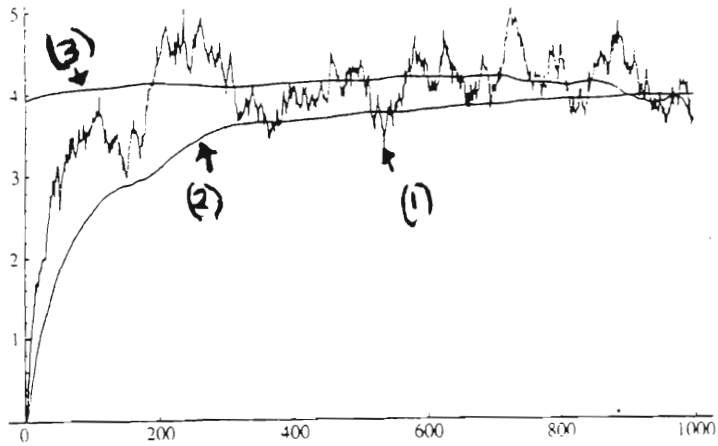

Figure 3(b). The graphs of $L_{zn'1}$; $L_{1n'z}$ and $L_{zn',y'-z+1}$ versus z (MC step) for n′=100 and y′=1000 [59].

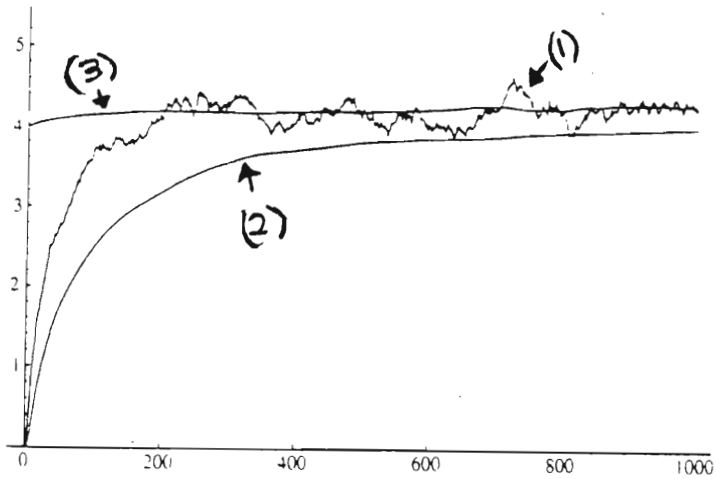

Figure 3(c). The graphs of $L_{zn'1}$; $L_{1n'z}$ and $L_{zn',y'-z+1}$ versus z (MC step) for n′=1000 and y′=1000 [59].

In the Figures 3(a), 3(b), and 3(c) the fluctuations decrease as n′ increases. Figure 3(c) yields a more reliable q value than do the first two figures. However, in practice one would rarely perform n′>1 replications. The Figures 4(a) and 4(b) below show how a small value of n′ and y′ can be misleading in choosing an 'adequate' q value.

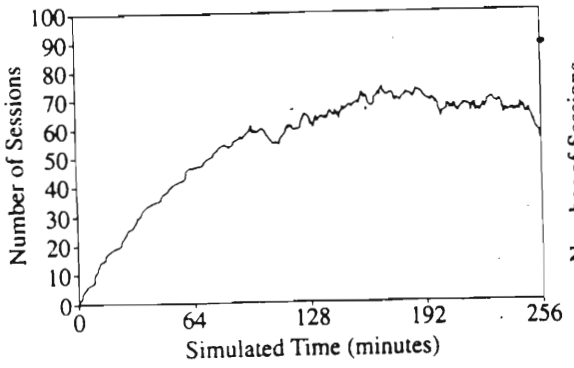

Figure 4(a)

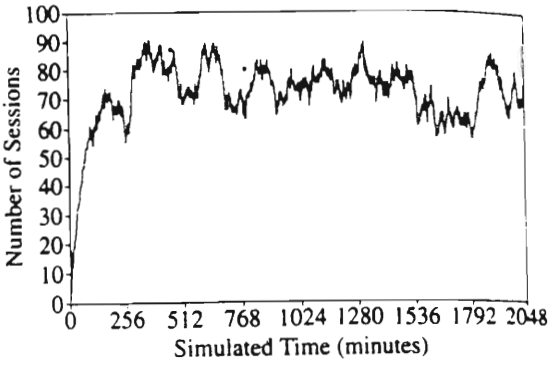

Figure 4(b)

In the both figures a single replication (n′=1) has been considered [59].

These figures represent part of a telecommunication network simulation. Figure 4(a) suggests that the number of active sessions at 15-seconds intervals builds up to a steady-state level between 60 and 70, immediately after 128 minutes (ie after q=512). While Figure 4(b) suggests that the number of sessions becomes steady between 70 and 80 and after 256 minutes (q> 1024). It follows that y′ must be long enough so that a graphical analysis does not confuse a local stabilization in Figure 4(a) and a steady-state in Figure 4(b). Choosing n′>1 can weaken this tendency toward a local stabilization in $L_{zn'1}$.

When fluctuations are to be eliminated, it is useful to start from the same state in each replication, since this will allow for an effective control of the fluctuations in the transient

behaviour of $\{L_{1n'z}\}$ and $\{L_{zn'1}\}$. However, some choices of the initial state may induce excessively long transients to lessen the influence of the initial conditions, and if all the chosen states are the same then they will all be misleading. Moreover, starting all replication in the same state leaves the possibility that a particular convergence may be due to a local equilibrium and not to the desired global equilibrium [59,61,62]. Local stagnation of a process can occur when its equilibrium distribution Γ is multimodal and its transition probability P makes one-step transitions only in a small neighbourhood around the current state of the process.

The second strategy for choosing initial states, starts in the different states, and it can dissipate this effect. Suppose that one assigns $\mathbf{V}_0^{(r)} = \mathbf{v}^{(r)}$ as the initial state on replication r, and then generates an independent sample chain of y′ steps. If the graphical analysis of the n′ independent sample chains $\{\mathbf{L}_z^{(r)}, 0 \leq z \leq y'\}$, $1 \leq r \leq n'$, reveals a positive integer $q < y'$ such that all n′ sample chains(without the influence of the initial conditions); $\{\mathbf{L}_{(z)}^{(1)}, q \leq z \leq y'\}, \ldots, \{\mathbf{L}_{(z)}^{(n')}, q \leq z \leq y'\}$ have converged to a common region and repeatedly intersect each other, then the choice of q as an adequate thermalising interval is justified. In addition, the possibility of a local equilibrium is considerably less than when all replication starts in the same state. Figure 5 below shows an example from gauge theory, where MC methods are applied on the group $SU(2)$[61]. For each lattice size, two distinct initial configurations were studied. The + symbols represent an ordered start, whereas x symbols a random start. Simulations are on the four-dimensional lattices of various sizes ;4^4, 6^4, 8^4, and 10^4 respectively.

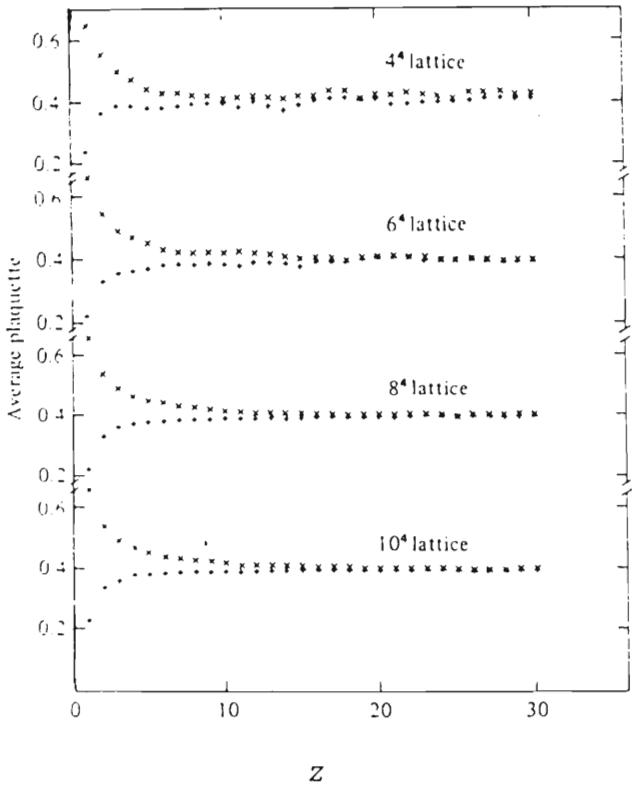

Figure 5. (from Ref. 61).

With the increasing lattice size, the fluctuations become less. An analysis of the individual sample paths $\{ \mathbf{L}_{(z)}{}^{(r)},\ 1 \leq z \leq y' \}$, $1 \leq r \leq n'$, may identify the states that lead to a considerably faster convergence than others. If all but one sample chain converge to a common region, the nonconverging behaviour of the remaining sample chain r may indicate that starting in the initial state $\mathbf{V}_o{}^{(r)} = \mathbf{v}^{(r)}$ induces exceptionally long convergence time. One should then omit chain r from further analysis, and carry out the sampling experiment for the $n'-1$ remaining chains. A non-converging behaviour may also be due to a distribution of $m(\mathbf{V}_z)$ that is multimodal with clustering occurring in the neighbourhoods of the modal values.

The third strategy that chooses initial states in a random tour, samples $\mathbf{V}_o^{(r)}$ randomly from a non-degenerate Γ_0. For a sufficiently large y', a graph of $\{L_{zn'1}\}$ should reveal fluctuations that decrease to a relatively constant level as z increases. If this occur for some $z=q \leq y'$, it suggests that $\{L_{zn'1}, q \leq z \leq y'\}$ is relatively free from the influence of the initial conditions. In general to reduce bias one is encouraged to choose an initial state for which Γ_0 is closer to Γ. However, such a choice relies on ones own ability to infer properties of Γ, presumably from a priori information available about the problem under study.

2.4 A Problem in Statistical Mechanics: A Lattice model

Consider a physical system with g degrees of freedom at a temperature T and energy $E(\mathbf{V}\equiv v_1, v_2, .., v_g) = E(\mathbf{V})$. The observable $A(\mathbf{V})$ for a canonical ensemble with discrete states is

$$\langle A(\mathbf{V}) \rangle = Z^{-1} \sum A(\mathbf{V})\ e^{-\{E(\mathbf{V})/kT\}}\ , \qquad (2.4\text{-}1)$$

where k is the Boltzman constant. The sum is over all states of the system. The partition function Z is

$$Z = \sum e^{-\{E(\mathbf{V})/kT\}}\ .$$

Again the sum is over all states of the system. If $\mathbf{V}$ varies continuously, the sum is replaced by an integral. For a typical system g could be as large as 10^{23} (≡ number of particles in a particular system). In the ASYNNNI model considered in this

thesis with N lattice sites and a maximum N/2 oxygen atoms, the sum is over all the configurational states. Each site can either be occupied by an oxygen atom or not (ie each site can be in two states) and, by changing the occupational state of just one site a new configuration is produced. The number of terms in the sum increases rapidly with the size of the lattice. Even for the lattice size 200x200, the total number of possible configurations is too large for a direct evaluation of the sum by manual methods. The probability that the system has energy $E(\mathbf{V})$, (with uncertainty $\delta E(\mathbf{V})$) is

$$P[E(\mathbf{V})] = \Omega[E(\mathbf{V})]\ e^{-\beta E(\mathbf{V})}, \qquad (2.4\text{-}2)$$

where $\beta=(kT)^{-1}$ and $\Omega[E(\mathbf{V})]$ is the number of configurational states in the energy interval $E(\mathbf{V})$ to $E(\mathbf{V})+\delta E(\mathbf{V})$. In order to evaluate expression (2.4-1), the MC approach uses a Metropolis algorithm to generate the configurational states distributed according to expression (2.4-2) [-which has a Boltzman factor]. Like-wise the probability that the system is in the i^{th} configurational state with energy $E(\mathbf{V_i})$, has a Boltzman factor (which results to a Boltzman distribution) and is given by

$$P_i[E(\mathbf{V_i})] = Z^{-1}\ e^{-\beta E(V_i)}.$$

The Boltzman factor varies rapidly with energy, and so using a randomly chosen sample of configurations without any guidance as to which states to average over, for the evaluation (2.4-1), will give an unreliable estimate to the solution. This is because very few of the chosen configurations will be weighted by a sufficiently large factor to make a significant contribution to the average [62]. From statistical mechanics, the PDF has a sharp maximum centred around a minimum energy $\langle E(\mathbf{V})\rangle$ [the average energy at equilibrium]. As the system under study becomes larger, the

maximum becomes sharper. Restricting sampling to those states that contribute the most in the summation, (ie those with a relatively large probability), around the peak, will result to a reliable estimate, hence importance sampling. The probability that the system is allowed to move from state $\mathbf{V}_i$ to state $\mathbf{V}_j$ is

$$P\{\mathbf{V}_i \rightarrow \mathbf{V}_j\} = \left\{ P_j[E(\mathbf{V}_j)] \right\} . \left\{ P_i[E(\mathbf{V}_i)] \right\}^{-1}$$

$$= e^{-\beta[E(V_j)-E(V_i)]}$$

$$= \mu .$$

CHAPTER 3

Phase Structure of Oxygen Configurations in the ASYNNNI model

3.1 Introduction

Equilibrium configurations of oxygen in the canonical ensemble obtained from a random start, as well as from a uniform start, have been used to obtain the tracer diffusion coefficients D^* from the MC simulations of the ASYNNNI model [9,35,39]. Since these attempts have failed to obtain the values of D^* in agreement with the experiments, it is worthwhile to try other modifications of this model and of the way it is implemented, in an attempt to reproduce the experimental observations. Using a completely different initial start in the ASYNNNI model with the hope that other equilibrium configurations than those obtained in Refs.9, 35 and 39, may be found, is the modification considered here.

If the free energy of this model has multi-minima, then the Markovian random walks which begin from a particular type of initial configuration could be trapped by one of the minima(not necessary the one corresponding to the lowest value of the free energy) while simulations starting from a different type of the initial configuration may end up being trapped by another minimum of the free energy, thus leading to different values of the observables. To see whether the free energy of this model possesses multi-minima and whether, for certain values of the temperature T and the oxygen concentration c these minima are separated by impenetrable barriers, the MC simulations from a "block" start (described below) were performed and the evolution

of the microstructures as functions of T and c studied.

3.2 The Simulation Method

A two-dimensional lattice gas model (the ASYNNNI model) was used to study the motion of the oxygen atoms in the basal planes of $YBa_2Cu_3O_{7-x}$. The lattice has size n_x, xn_y and the number of the oxygen atoms is $N=0.5xn_x,n_y$, where $x=2c$. Periodic boundary conditions are used. The MC simulations using the Metropolis algorithm were employed in obtaining the observables. The values of the EPI were chosen as V_1=0.19eV, V_2=-0.136eV and V_3=0.054eV [35]. The initial configurations in which all oxygens were ordered with maximum density at one side of the lattice leaving the rest of the lattice unoccupied are here referred to as a block start. Examples of the random and the block starts are shown in Figures 1(a) and 1(b) respectively, where the small circles represent oxygen ions. Empty spaces along the rows represent oxygen vacancies.

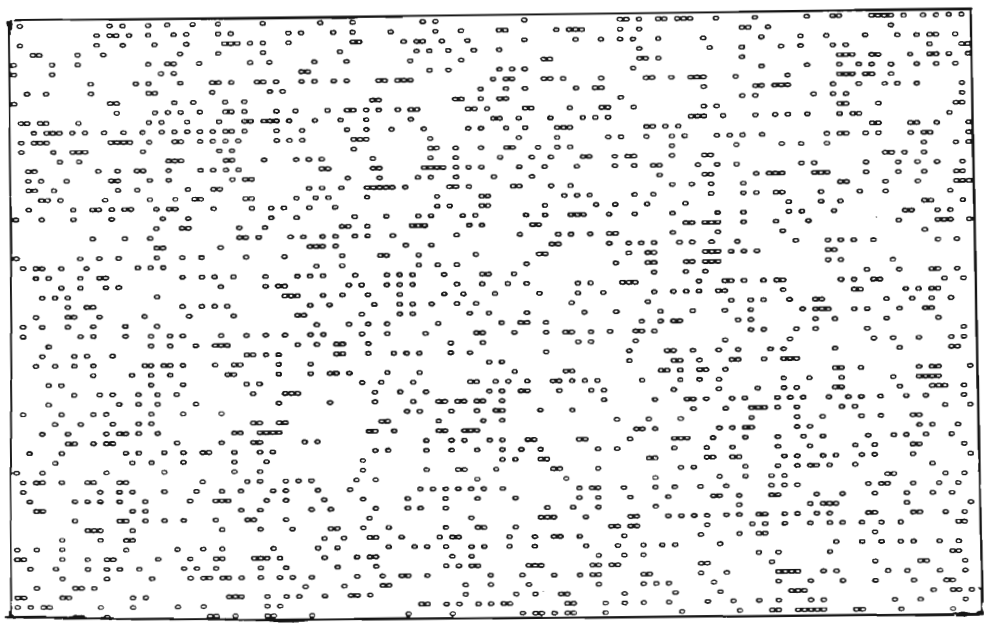

Figure 1(a). A lattice configuration of the oxygen atoms showing a random start with x=0.4. The lattice is 150x62.

It was anticipated that the block start is far from equilibrium, therefore the system was thermalised through hundreds of thousands of MC steps. Since the distribution of oxygen corresponding to a block start is highly inhomogeneous, it was expected that, at least for low temperatures, some relic of this inhomogeneity will survive thermalization over many hundreds of thousands and even millions of MC steps, thus signalling a distinct phase in the model.

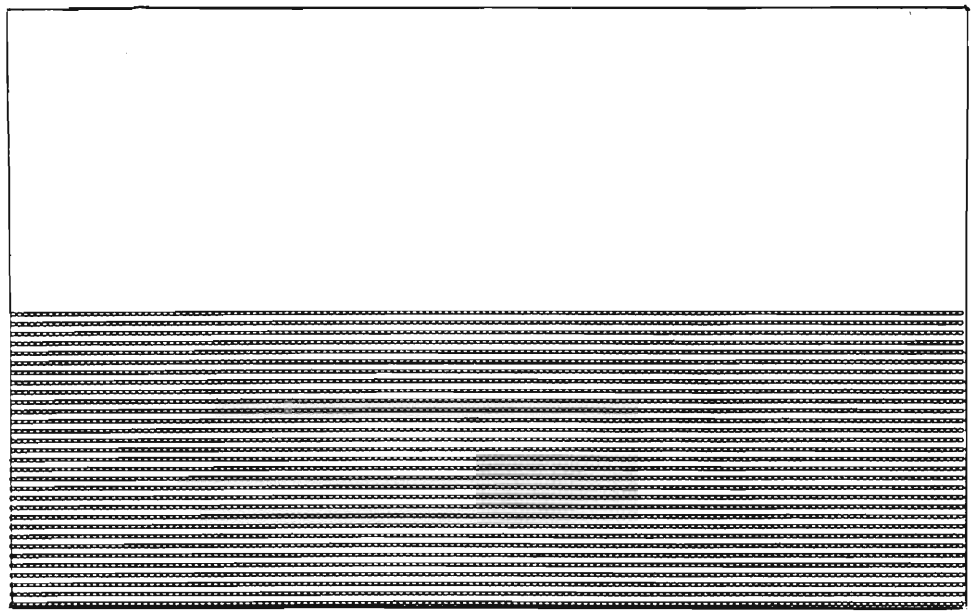

Figure 1(b).The lattice configurations of oxygen showing a block start with x=1. The lattice is 150x62.

In the simulation method, each oxygen ion is only allowed to jump to either one of its four nearest neighbour(NN) accessible sites or one of its two next-to-nearest neighbour(NNN) accessible sites with equal probability. The jumps over Cu ions from one O(1) site to another are not allowed. Only one oxygen ion can occupy a particular site at a time. Each site can therefore be in two states, occupied and unoccupied. A randomly selected ion may jump to any NN or NNN accessible site according to the value of the configurational energy change ΔH between the initial configuration (before the jump is made) and the final configuration (after the jump has been made). The energy of a randomly selected ion is calculated as the sum of all the interactions with occupied NN and NNN sites. So for each ion a maximum of eight occupied sites contribute to H (four NN and four NNN sites respectively). The configurational energy of the system is given by,

$$H = V_1 \sum_{<ij>} c_i c_j + V_2 \sum_{[ij]} c_i c_j + V_3 \sum_{\{ij\}} c_i c_j,$$

where the first sum is over NN pairs <ij> , the second sum is over NNN pairs over Cu [ij], and the last term is a sum over NNN pairs not over Cu {ij} and V_1, V_2, and V_3 are EPI's. The occupational numbers for site i and j are c_i and c_j respectively and when c_i=1 or 0, site i is occupied or empty. If $\Delta H = H_f - H_i < 0$, where H_f and H_i are the final and the initial energy after and before the jump is made, a jump is allowed, otherwise a random number $\sigma \in [0,1]$ is generated and if $\sigma < \exp(\Delta H/kT)$, a jump is allowed, otherwise another occupied site is randomly selected.

The simulations were performed on a dual processor Origin 200 Silicon Graphics workstation. The program was written in FORTRAN 90 using a multi-spin coding technique [63]. When a site is occupied the bit is set to one and when empty set to zero. The whole array of bits is stored as an integer in the computer memory. The general structure of the program and the main subroutines used in the simulations are listed in the Appendix. Time is measured in MC steps per site. One iteration/MC step (MCS) consists of an attempt to update each site of the lattice once.

3.3 Phase Structure and the Oxygen Density Profile.

The simulations with the same values of EPI's, but from a random start were also performed for a direct comparison with the results of the other workers. The oxygen density profile was also monitored, by plotting the ratio of the occupied sites in each row of the lattice. Simulations from a random start reproduced the lattice configurations and the D^* values in [9], whereas

simulations from a block start revealed additional stable configurations. Here only the representative oxygen lattice configurations will be shown.

The lattice configuration in Figure 2(a) shows a general pattern of oxygen ordering at lower temperatures obtained from a random start. These microstructures do not show any significant deviation from a homogeneous distribution of oxygen. The short Cu-O chains appear with equal probability along the O(1) and O(5) sites. A graphical representation of the oxygen density profile ρ in the lattice rows shown in Figure 2(b) confirms the almost homogeneous distribution of oxygen ions in the rows of the lattice. The equilibrium ρ of the occupied sites in the rows of the two lattices does not show any variation above statistical noise, and equilibrated to ≈ 0.2 within 100 MC steps and stayed so for at least the next 51k MC steps. However as the number of MC steps increases fluctuations decrease. A plot of ρ per slice against the MC step reveals the same information as that of ρ versus the row number after 51k MC (Figure 2(c)). (For the lattices with 52 and 62 rows, each slice consist of 5 and 6 consecutive rows respectively). The average energy per ion in a slice, plotted against MC steps shows that the average energy of each slice is almost the same throughout the lattice (Figure 2(d)). A negative value of the energy indicates that the dominant interaction is V_2. When the total energy in the slices was plotted against the number of slices (not shown here), similar information to Figure 2(d) was revealed. However the average energy seemed more stable.

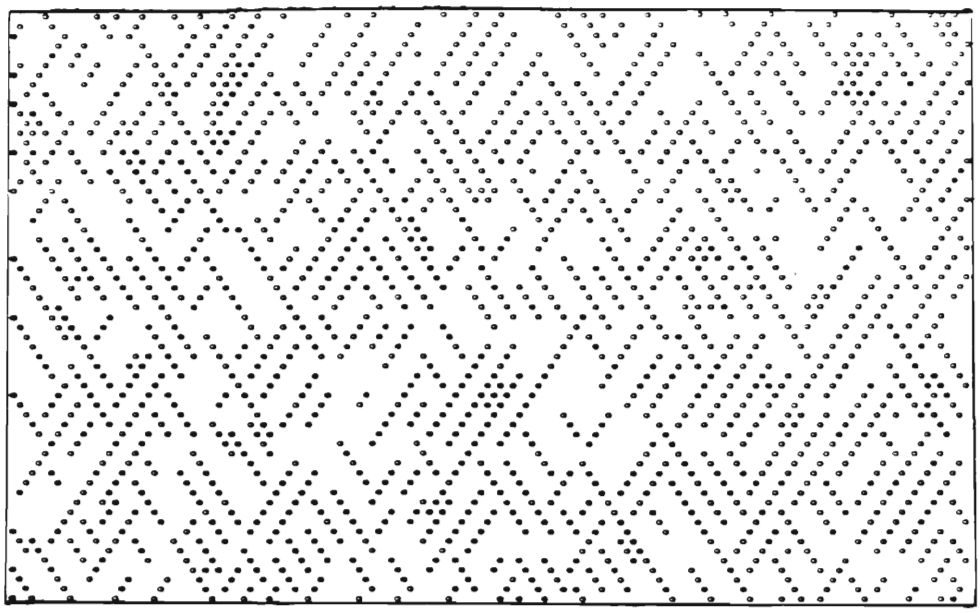

Figure 2(a). A lattice oxygen configuration for x=0.4 and T=0.02eV after 1k MC steps from a random start. The lattice is 150x62.

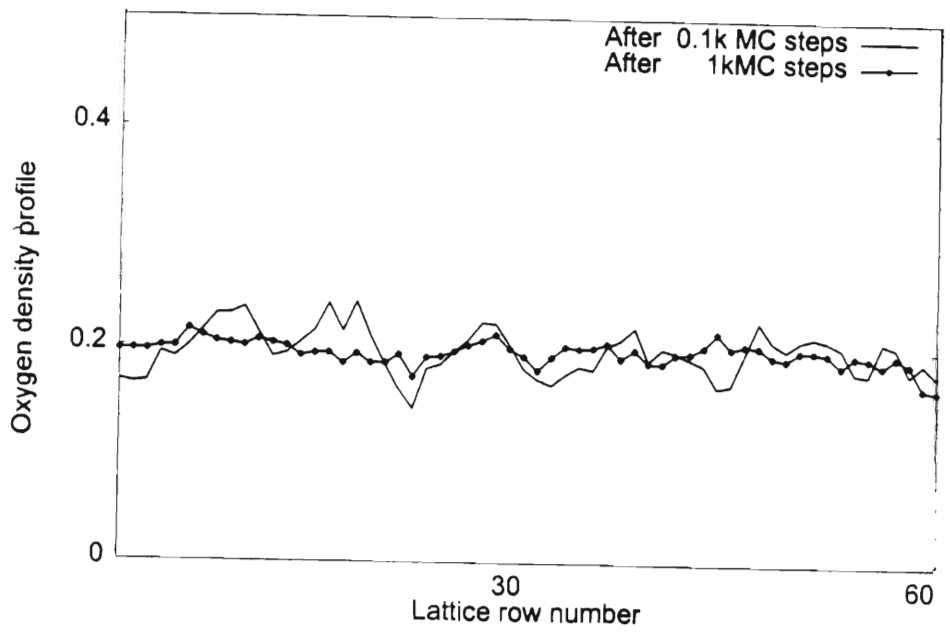

Figure 2(b). The oxygen density profile versus the number of the row for x=0.4 and T=0.02eV. The lattice is 150x62.

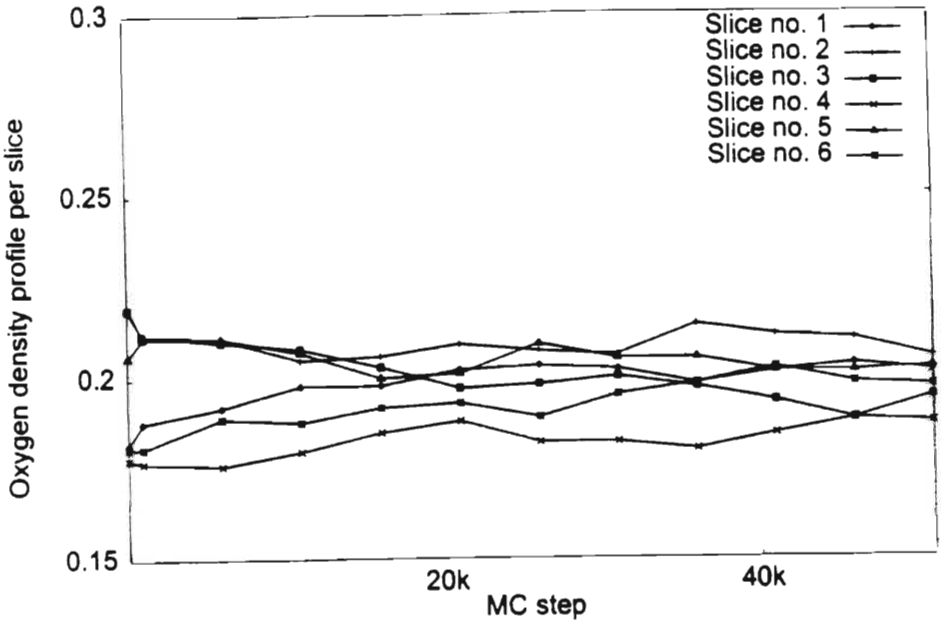

Figure 2(c).The oxygen density profile per slice after various MC steps for x=0.4 and *T*=0.02eV. The lattice is 150x62.

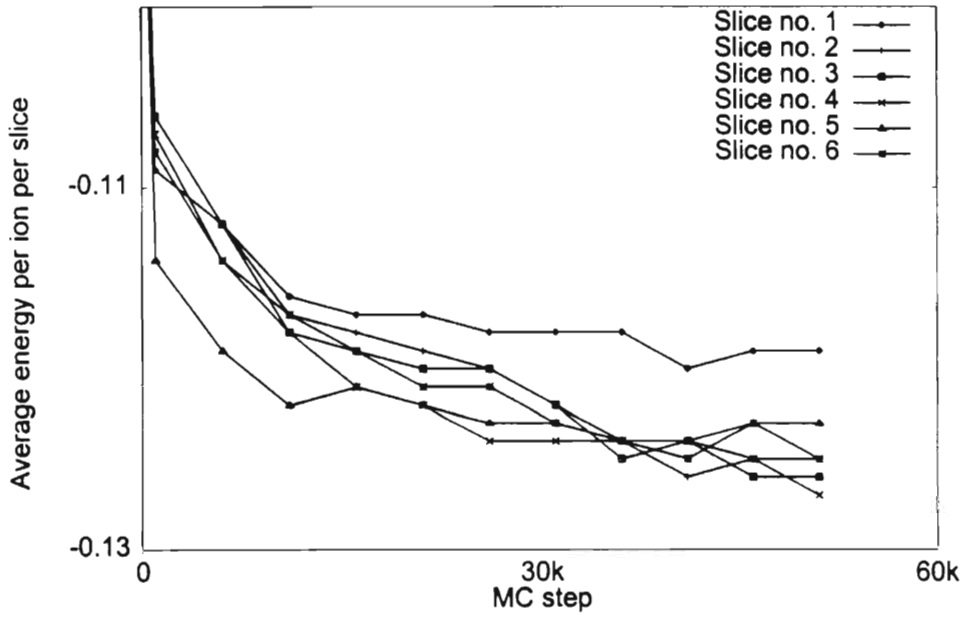

Figure 2(d). The average energy per oxygen ion per slice after various values of MC steps for x=0.4 and *T*=0.02eV. The lattice is 150x62.

The homogeneous phase can be denoted H_{10} where the first subscript indicates the presence of the chains and the second that these are not preferentially oriented along either the O(1)

or O(5) directions. (The OrthoI structure (x=1) is a particular case of the H_{10} phase). When T is increased, and for x<1, the Cu-O chains appear less frequently and eventually disappear completely: the high temperature phase is characterised by a homogeneous and a disordered distribution of oxygen (denoted by H_0 where the subscript 0 indicates the absence of chains), which is essentially the same as the random initial configuration used in the simulations. These are all the phases of the ASYNNNI model which can be reached by MC simulations from a random start. A homogeneous lattice configuration with chains orientated along one preferred direction has been obtained from a random start [39].

When the model is simulated from the block start, a richer phase structure is revealed. For the lowest temperature studied (0.02eV) the system stabilizes at a markedly inhomogeneous oxygen distribution. The oxygen ions tend to stay together and this effect is most pronounced for x=0.4 and 0.6. Examples of the lattice configurations at various MC steps, together with the oxygen density profiles and the average energy per oxygen ion per slice are shown in Figures 3 and 4. Clearly Cu-O chains are much longer when simulating from a block start (Figures 3(a) and 4(a)). These inhomogeneous configurations can be classified as belonging to the phase I_{11} of the model. Here the first subscript indicates that there are chains and the second that they tend to be preferentially ordered in either the O(1) or the O(5) directions.

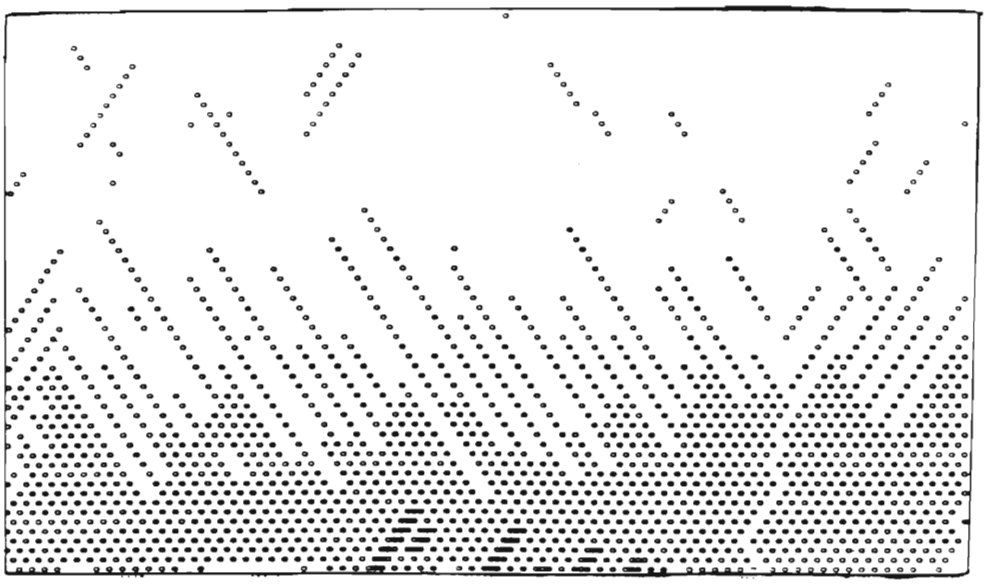

Figure 3(a)(i).A lattice oxygen configuration for x=0.4 and T=0.02eV after 100k MC steps from a block start. The lattice is 150x62.

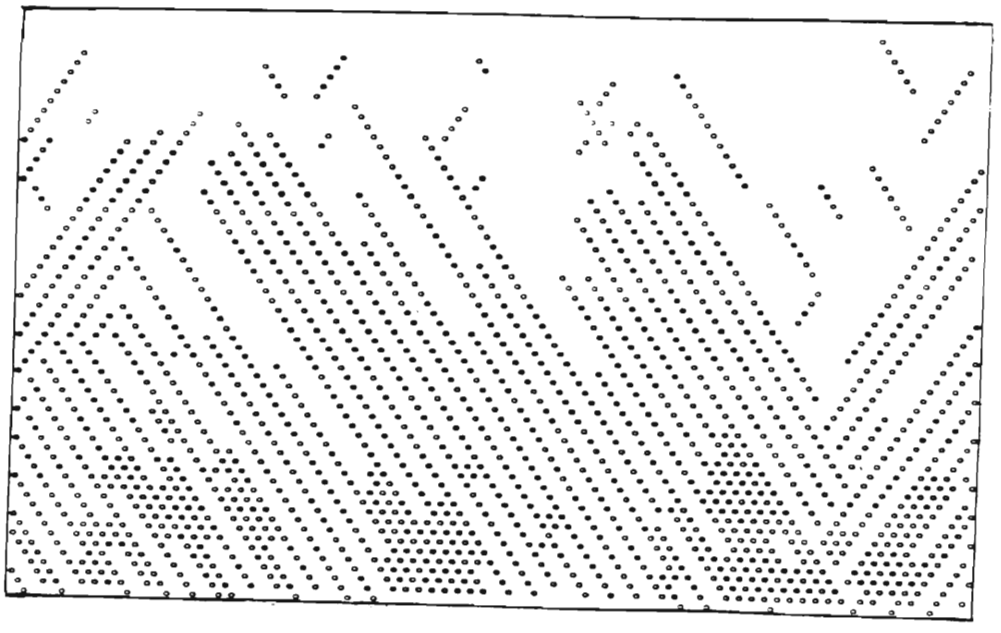

Figure 3(a)(ii).As in Figure 3(a)(i), but after 10^6 (1M) MC steps.

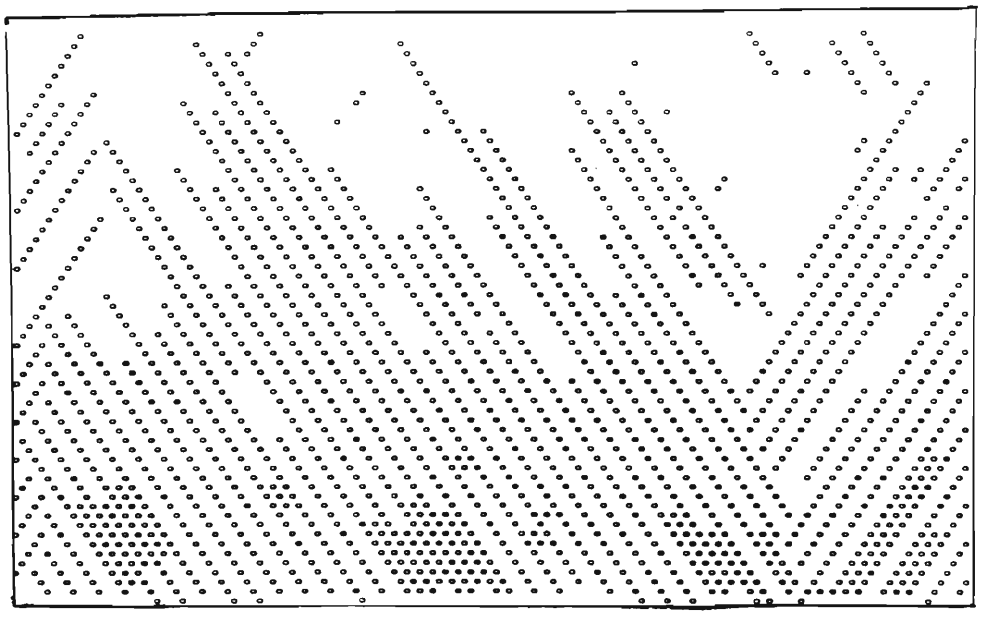

Figure 3(a)(iii).As in Figure 3(a)(i), but after $2x10^6$ (2M) MC steps.

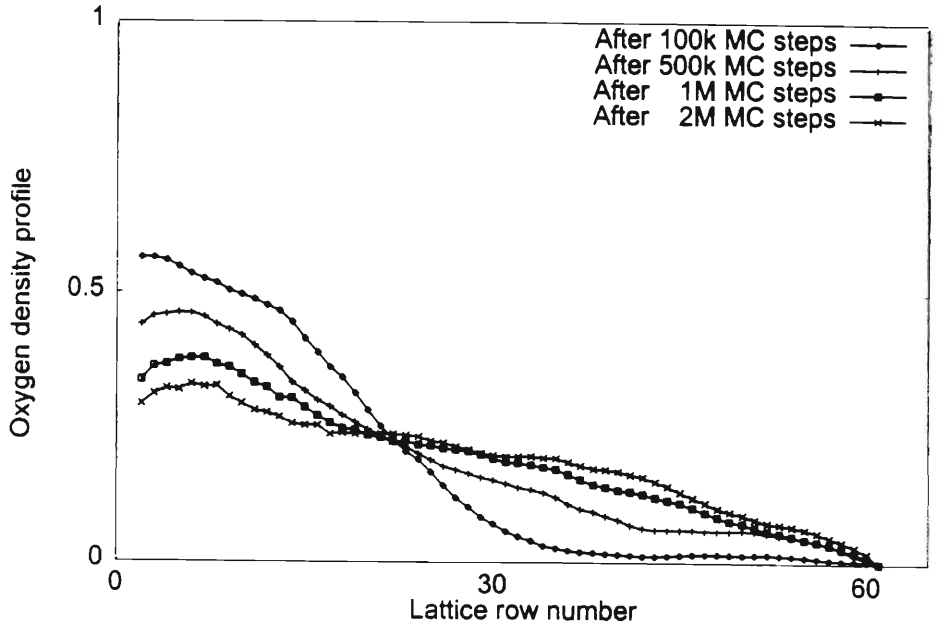

Figure 3(b).The oxygen density profile versus row number for x=0.4 and T=0.02eV. The lattice is 150x62.

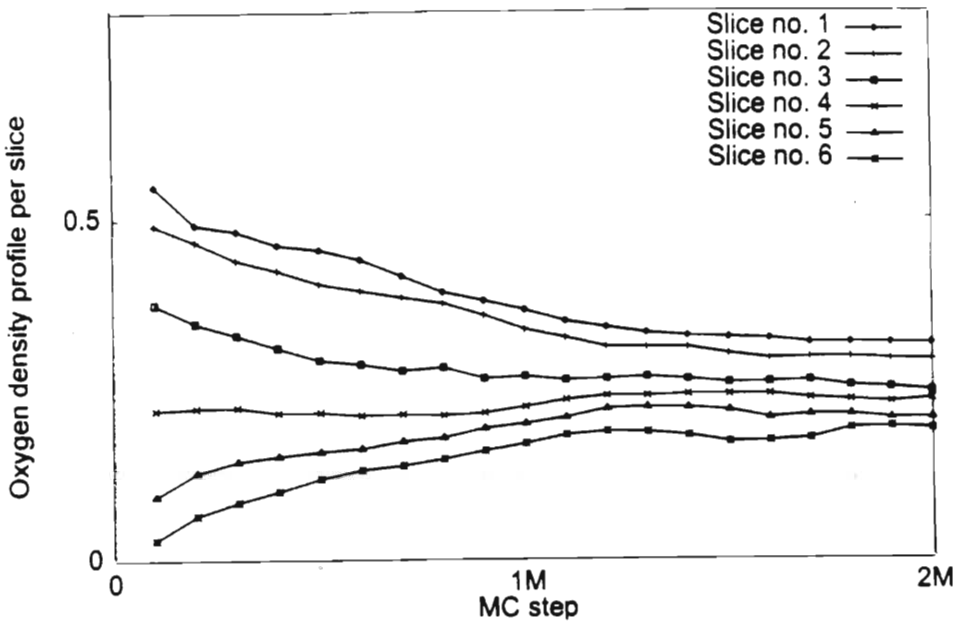

Figure 3(c). The oxygen density profile per slice versus the number of the MC steps for x=0.4 and *T*=0.02eV. The lattice is 150x62.

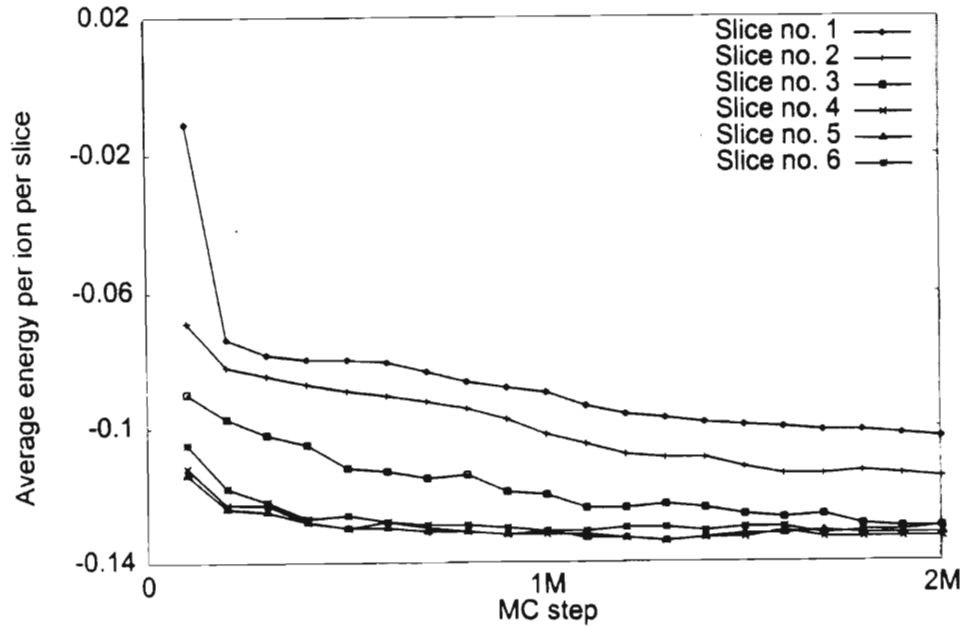

Figure 3(d). The average energy per oxygen ion per slice versus the number of the MC steps for x=0.4 and *T*=0.02eV. The lattice is 150x62.

The lattice from a block start takes longer to stabilize than the one from a random start. The inhomogeneity of the oxygen distribution in the lattice is evident from Figures 3(b) and 4(b. The oxygen density profile in the rows shows that the oxygen density is not evenly distributed throughout the lattice even after $2x10^6$ (2M) MC steps. For x=0.4 the lattice stabilizes above 1.5×10^6 MC steps (Figure 3(c)), whereas for x=0.6 above 500k MC steps (Figure 4(c)). The average energy per oxygen ion per slice shows a bigger variation from one slice to the other than for a random start, due to inhomogeneity (Figures 3(d) and 4(d)). However there still remains some slices with almost a similar average energy.

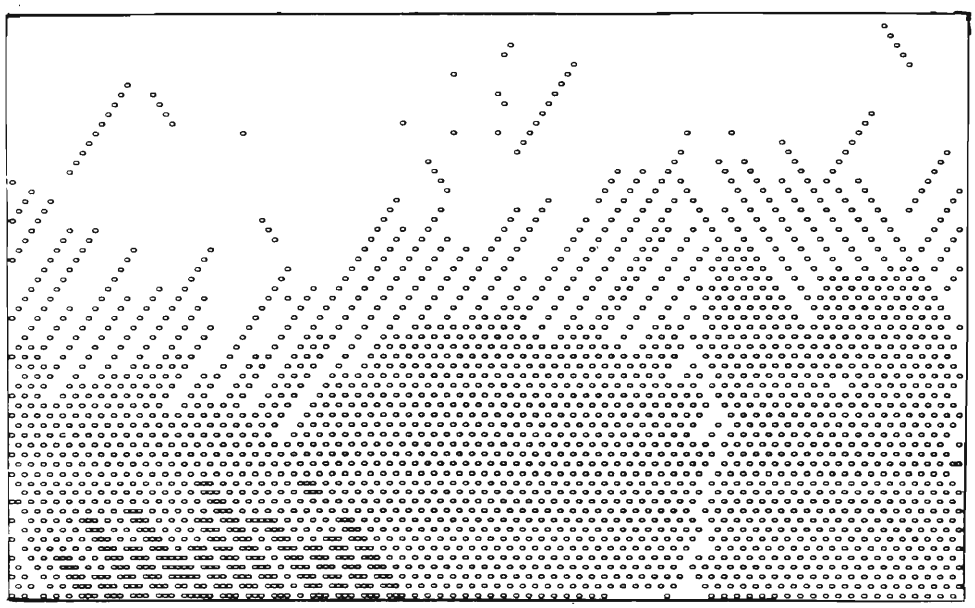

Figure 4(a)(i).A lattice oxygen configuration for x=0.6 and T=0.02eV after 100k MC steps from a block start. The lattice is 150x62.

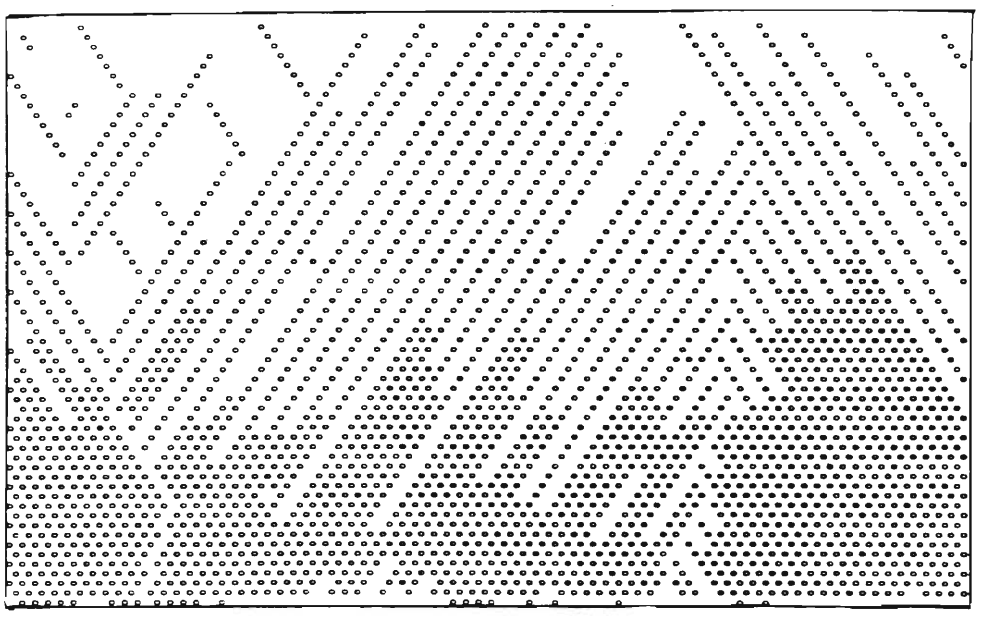

Figure 4(a)(ii).As in Figure 4(a)(i), but after 10^6 (1M) MC steps.

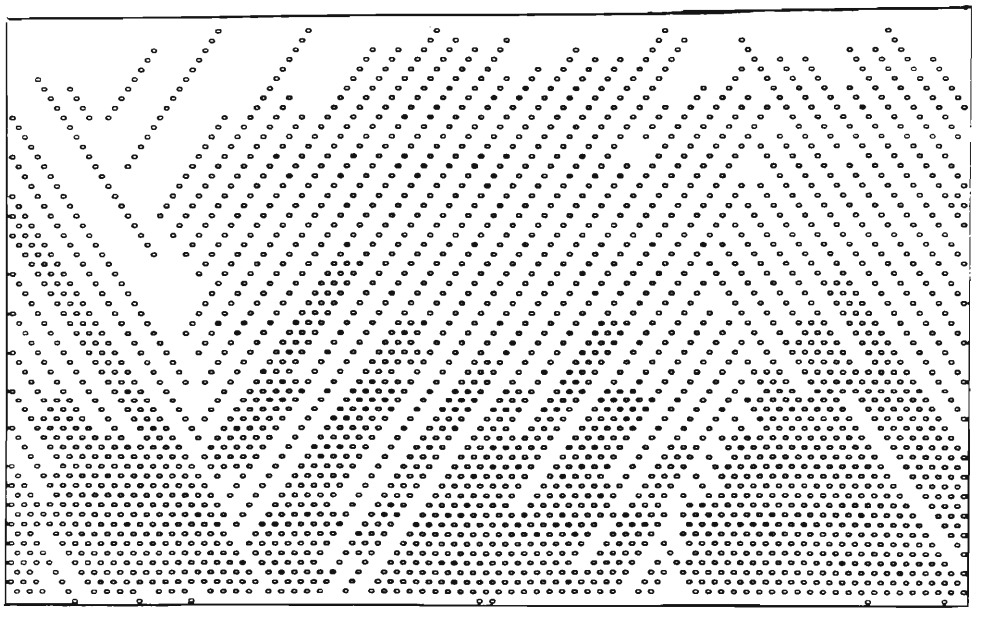

Figure 4(a)(iii). As in Figure 4(a)(i), but after $2x10^6$ (2M) MC steps

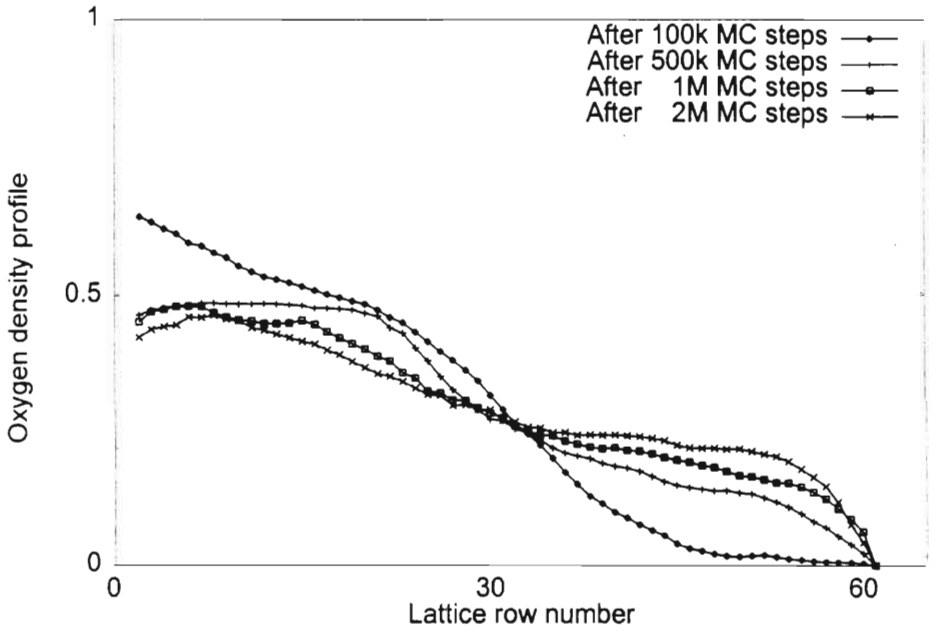

Figure 4(b). The oxygen density profile versus row number for x=0.6 and *T*=0.02eV. The lattice is 150x62.

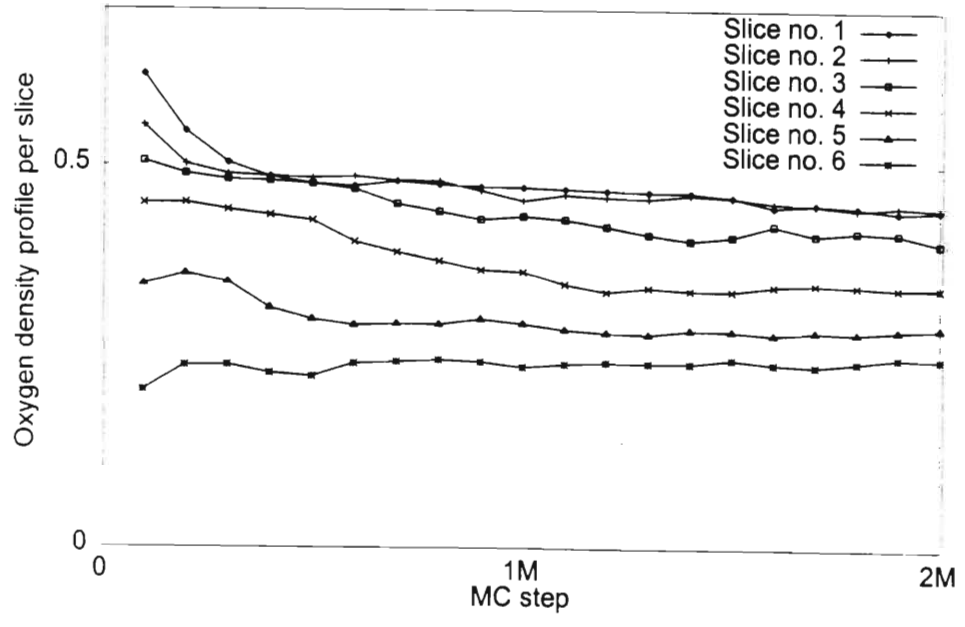

Figure 4(c). The oxygen density profile per slice versus the number of the MC steps for x=0.6 and *T*=0.02eV. The lattice is 150x62.

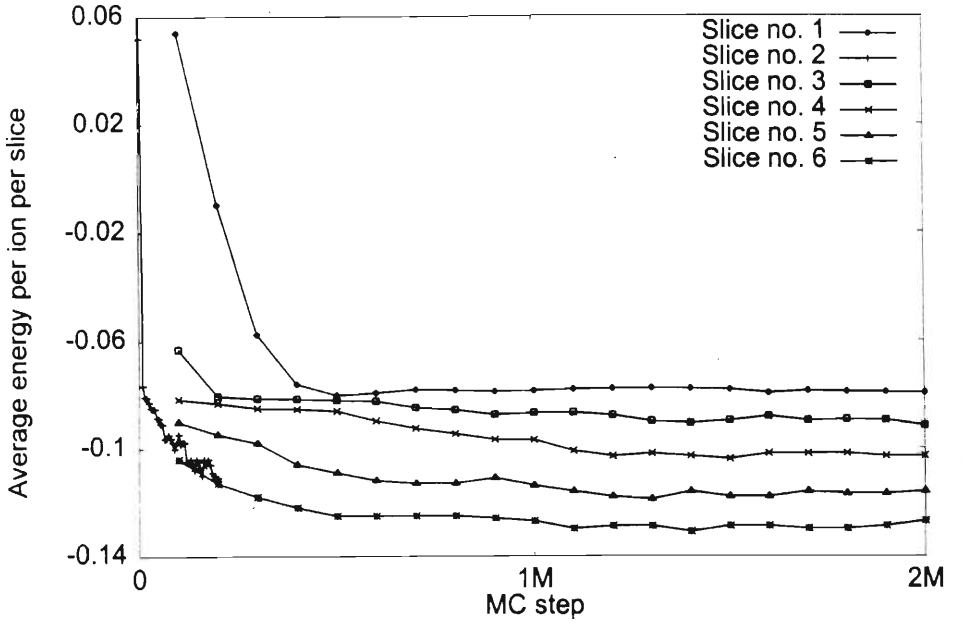

Figure 4(d).The average energy per oxygen ion per slice versus the number of the MC steps fro x=0.6 and *T*=0.02eV. The lattice is 150x62.

There are three features, in particular, of the above stable microstructures and the density profiles worth noting. First, chains of vacancies seem to appear together with the typical oxygen chains (Figures 3 and 4, a(ii)-a(iii)). Other irregular clusters of the vacancies are also present. These features are easier to identify at higher oxygen concentration than that in Figure 4 (see Figure 6(a)). A chain of vacancies immersed in a locally homogeneous environment could move, in principle, without dissipation of energy, and hence without "friction". The formation of the vacancies requires both a particular temperature interval and an oxygen concentration which is neither too low nor too high. It is an open question whether this is an artifact of the model or has some bearing on the transport phenomena in YBCO. Second, the oxygen density profiles for different numbers of MC steps seem to pass through the same point (Figures 3(b) and 4(b)). (This feature is also observed at other values of c and

T. It is, however, less defined at low concentrations and/or high temperatures). This could correspond to a characteristic length scale associated with the inhomogeneous phases. The dependence of this length on c and *T* is left as a subject for further research. Third, the microstructures of the configurations reached from a block start at low *T* are anisotropic since one type of a oxygen chain (say O(1)) clearly dominates over the other. The system can end up in either of the two ordered states with equal probability, which is indicative of spontaneous symmetry breaking. This long-range order is typical for systems of the same universality class as the Ising model for a 2-dimensional ferromagnet.

At lower concentrations the oxygen inhomogeneity seems to dissolve away after a certain number of MC steps (Figure 5(a)). The chains seem longer for x=0.2 than for x=0.1. The point through which the oxygen density profiles for different MC steps pass is not as well defined as in Figures 3(b) and 4(b)(Figure 5(b)). Stability is attained above 300k MC steps (Figure 5(c)). There are more fluctuations for the low values of the MC steps. The average energy per oxygen ion in each slice shows that the energy values for all the six slices are converging to an almost similar value (Figure 5(d)).

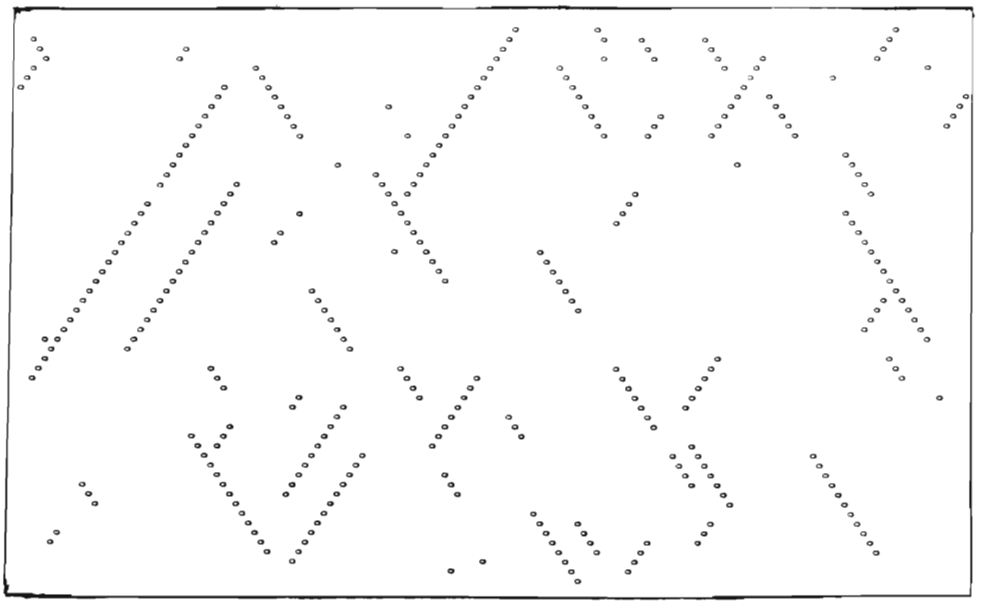

Figure 5(a)(i).A lattice oxygen configuration for x=0.1 and T=0.02eV after 800k MC steps from a block start. The lattice is 150x62.

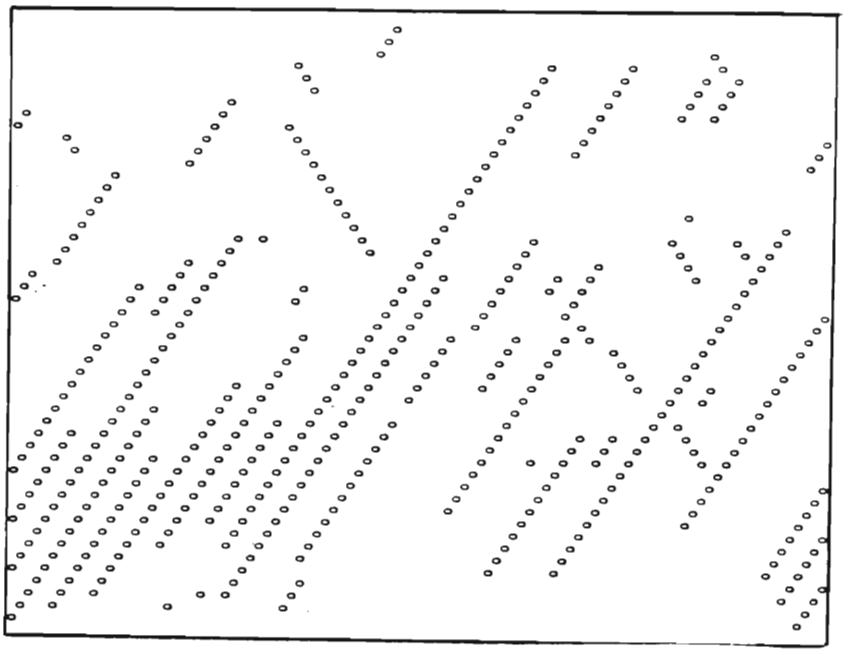

Figure 5(a)(ii). A lattice oxygen configuration for x=0.2 and T=0.02eV after 10^6 (1M) MC steps from a block start. The lattice is 100x52.

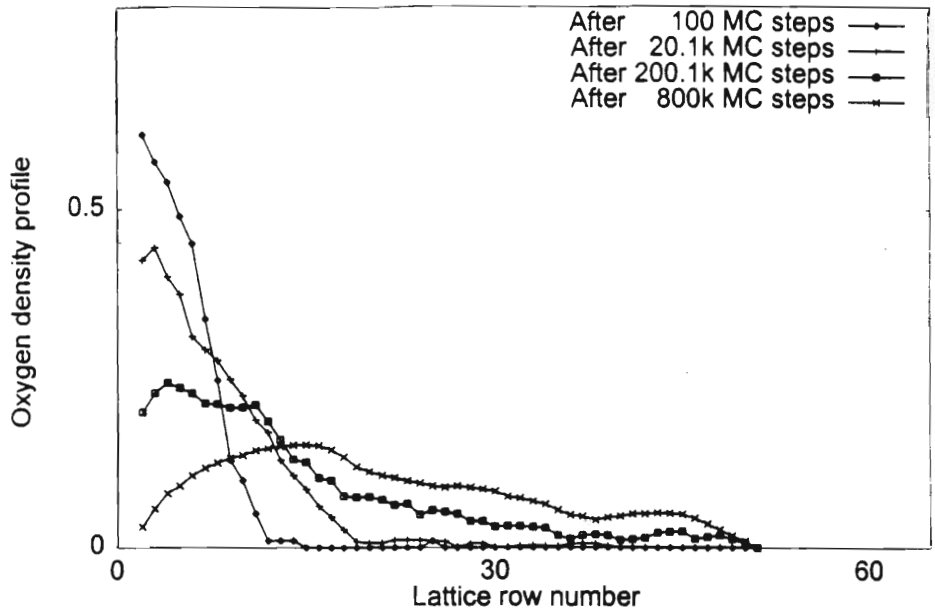

Figure 5(b).The oxygen density profile versus row number for x=0.2 and *T*=0.02eV. The lattice is 100x52.

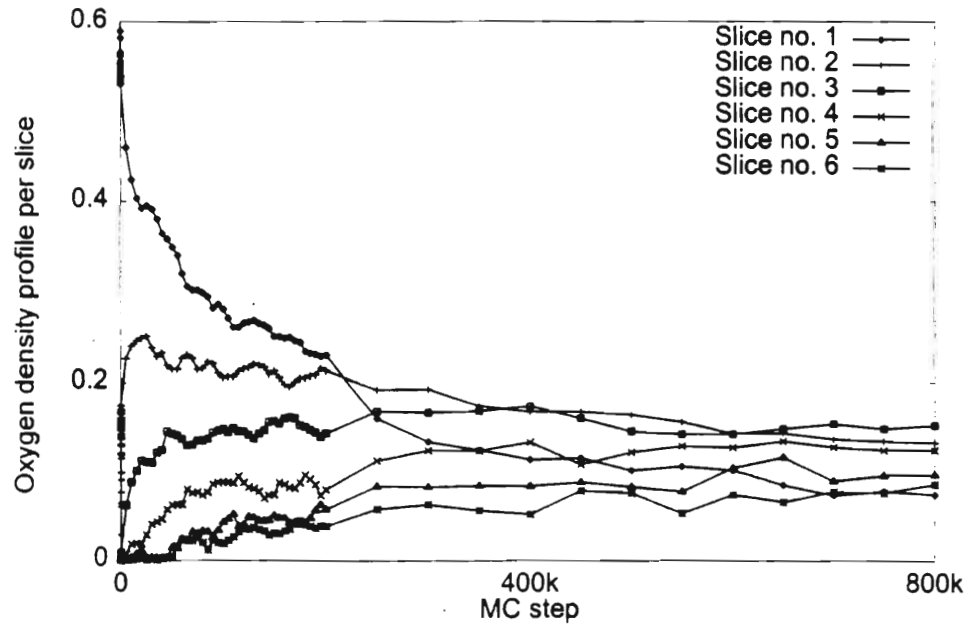

Figure 5(c).The oxygen density profile in the slices against MC step for x=0.2 and *T*=0.02eV. The lattice is 100x52.

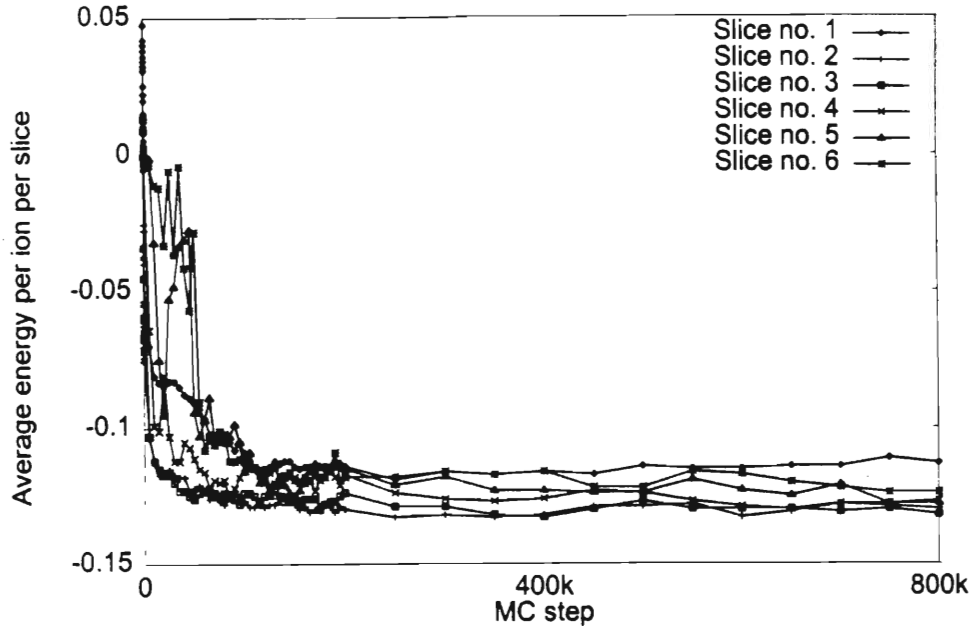

Figure 5(d). The average energy per ion per slice versus the number of MC steps for x=0.2 and *T*=0.02eV. The lattice is 100x52.

The evolution of the configuration for x=0.8 and *T*=0.02 is shown in Figures 6(a)(i) and (ii). After 10^6 (1M) MC steps, one side of the lattice seemed to have formed chains of both the oxygen atoms and the oxygen vacancies, whereas the other side appears to be the orthorhombic phase (Figure 6(a)(ii)). The fact that the oxygen density profile after 1M MC steps seems to form two plateaus at different values (Figure 6(b)), confirms the co-existence of two stable microstructures. More simulations above 1M steps would have provided a much more complete picture at this concentration and temperature. Nevertheless, the general trend of the behaviour of the oxygen density per slice to stabilize after a certain number of MC steps, and early stabilization in the rows where the lattice was initially empty remains (figure 6(c) and (d)).

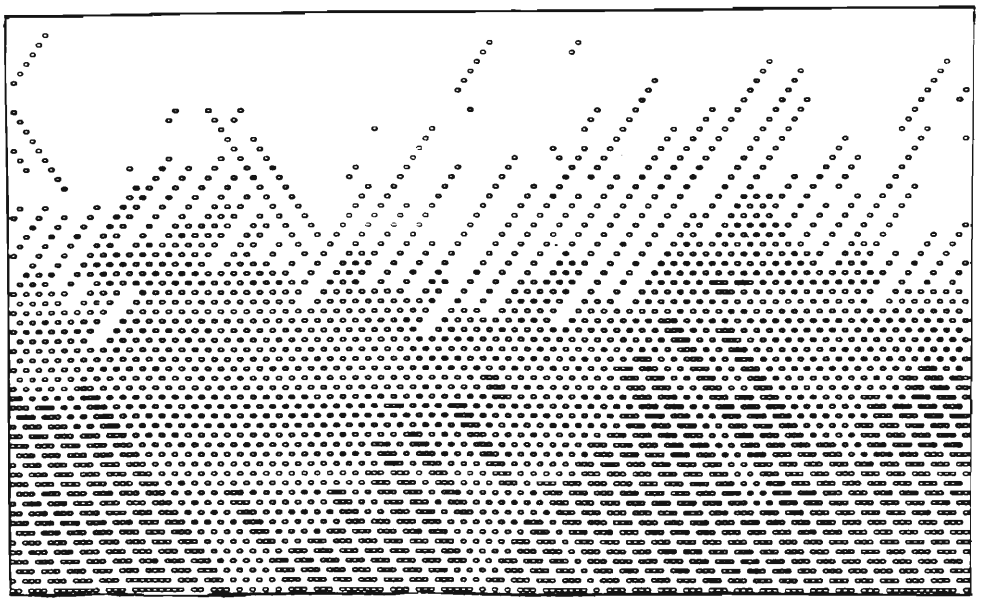

Figure 6(a)(i). A lattice oxygen configuration for x=0.8 and T=0.02eV after 100k MC steps from a block start. The lattice is 150x62.

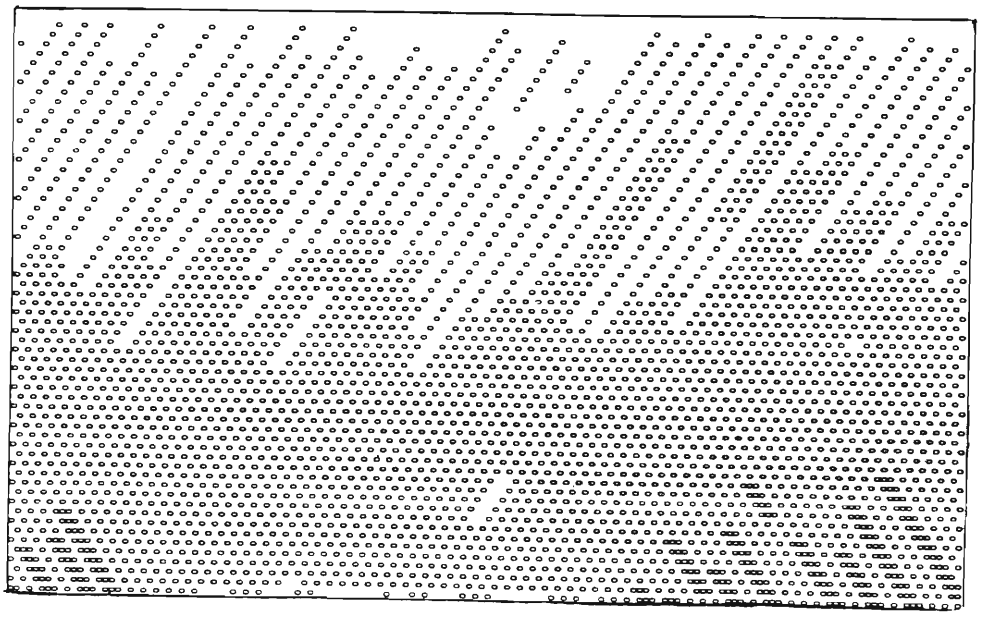

Figure 6(a)(ii). A lattice oxygen configuration for x=0.8 and T=0.02eV after 10^6(1M) MC steps from a block start. The lattice is 150x62.

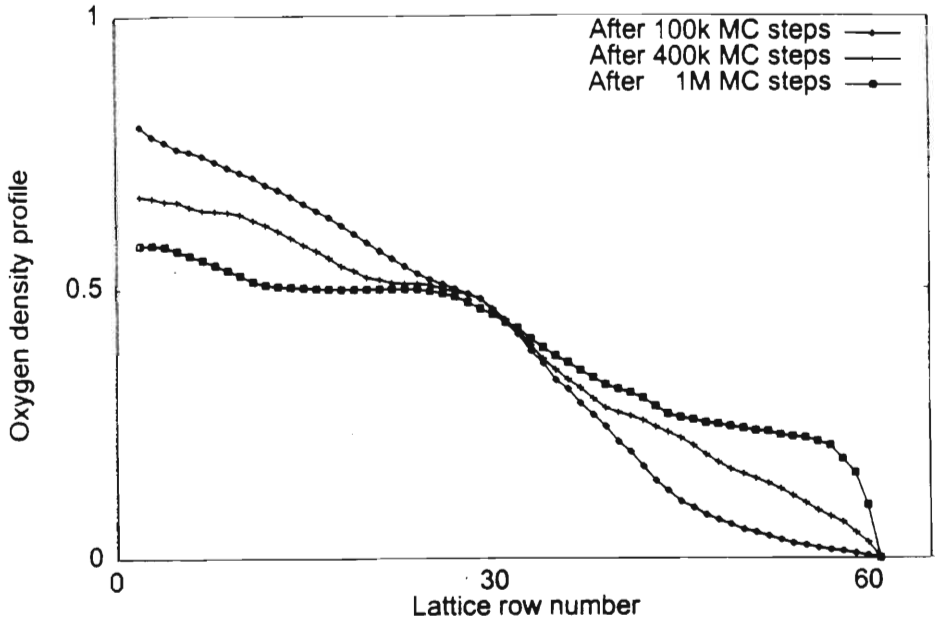

Figure 6(b). The oxygen density profile versus row number for x=0.8 and T=0.02eV. The lattice is 150x62.

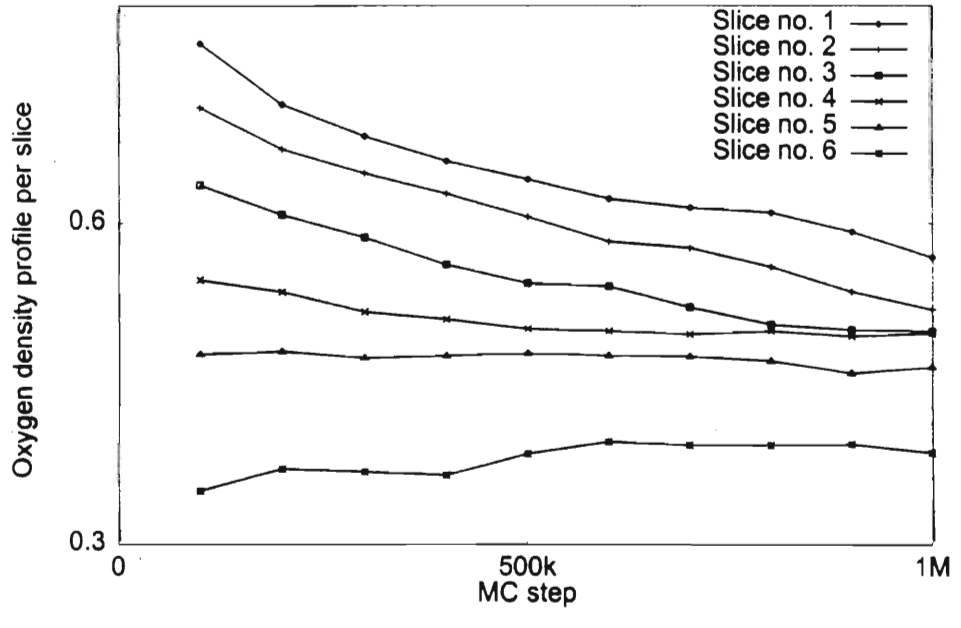

Figure 6(c). The oxygen density profile per slice against the MC step for x=0.8 and T=0.02eV. The lattice is 150x62.

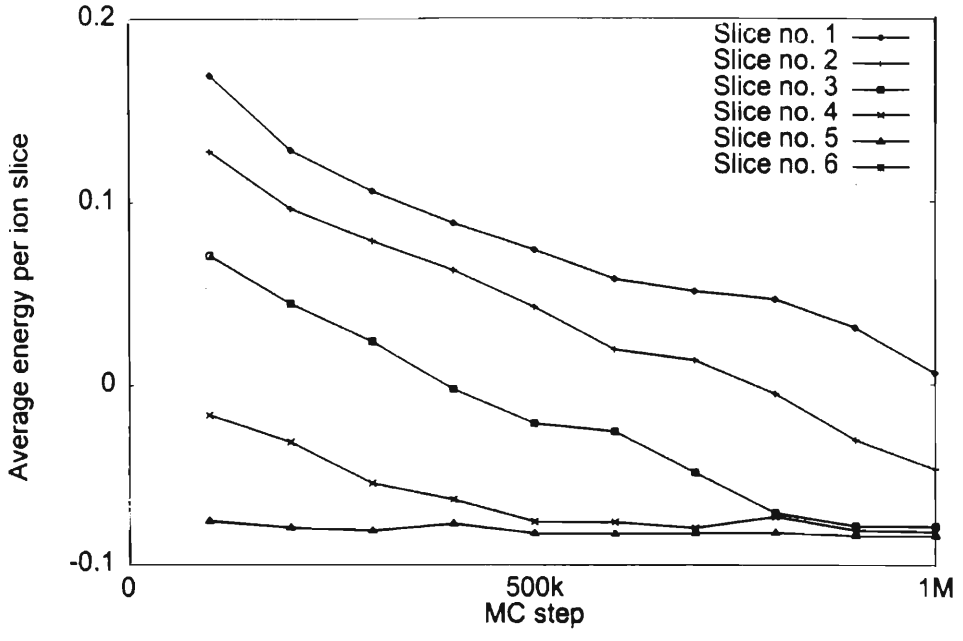

Figure 6(d). The average energy per oxygen ion per slice versus the number of MC steps for x=0.8 and T=0.02. The lattice is 150x62.

For x=0.8 the configurations tend towards the ordered orthorhombic phase (Figure 7(a)). After only 700k MC steps the oxygen ions are evenly distributed over the lattice (Figure.7(b)). However, individual ions at high concentrations have to travel a shorter empty distance across the lattice than for low concentration in a block start. The oxygen density profile per slice would have stabilized quickly around 0.5 from close to unity and from close to zero if plotted, and average energies per oxygen ion per slice would have converged to almost a similar value in all the slices.

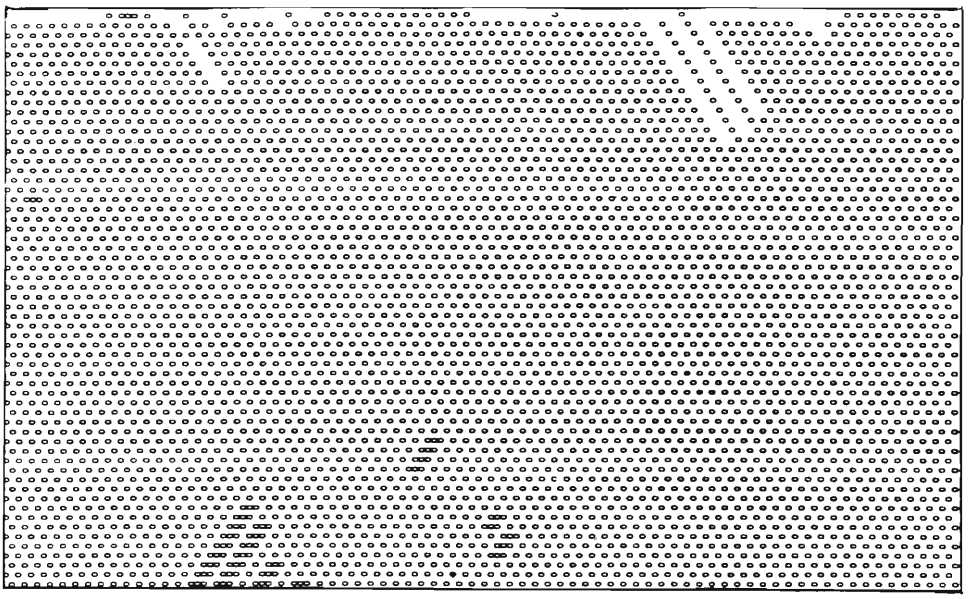

Figure 7(a). A lattice oxygen configuration obtained from a block start for x=1.0 and T=0.02eV after 700k MC steps . The lattice is 150x62.

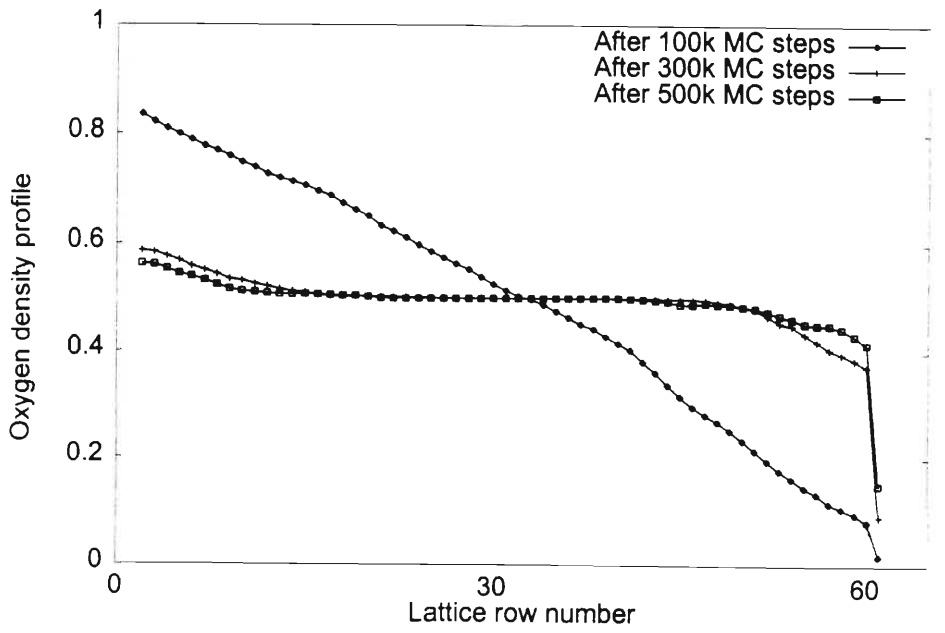

Figure 7(b). The oxygen density profile in the rows for x=1.0 and T=0.02eV. The lattice is 150x62.

When x is kept fixed and the temperature is increased, the inhomogeneity of the block disappears (Figure 8(a)). Initially the anisotropy in the orientation of the oxygen chains persists (see Figure 8 (a)(i)) and the phase is denoted H_{11}. At higher temperatures the anisotropy is diminished (see Figure 8(a)(ii)) and the phase is H_{10}, becoming H_0 at even higher temperatures (Figure 8 (a) (iii). The point at which the oxygen density profiles in the rows are equal for the various numbers of MC steps is again not as well defined as in low concentrations (see Figure 8 (b)). The variation of the oxygen density profile with lattice row number after equilibrating for 200k MC steps from a block start is similar to that obtained from a random start after 0.1k MC steps (compare Figures 2(a)and 2(b) with Figures 8(a)(i) and 8(b))even if the two lattices have different types of distribution. The oxygen density profile per slice shows clearly that the density of each slice converges to about 0.3 on stabilization, thus confirming a uniform distribution of oxygen ions (Figure 8(c)). The average energy per oxygen ion per slice is similar for each slice and is roughly constant after about 100k MC steps (Figure 8(d)).

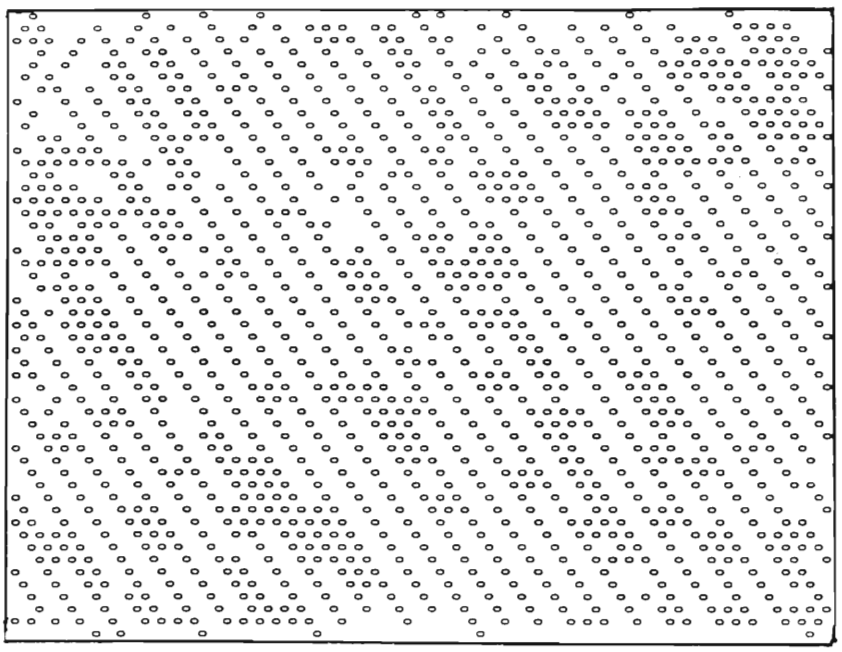

Figure 8(a)(i).A lattice oxygen configuration for x=0.6 and T=0.04eV obtained from a block start after 200k MC steps. The lattice is 100x52.

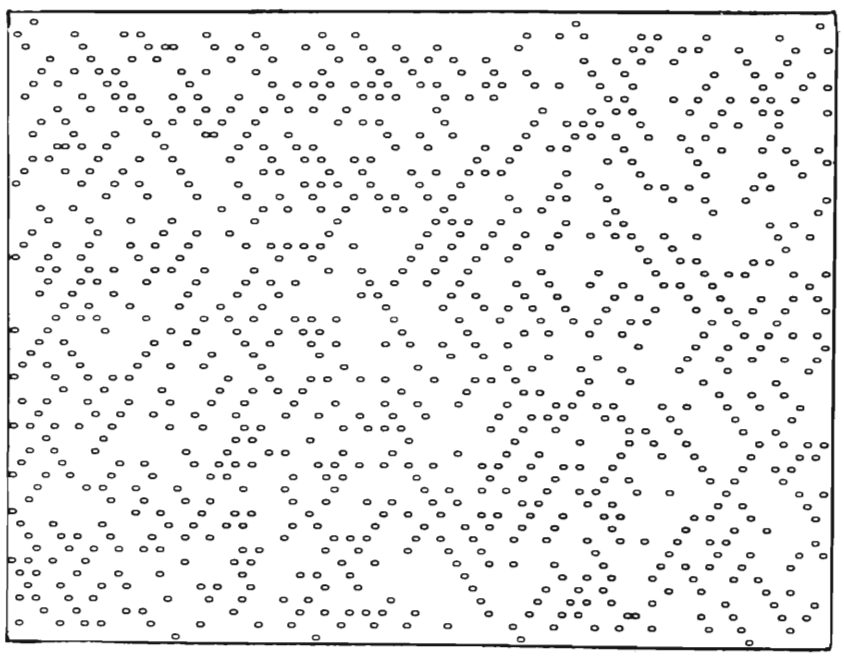

Figure 8(a)(ii). As in Figure 8(a)(i), but for x=0.4 and T=0.06eV.

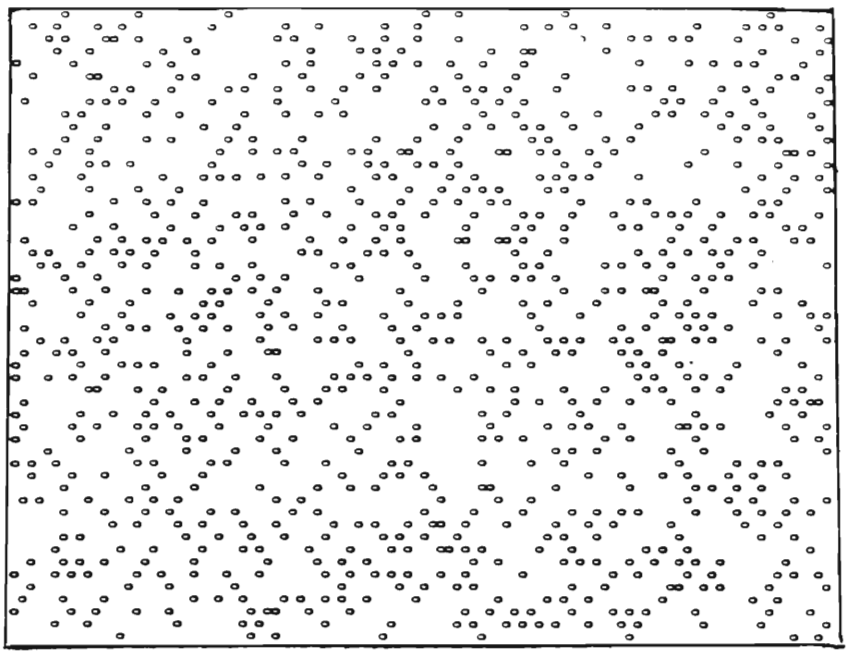

Figure 8(a)(iii). As in Figure 8(a)(ii), but for x=0.4 and *T*=0.10eV.

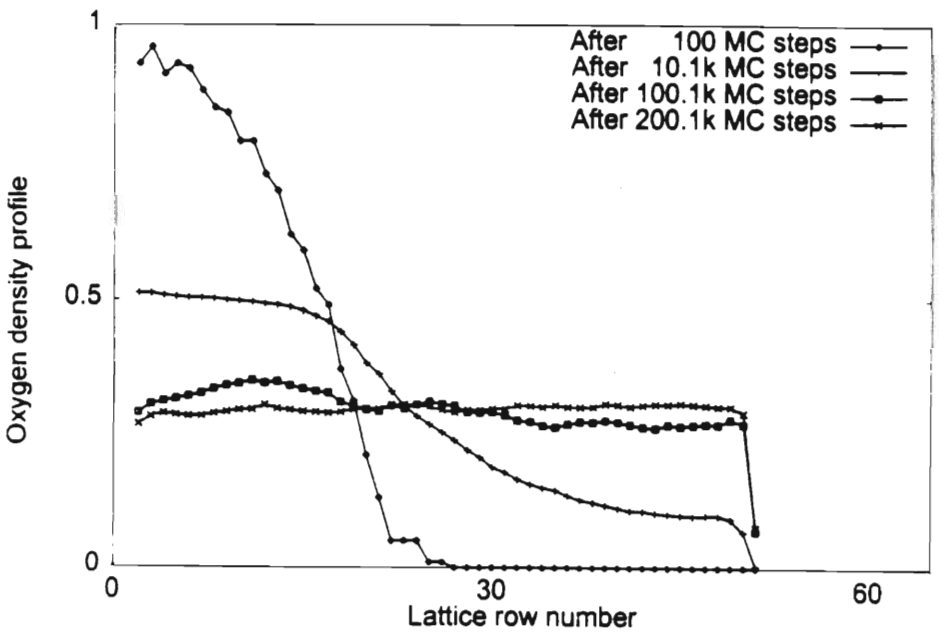

Figure 8(b). The oxygen density profile versus row number for x=0.6 and *T*=0.04eV. The lattice is 100x52.

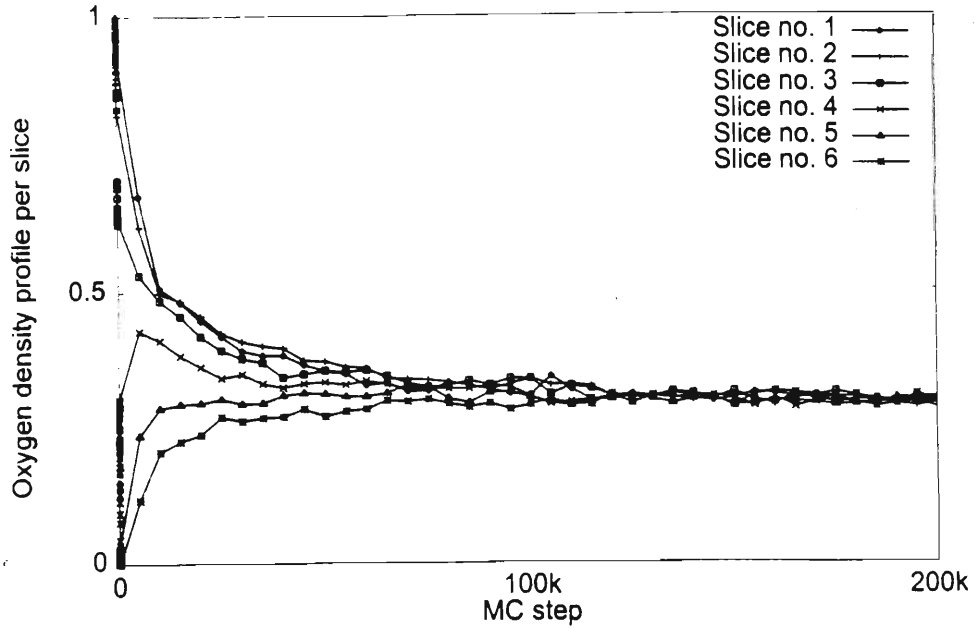

Figure 8(c). The oxygen density profile per slice versus the number of the MC steps for x=0.6 and *T*=0.04eV. The lattice is 100x52.

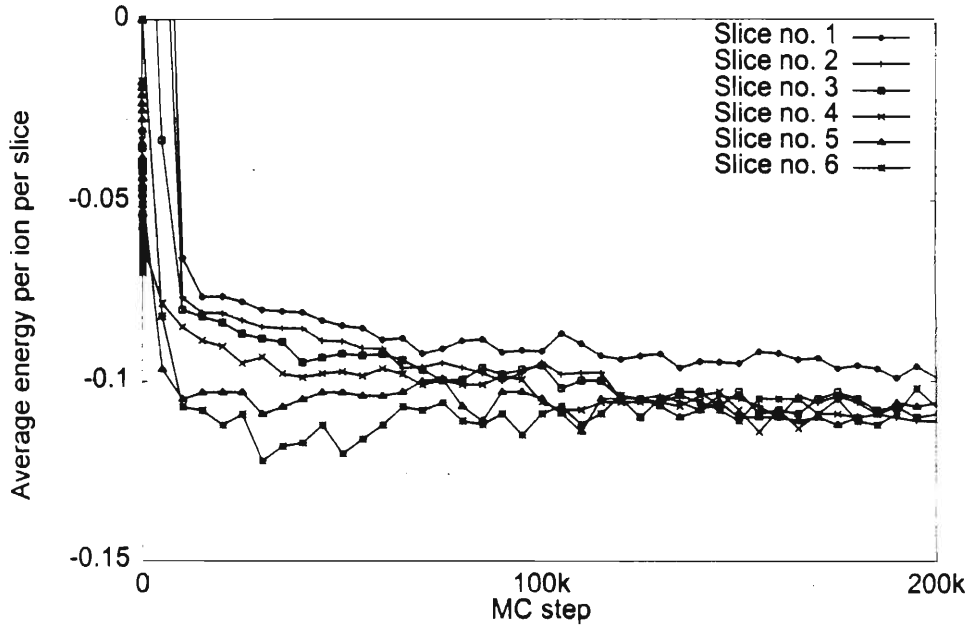

Figure 8(d). The average energy per oxygen ion per slice versus the number of the MC steps for x=0.6 and *T*=0.04. The lattice is 100x52.

It should be noted that the microstructures of the configurations reached from a block start at lower T values are anisotropic since one type of oxygen chain (say 0(1)) clearly dominates over the other (see Figure 8(a)(i)). The system can end up in either of the two ordered states with equal probability. A critical transition between the phases, H_{11} and H_{10}, is therefore expected.

It is clear that, in addition to known phases of the ASYNNNI model known (H_{10}, H_0 and the OrthoI phase) two more phases have been identified, namely H_{11} and I_{11}. The results for the model can be summarized in the schematic phase diagram shown in Figure 9. At high concentrations ($x \geq 0.8$) and low temperatures, the orthorhombic phase forms. A decrease in the concentration below 0.8 results in the phase I_{11} . Increasing the temperature for a fixed x destroys the inhomogeneity but not the anisotropy (see the phase H_{11} in Figure 9). As the temperature is increased further, the chains loose their preferred orientation and the phase becomes H_{10} in Figure 9. Further increase in the temperature completely destroys the chains and H_0 forms.

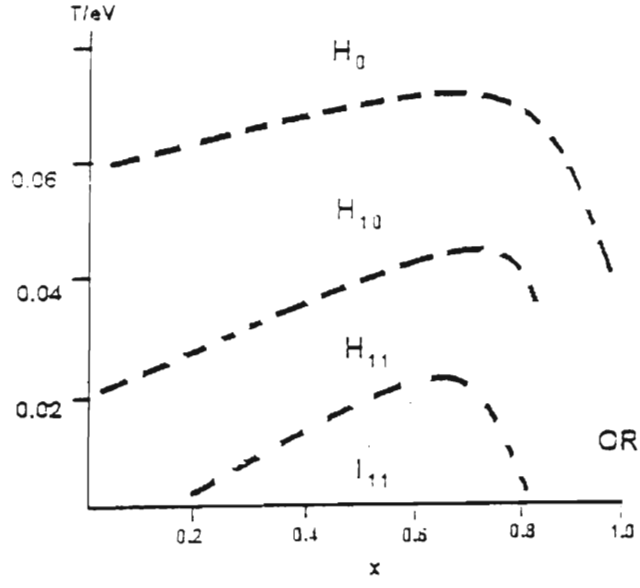

Figure 9. A schematic phase diagram for the ASYNNNI model. OR denotes the OrthoI phase, I_{11} denotes an inhomogeneous phase with preferentially ordered chains, H_{11} denotes a homogeneous phase with preferentially ordered chains. In H_0 the chains are not ordered. H_0 is a homogeneous phase without chains.

The fact that the configurations obtained from a block start remained inhomogeneous even after many MC steps ($2x10^6$) and seemed to be at equilibrium, indicate that such configurations are at least metastable. (It is clear from this chapter that after a certain number of MC steps the distribution of the oxygen atoms in the lattice obtained from a block start is not changing with an increase in the number of MC steps, and hence they are probably in equilibrium). These configurations may not correspond to the lowest free energy of the ASYNNNI model, but what is important is that they do exist. This is a new feature of the ASYNNNI model. The energy barriers between the homogeneous and inhomogeneous configurations and the differences of the energy minima were not investigated further.

We remark that the total energy of oxygen ions per slice after various MC steps (not shown here) revealed almost a similar information to the graphs of the average energy per ion per slice throughout the simulations.

CHAPTER 4

Tracer Diffusion Coefficients from Uniform and Nonuniform Equilibrium Configurations.

4.1 The Simulation Method

The tracer diffusion coefficients are defined through the time dependence of the mean square displacement of tagged ions (tracers) [4,64]. In Monte Carlo simulated self-diffusion time is measured as the number of attempted hops/moves of the oxygen ions in the lattice. If x is the displacement of a tracer in a particular direction for m Monte Carlo hops, then the corresponding tracer diffusion coefficient D_x^* is defined as,

$$D_x^* = \langle x^2 \rangle / 2m \qquad (4.1\text{-}1)$$

,where the averaging is over a large number of tracers in an ensemble of lattice configurations at equilibrium for a given value of the temperature T and concentration c.

The over-all tracer diffusion coefficient D^* is defined as,

$$D^* = 1/2(D_x^* + D_y^*)$$

,which is equivalent to,

$$D^* = \langle x^2 + y^2 \rangle / 4m \qquad (4.1\text{-}2)$$

For clarity it is important to differentiate between chemical diffusion coefficient D of oxygen in YBCO, which is usually measured by following the relaxation of some physical quantity (eg weight) as the sample gains up or losses oxygen and D^* usually measured by obtaining the mean-square displacement of the tracer [4]. Chemical diffusion is driven by the chemical potential gradient and D^* is largely depended on the temperature. The two types of diffusion are related to one another by the thermodynamic factor. The equations for D and D* are given in the Appendix.

In the present simulations the tracer diffusion coefficients were evaluated from the mean-square displacement of the tracer oxygen ions hopping to accessible NN and NNN sites in a sample of lattices from a canonical ensemble at a temperature *T* and oxygen concentration c. The duration in number of tracer attempted moves of the tracer walks was varied from m=3 to m=7. For each value of *T* and c the tracer diffusion coefficient D* was obtained as follows: the oxygen ions in a thermalised lattice were selected one by one as tracers and allowed to drift for a total of 7 MC steps while the other ions were kept fixed. The mean square displacement $\langle x^2 \rangle$ and $\langle y^2 \rangle$ were evaluated for different values of the walks durations, ie m=3,4,5,6,7, over a large number of tracers and decorrelated lattice configurations. The tracer diffusion coefficients D_x^* and D_y^* were obtained from the least-square linear fit of $\langle x^2 \rangle$ and $\langle y^2 \rangle$ as a function of m, the walk duration, and follows from expression 4.1-1. D* was then evaluated from expression 4.1-2.

The procedure for updating the lattice configurations is the same as in Chapter 3. The results reported here correspond to Q=0, where Q is the barrier for a jump to a next-to-nearest neighbour vacant site (It is not yet established whether the NNN jumps require more energy than the NN ones [9]). For conformity of

the algorithm with the detailed balance condition, destinations for the jumps were chosen uniformly from all the available vacant sites in the vicinity of a given oxygen ion. Since the quality of the sample is of crucial importance for the reliability of the results, it was ensured that the sample contains lattices which are at equilibrium for the chosen values of T and c, and that correlations between the members of the sample are minimised. Ideally, each member of the sample should be produced as the end-point of a separate Markovian process starting from significantly different initial configurations. Because this turns out to be prohibitively expensive in terms of computer time, one has to settle for a sample of reasonable quality. Usually only one process is generated and after allowing it to equilibrate (after a certain number of the MC steps) it is assumed that the process has converged to a configuration belonging to the ensemble, as discussed in Chapter 2. At this stage one can either count each consecutive lattice configuration as a member of the sample and use it for evaluating the statistical averages of the observable or decide to skip a number of MC steps before including a configuration in the sample thus reducing the correlations between the lattices. In these simulations the Metropolis acceptance rate was monitored and according to its current value the number of decorrelation steps was set (typically $\approx$100 MC steps). If the space of all the lattice configurations in equilibrium with a reservoir at a temperature T and corresponding to a given concentration c consist of subsets separated by energy barriers, then it may occur that the Markovian process is trapped in one of these subsets and the rest of the ensemble remains "invisible". This can be avoided by repeating the simulations for several different choices of the initial configuration; such repeated simulations are expected to yield similar results. The tracer diffusion coefficient and the oxygen density were monitored for approach to their respective equilibrium values.

The tracer diffusion coefficients were evaluated for the nonuniform equilibrium configurations obtained from a block start, which were described in the previous chapter. In order to detect any local dependence of the observables in these nonuniform configurations, the lattice was divided into a number of slices. For each slice the corresponding values of the tracer diffusion coefficient D^* and the density ρ were measured. The local densities (the oxygen density profiles per slice) were used, after normalization, as weights for evaluating the global tracer diffusion coefficients from the corresponding values in the slices.

From the last chapter it is clear that the free energy of the ASYNNNI model possesses multi-minima and that, as a consequence, nonuniform equilibrium configurations of the oxygen ions can occur, in addition to the uniform equilibrium configurations for the same values of T and c. In the present chapter, the effect of this property of the ASYNNNI model on D^* is investigated.

4.2 Comparison of Tracer Diffusion Coefficients from Nonuniform and Uniform Configurations.

The inhomogeneous oxygen distribution observed at low temperatures (≈0.02eV) were found for values of x between 0.4 and 0.6 (Chapter 3). The local values of D^* for T=0.02eV and various concentrations are shown in Figure 1(a) after 200k MC steps. The corresponding oxygen densities per slice are shown in Figure 1(b). The local values of D^* in Figure 1(a) exhibit considerable fluctuations due to a low temperature, as well as the low number of oxygen ions in the slices. The corresponding local oxygen densities have lesser fluctuations (Figure 1(b)).

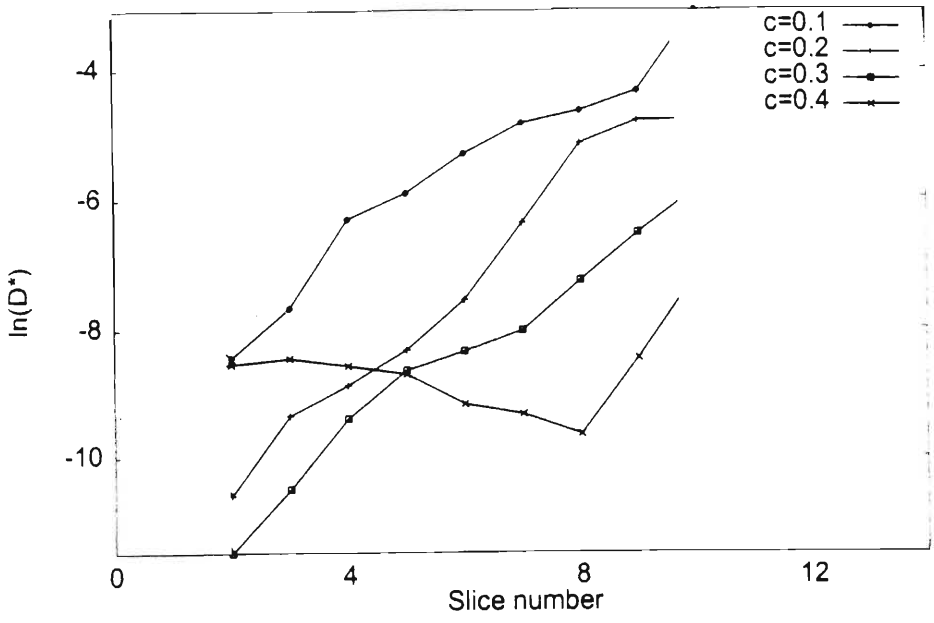

Figure 1(a).The tracer diffusion coefficients in various lattice slices for a nonuniform equilibrium oxygen configuration (obtained from a block start after 200k MC steps) at T=0.02eV, and for various concentrations of oxygen. The lattice is 100x52.

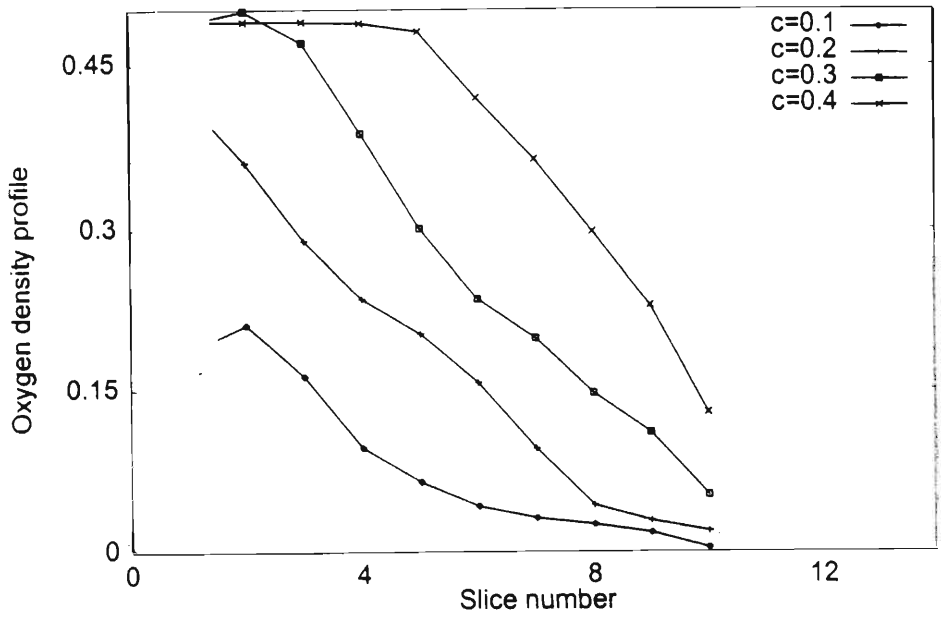

Figure 1(b).The oxygen density profiles in the various lattice slices for a nonuniform equilibrium oxygen configuration (obtained from a block start after 200k MC step) at T=0.02eV, and for various concentrations of oxygen. The lattice is 100x52.

It is clear from Figure 1 that the values of D^* are largest where ρ is smallest. In general, an increase in concentration decreases D^*. The simulations show that D^* is inversely proportional to ρ and c, which points to a concentration dependent D^*. In Figure 1(b) at some point ρ is the same for c=0.3 and c=0.4 (for low slice numbers) but the corresponding D^* values are not the same, indicating that the increase in D^* is possibly due to ordering of oxygen ions for c=0.4. This effect has also been observed (both in the simulations and in the experiments) at low T and close to c=0.5 [9,55,56] and attributed both to ordering and interstitial diffusion.

As the temperature is increased the local dependence of tracer diffusion coefficient throughout the lattice decreases (Figures 2(a) and 3(a)), since the oxygen density in the slices tends to be homogeneous (Figures 2(b) and 3(b)) throughout the lattice. The fluctuations are also minimised. Clearly, when the concentration is low, $\ln(D^*)$ is high.

The values of $\ln(D^*)$ for T=0.04 eV and c=0.3 and 0.4 are surprisingly almost the same in Figure 2(a). The dependence of D^* on the oxygen concentration seems to decrease with increasing the temperature (Figure 3(a)). In general $\ln(D^*)$ increases with T, ie the oxygen mobility is enhanced by the rise in temperature. Since the oxygen ions are disordered into O(5) sites at high temperatures, they must have moved to O(5) sites either through path O(1)-O(1)-O(5) or O(1)-O(5) or some other path. However, at the low temperatures the ions probably follow the path O(1)-O(5)-O(1), since the O(5) sites are empty.

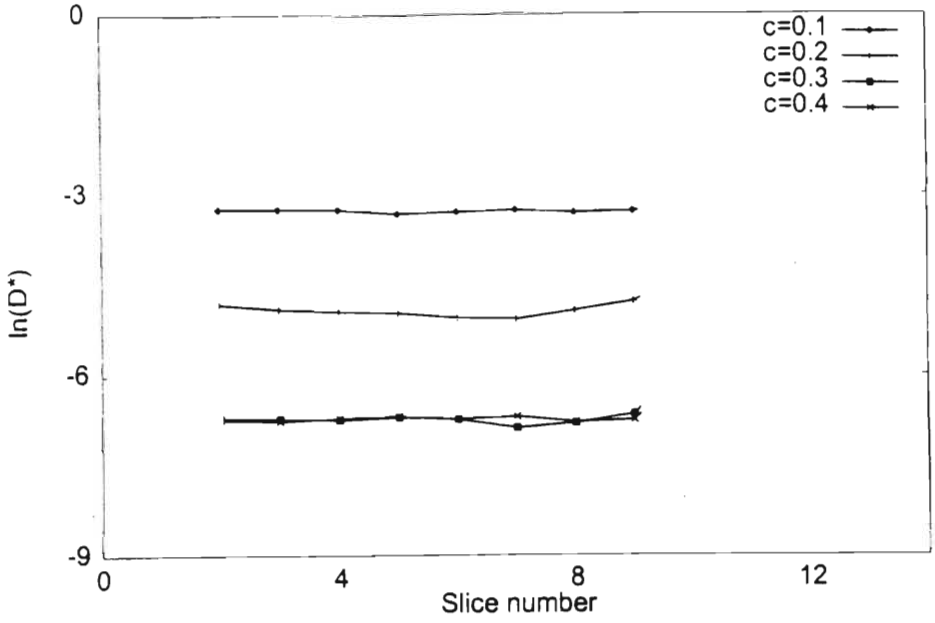

Figure 2(a). The tracer diffusion coefficients in the various lattice slices for a nonuniform equilibrium oxygen configuration (obtained from a block start after 200k MC steps) at T=0.04eV, and for various concentrations of oxygen. The lattice is 100x52.

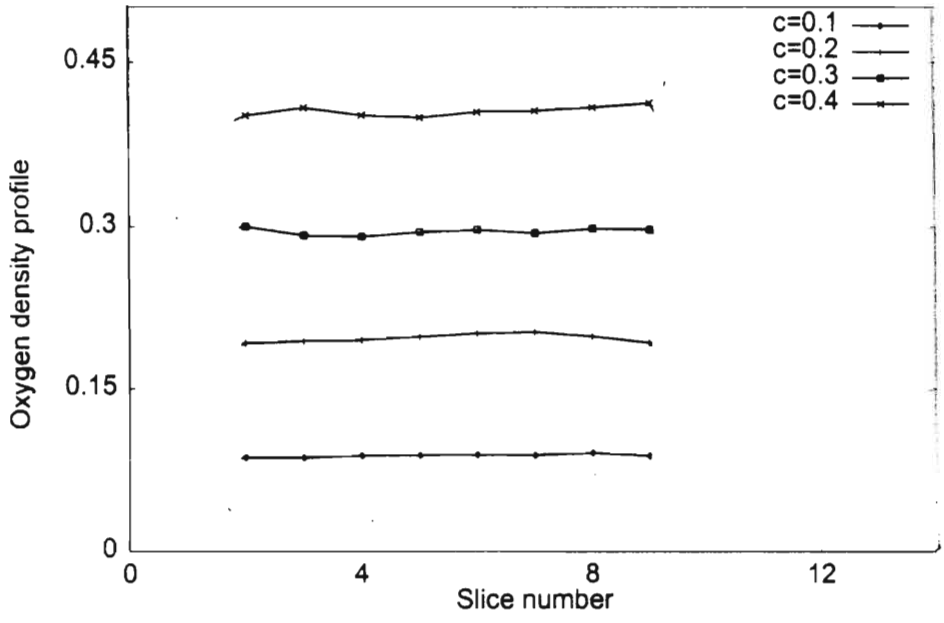

Figure 2 (b). The oxygen density profiles in the various lattice slices for a nonuniform equilibrium oxygen configuration (obtained from a block start after 200k MC step) at T=0.04eV, and for various concentrations of oxygen. The lattice is 100x52.

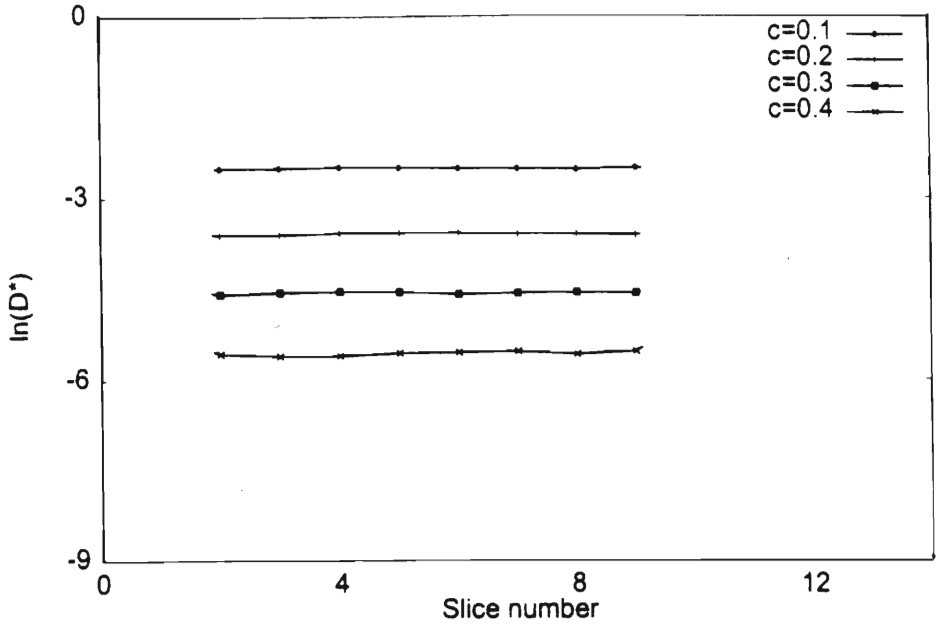

Figure 3(a). The tracer diffusion coefficients in the various lattice slices for a nonuniform equilibrium oxygen configuration (obtained from a block start after 200k MC steps) at T=0.06eV, and various concentrations of oxygen. The lattice is 100x52.

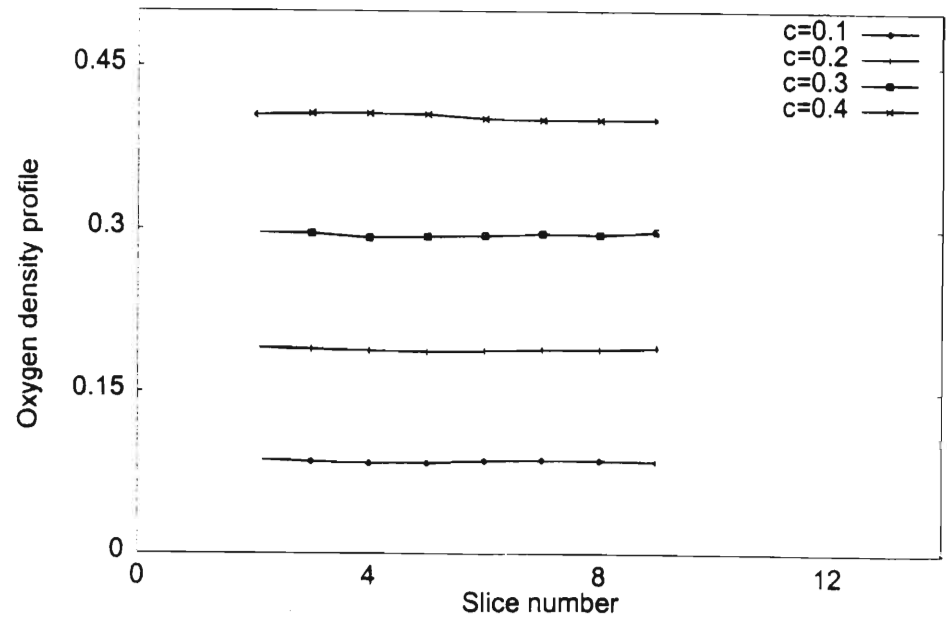

Figure 3(b). The oxygen density profiles in the various lattice slices for a nonuniform equilibrium oxygen configuration (obtained from a block start after 200k MC step) at T=0.06eV, and for various concentrations of oxygen. The lattice is 100x52.

When the local values of D^* in the slices were summed up with the corresponding statistical weights as obtained from the local oxygen density distribution, the values which are only slightly different from the corresponding results obtained by simulating the model from a completely random initial configuration were obtained. The difference is noticeable only for the lowest temperature studied (T=0.02eV). The global values for the tracer diffusion coefficients obtained from a block start at T=0.02 eV together with published results in Ref.9, for a random start, are shown in Figure 4. It is evident that the nonuniform equilibrium configurations do not result in the tracer diffusion coefficients that are very different from those for the uniform equilibrium configurations. It was found that, as the temperature is increased, this slight difference between the tracer diffusion coefficients measured by the MC simulations from the different initial configurations disappears. This is expected since the lattice configurations from the random and the block starts at high temperatures are similar to each other.

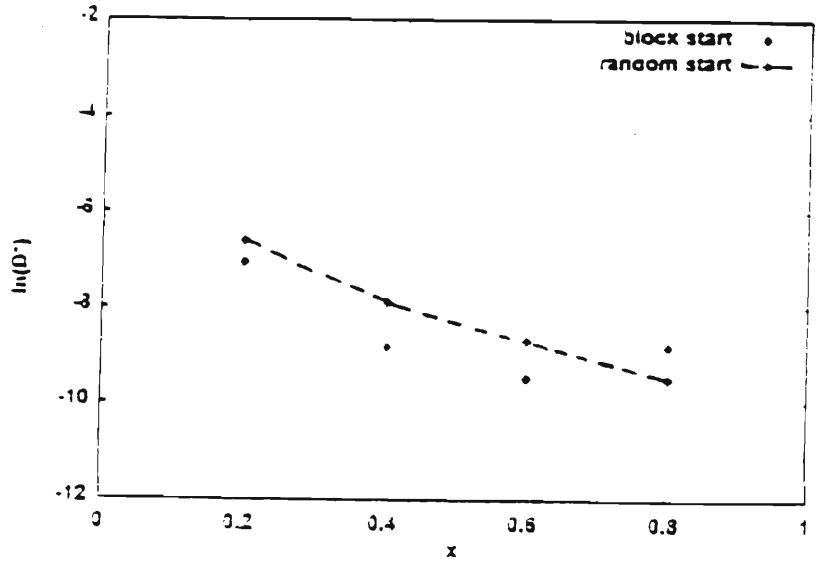

Figure 4.The tracer diffusion coefficients for a block start and for T=0.02eV compared with those from a random start from Ref.9.

4.3 Summary and Conclusion

In summary, a two-dimensional lattice gas ASYNNNI model was employed to study the tracer diffusion coefficients for oxygen in the basal plane of YBCO. A different type of initial configuration (other than the random and the uniform starts considered by the previous workers), was used to obtain the equilibrium configurations, which might yield a concentration independent D^* value. However, the inhomogeneous equilibrium configurations obtained did not produce a concentration independent D^*. An important aspect of the ASYNNNI model was discovered, namely that its free energy possesses multi-minima as revealed by the occurrence of the stable homogeneous and inhomogeneous configurations for the same values of T and c. The nonuniform equilibrium configurations have interesting features which merit further investigation as mentioned in pages 63 and 64.

It was expected that the tracer diffusion coefficients calculated from the nonuniform equilibrium configurations will be different from those calculated for the uniform equilibrium configurations, since the ordering in the two types of configurations is completely different. As this was not the case, it therefore means that the different structural phases observed in the ASYNNNI model in Chapter 3 are not characterised by different values of the tracer diffusion coefficients. A possible explanation of this fact could be that the difference between the configurations reached from random and block starts is in the long-range ordering with little effect on the individual mobility of the oxygen ions.

In principle, a weak dependence of the tracer diffusion coefficients on the oxygen concentration should follow from any

realistic model of the self-diffusion in YBCO. Therefore, the incorrect D^* results thus far reported, casts doubt on the reliability of the ASYNNNI model or the way it has been exploited. It is evident that the model cannot even account qualitatively for the oxygen concentration dependency of D* in the basal plane. It is then worthwhile to attempt other modifications and/or analyse assumptions made in the model.

One possible modification is to simulate the micro-canonical ensemble for the same system, thereby departing completely from the simple application of the Metropolis algorithm. The fact that there are homogeneous and inhomogeneous equilibrium configurations corresponding to a particular value of T and c (indicating that more than one minima correspond to a single temperature T) indicates that such an approach could lead to different results for D^*, since in the micro-canonical ensemble the energy is fixed and the temperature is varied until it corresponds to the chosen energy.

In the ASYNNNI model the atomic relaxations, and hence lattice distortions, have thus far been neglected. It is assumed that the possible relaxations of the surrounding atoms due to the tracer motion does not affect D* of the tracer itself. Though it is known that the lattice constants in the a- and b- directions do change as the YBCO goes through various phases, this has been neglected in the model. It is interesting to note that in the Ortho phase the lattice constant in the b-direction is slightly greater than in the a-direction but the diffusion is greater in the b-direction than in the a-direction. In general, however, another refinement to the model could be to account for the atomic relaxations and see how much the lattice distortions affect the EPI's and consequently the probability for a jump to be taken.

It has also been assumed that the interactions between the oxygen atoms is confined to only two nearest oxygen atoms, ie only pair interactions are considered. In reality, it is the many-body interactions (beyond two) that actually exist in real crystals. It is the success of the Ising model using the pair effective interactions in reproducing some experimentally observed features of the YBCO, in particular the ordering of atoms, that has also motivated the choice of this model in studying the tracer diffusion coefficient. It could be that for studying diffusion in YBCO three-body interactions or even four-body interactions are necessary in the calculations.

The difficulty in obtaining the reliable experimental data for both the chemical and the tracer diffusion coefficients and a lack of computer simulations have impeded a quicker progress in elucidating the exact atomic diffusion mechanism of the oxygen atoms. The data from the experiments and the models can, together be used to formulate important concepts and principles that can be used in the eventual formulation of a theory of oxygen diffusion in this material.

REFERENCES

[1] A.S. ILCHEV, O.L. DE LANGE, AND S. GUMEDE, *Phase Structure in the ASYNNNI model for the self-diffusion of Oxygen in 123YBCO*, in Chemistry and Technology of High-Temperature and Related Advanced Materials, ed. G van Tendeloo (Kluwer, Dordrecht) in press.

[2] A.S. ILCHEV, O.L. DE LANGE, AND S. GUMEDE, *Tracer Diffusion of Oxygen in 123YBCO from Monte Carlo Simulations of the ASYNNNI model*, in Chemistry and Technology of High-Temperature and Related Advanced Materials, ed. G van Tendeloo (Kluwer, Dordrecht) in press.

[3] X.M. XIE, T.G. CHEN, AND Z.L. WU, *Phys. Rev. B* **40**, 4549 (1989).

[4] S.J. ROTHMAN, J.L. ROUTBORT, AND J.E. BAKER, *Phys. Rev. B* **40**, 8852 (1989).

[5] J.L. ROUTBORT AND S.J. ROTHMAN, *J. Appl. Phys.* **76**, 5615 (1994).

[6] K.N.TU, N.C. YEH, S.I.PARK, AND C.C.TSUEI, *Phys. Rev. B.* **39**, 304 (1989).

[7] L.T. WILLE, *Phys. Rev. B* **40**, 6931 (1989).

[8] L.T. WILLE, A.BERERA AND D. de FONTAINE, *Phys. Rev. Lett.* **60**, 1065 (1988).

[9] M. AUSLOOS AND A.PEKALSKI, *Phys. Rev. B* **52**,4577 (1995).

[10] P.J. FORD AND G.A SAUNDERS, *Contemp.Phys.* **38**,63(1997).

[11] R. de BRUYN OUBOTER, *Sci. Am.* **276**, March 84 (1997).

[12] D. SHOENBERG. *Superconductivity*. (Cambridge University Press, 1965).

[13] G. BURNS. *High-Temperature Superconductivity-An introduction*.(Harcourt Brace Jovanovich,1992).

[14] E.A. LYNTON. *Superconductivity*. (Spottiswoode, Ballantyne & Co Ltd,London,1962).

[15] J.R. CHRISTMAN. *Fundamentals Of Solid State Physics.* (John Wiley & Sons, 1988).

[16] S.CHU, C.COHEN-TANNOUDJI, AND W.D. PHILLIPS, *Sci. Am.* **278,** January 8(1998).

[17] C.G. KUPER. *An introduction To Theory of Superconductivity.*(Claredon Press Oxford,1968).

[18] A.C. ROSE-INNES AND E.H.RHODERICK. *Introduction To Superconductivity.* (Pergamon,1980).

[19] D. SAINT-JAMES, G.SARMA AND E.J. THOMAS. *Type II Superconductivity.* (Pergamon, 1969).

[20] M. TINKHAM. *Introduction To Superconductivity.* (McGraw-Hill,(1975).

[21] V.Z. KRESIN AND S.A.WOLF. *Fundamentals Of Superconductivity.* (Plenum Press, New York,1992).

[22] G. VIDALI. *Superconductivity-The next revolution?* (Cambridge University, 1993).

[23] J.R. KIRTLEY AND C.C. TSUEI, *Sci. Am.* **275**, August 50 (1996).

[24] G.W. CRABTREE AND D.R. NELSON, Phys. Today **50**, April 38 (1997).

[25] E.D. SPECHT, C.J. SPARKS, A.G. DHERE, J. BRYNESTAD, O.B. CAVIN, D.M. KROEGER, AND H.A. OYE, *Phys. Rev.B* **7**,7426 (1988).

[26] L.T. WILLE AND D. de FONTAINE, *Phys. Rev. B* **37**, 2227 (1988).

[27] E. SALOMONS, N. KOEMAN, R. BROUWER, D.G. de GROOT AND R. GRIESSEN, *Solid State Commun.* **64**, 1141 (1987).

[28] S.J. ROTHMAN, J.L. ROUTBORT, U. WELP, AND J.E. BAKER, *Phys. Rev. B* **44**, 2326 (1991).

[29] J.D. JORGENSEN, M.A. BENO, D.G. HINKS, L.SODERHOLM, K.J.VOLIN, R.L. HITTERMAN, J.D. GRACE, IVAN K. SCHULLER, C.U. SEGRE, K. ZHANG AND M.S. KLEEFISCH, *Phys. Rev. B* **36**, 3608 (1987).

[30] J.M. BELL, *Phys. Rev. B* **37**, 541 (1988).

[31] A.BERERA AND D. de FONTAINE, *Phys. Rev. B* **39**, 6727 (1989).

[32] W.R. McKINNON, M.L. POST, L.S. SELWYN, G. PLEIZIER, J.M. TARASCON, P.BARBOUX, L.H. GREENE, AND G.W. HULL, *Phys. Rev. B* **38**, 6543 (1988).

[33] J.M. SANCHEZ, F. MEJíA-LIRA AND MORAN-LÓPEZ, *Phys. Rev. B* **37**, 3678 (1988).

[34] S.G. BRUSH, *Rev. Of Mod. Phys.* **39**, 883 (1967).

[35] E.SALOMONS AND D. de FONTAINE, *Phys.Rev.B* **41**, 11 159 (1990).

[36] G. CEDER, M. ASTA, W.C. CARTER, M. KRAITCHMAN, D. de FONTAINE, M.E. MANN AND M.SLUITER, *Phys. Rev. B*, **41**, 8698 (1990).

[37] A.BERERA, L.T. WILLE, AND D. De FONTAINE, *Physica C* ***153-155***, 598 (1988).

[38] G.E. MURCH, *Phil. Mag. A* **41**, 701 (1980).

[39] A.PEKALSKI AND M. AUSLOOS, *Physica C* **226**, 188 (1994).

[40] H.BAKKER, J.P.A.WESTERVELD, D.M.R.LO CASCIO AND D.O.WELCH, *Physica C* **157**, 25 (1989).

[41] J. CHOI, M. SARIKAYA, I.A. AKSAY, AND R.KIKUCHI, *Phys. Rev.B* **42**, 4244 (1990).

[42] A. BERERA, L.T. WILLE, AND D. de FONTAINE, *J. Stat. Phys.* **50**,1245 (1988).

[43] A.G. KHACHATURYAN, SV SEMENOVSKAYA, AND J.W. MORRIS,Jr., *Phys. Rev. B* **37**, 2243 (1988).

[44] A.G. KHACHATURYAN AND J.W. MORRIS,Jr., *Phys. Rev. Lett.* **59**, 2776 (1987).

[45] S.SEMENOVSKAYA AND A.G. KHACHATURYAN, *Phys. Rev. B* **46**,6511 (1992).

[46] J.MAIER AND H.L. TULLER, *Phys. Rev. B* **47**, 8105 (1993).

[47] H. BAKKER, D.O. WELCH, AND O.W. LARARETH,Jr., *Solid State Commun.* **64**, 237 (1987).

[48] J.L. TALLON, *Phys. Rev. B.* **39**, 2784 (1989).

[49] H.SHAKED, J.D.JORGENSEN, J.FABER,Jr., D.G. HINKS, AND B. DABROWSKI, *Phys. Rev. B* **39**, 7363 (1989).

[50] D.de FONTAINE, L.T.WILLE, AND S.C. MOSS, *Phys. Rev. B* **36**, 5709 (1987).

[51] R.C. BAETZOLD, *Phys. Rev. B*, **42**, 56 (1990).

[52] X.ZHANG AND C.R.A. CATLOW, *Phys. Rev. B* **46**, 457 (1992).

[53] G.GANNELLI, R.CANTELLI, F. CORDERO, M.FERRETTI, AND L.VERDINI, *Phys. Rev. B* **42**, 7925 (1990).

[54] J.L.TALLON AND M.P.STAINES, *J. Appl. Phys.* **68**, 3998 (1990).

[55] J.R. LAGRAFF AND D.A.PAYNE, *Physica C* **212**, 470 (1993).

[56] Y.IKUMA AND S.AKIYOSHI, *J. Appl. Phys.* **64**, 3915 (1988).

[57] P.SINGH, M.N. NYAYATE, S.H. DEVARE, AND H.G. DEVARE, *Phys. Rev. B.* **39**, 2308 (1989).

[58] HAMMERSLEY J.M. AND D.C. HANDSCOMB. *Monte Carlo Methods* (Fletcher & Son, Norwich,1964).

[59] G.S. FISHMAN *Monte Carlo: Concepts, Algorithms, and Applications* (Springer-Verlag, New York, 1996).

[60] P.K. MACKEOWN AND D.J. NEWMAN. *Computational Techniques in Physics* (Adam Hilger, Bristol, 1987).

[61] M. CREUTZ. *Quarks, Gluons, and Lattices* (University Press, Cambridge, 1985).

[62] J.M. YEOMANS. *Statistical Mechanics of Phase Transitions* (Oxford University, New York, 1992).

[63] R. ZORN, H.J. HERRMANN, C.PEBBI, *Comp. Phys. Comm.* **23**, 337 (1981).

[64] L.F. PERONDI AND P.M. BINDER, *Phys. Rev. B* **47**, 14 221 (1993).

Appendix

A. THE GENERAL STRUCTURE OF THE PROGRAMME FOR SIMULATING OXYGEN DIFFUSION IN YBCO

The programme was divided into three parts: initialisation of the lattice, thermalisation of the lattice, and statistical evaluation of D* from an ensemble of decorrelated lattice configurations. The flow diagram showing the three parts in some details is given in the flow diagram on pages 97-99. The flow diagram for the structure of one MC step/iteration/sweep is shown on page 100.

The flow diagram showing the general structure of the programme that was used to calculate D*:

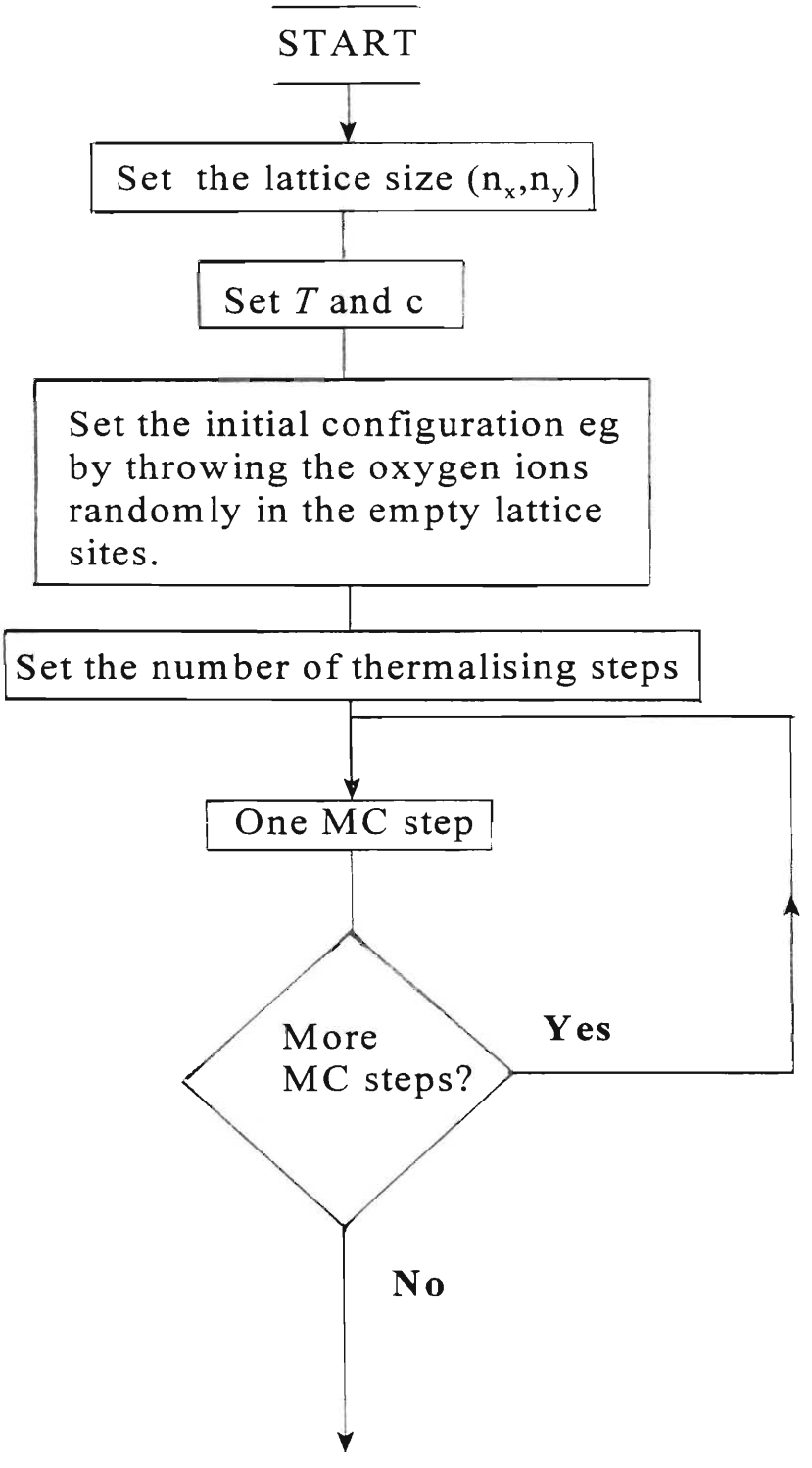

(To page 98)

(From page 97)

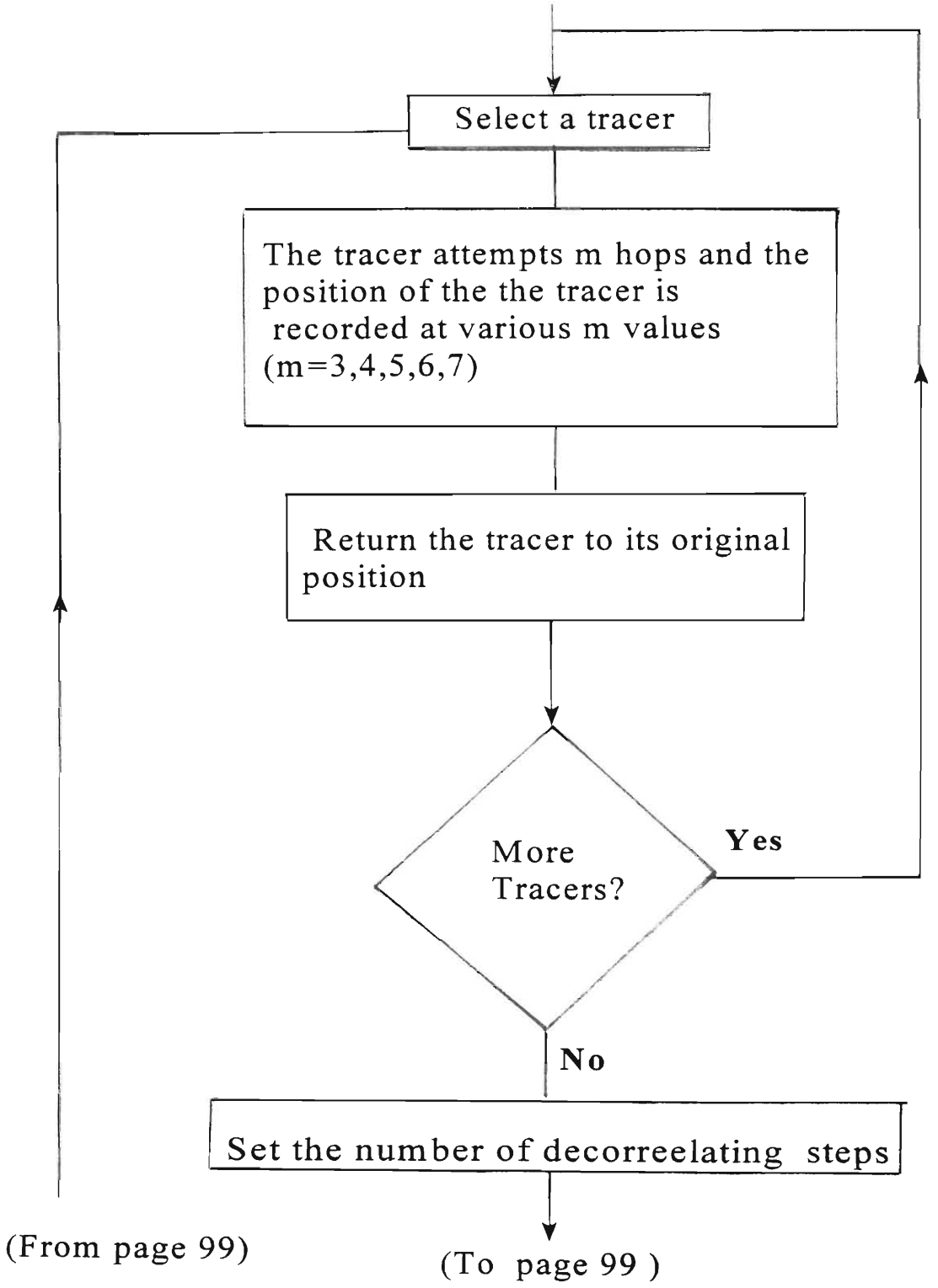

(From page 99)

(To page 99)

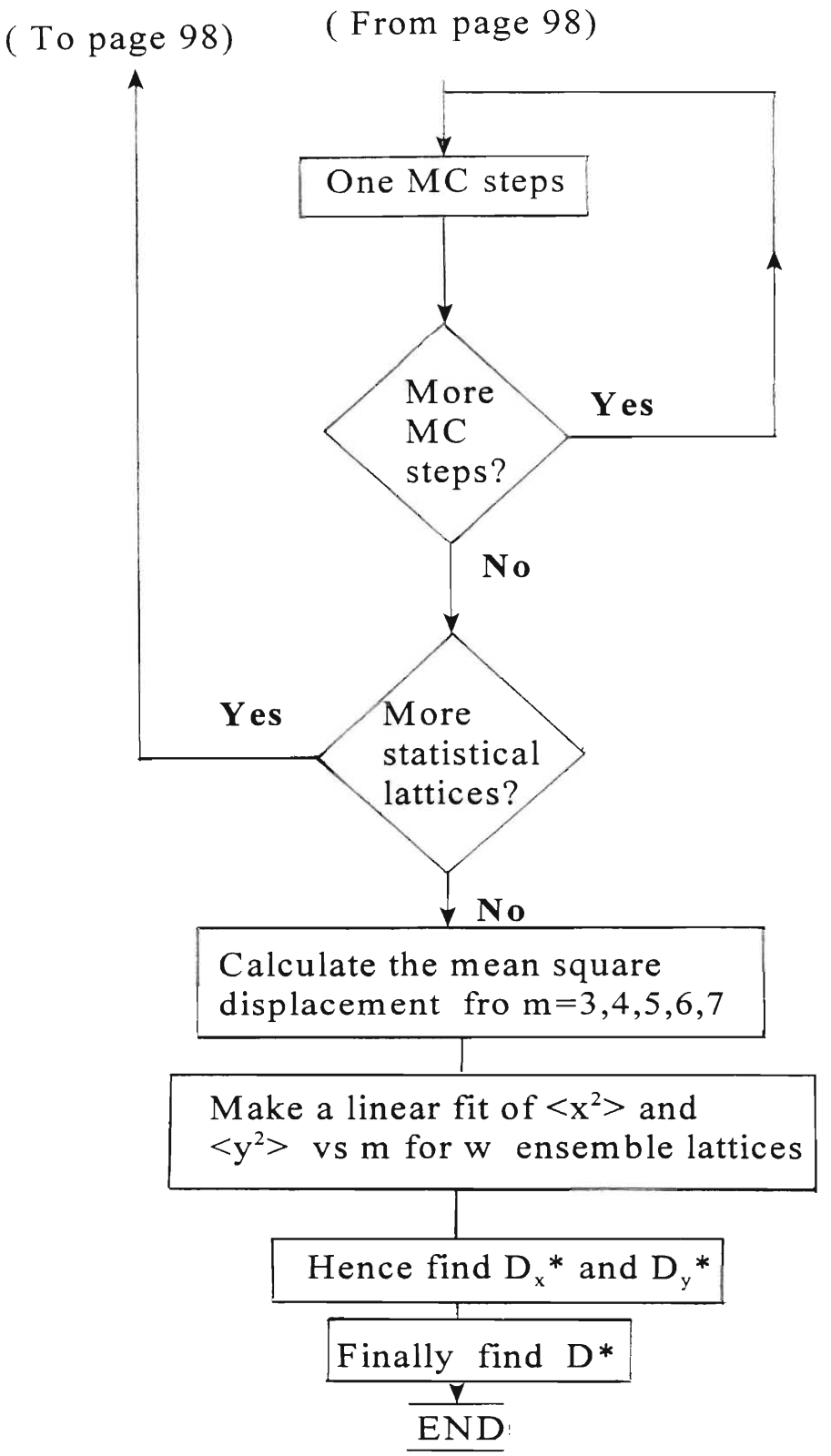
(To page 98)
(From page 98)
One MC steps
More MC steps?
Yes
No
More statistical lattices?
Yes
No
Calculate the mean square displacement fro m=3,4,5,6,7
Make a linear fit of <x²> and <y²> vs m for w ensemble lattices
Hence find Dx* and Dy*
Finally find D*
END

The flow diagram showing the structure of one MC step/iteration/sweep:

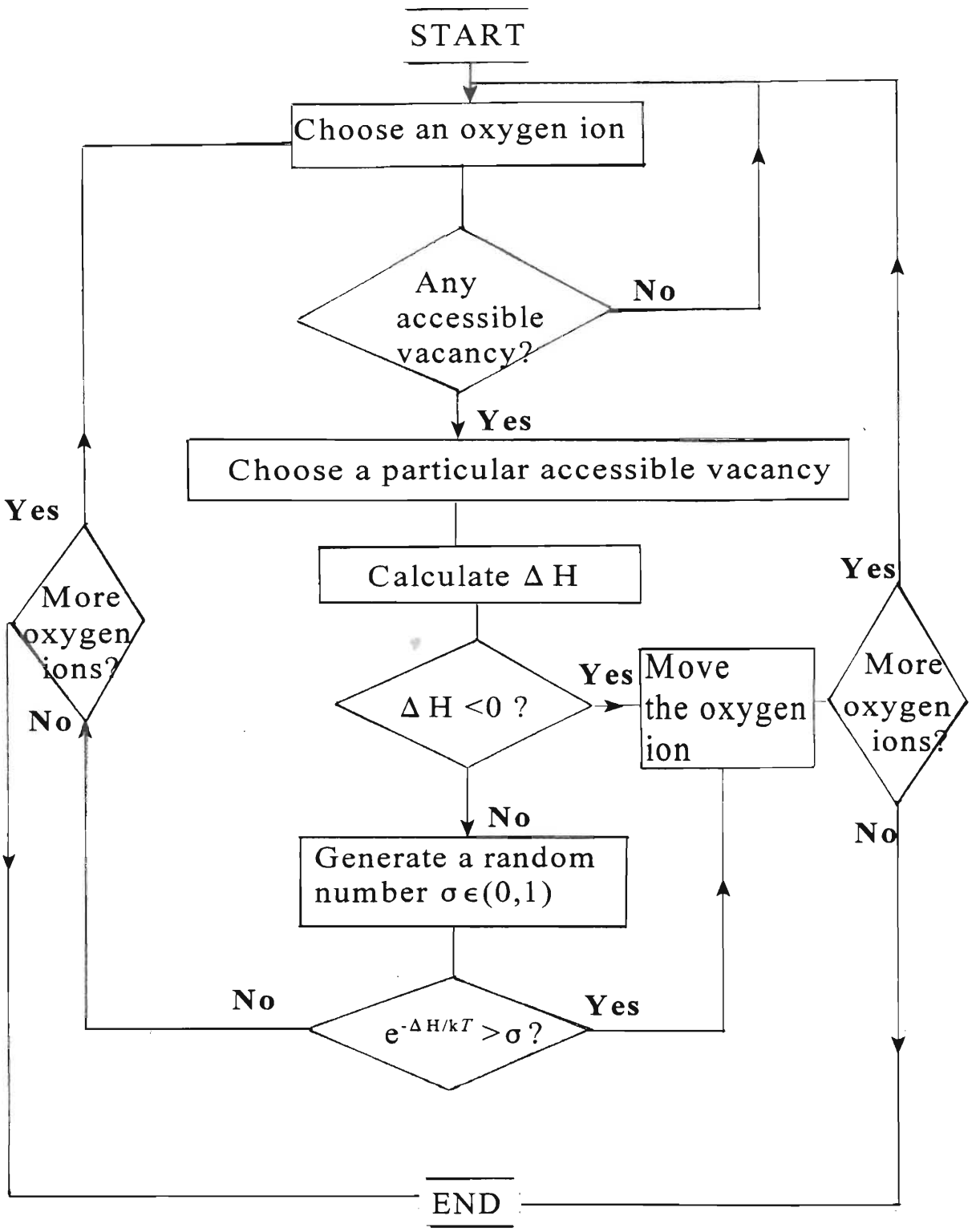

B. THE MAIN SUBROUTINES OF THE FORTRAN90 PROGRAMME FOR SIMULATING OXYGEN DIFFUSION IN YBCO

There are five subroutines shown here and one function. This represents a small but important part of the whole programme used. The first subroutine, *setlat*, allocated memory for the main lattice arrays. The second, *col_scol*, transformed general lattice coordinates into sliced lattice coordinates. This was done in order to accommodate large lattices. The function used, calculated the energy associated with a particular oxygen ion in a given lattice configuration. The third subroutine, *deltae*, evaluated the change of energy associated with the move of a given oxygen ion to an accessible vacancy. *Metrostep*, determined whether a single jump of an oxygen ion to an accessible vacancy should be accepted or not. Once the jump was accepted, *hop*, actually moved the oxygen ion to a vacancy.

```
subroutine setlat(nc,nr)
implicit none
integer,intent(in)::nc,nr
ncol=nc
nrow=nr
mcol=ncol-1
mrow=nrow-1
nsl=int(ncol/mbits)+1
allocate(blatt(nsl,0:mrow))
allocate(envir(0:mcol,0:mrow,-1:1,-1:1))
cshft(-1,:)=-1
cshft(0,:)=
cshft(1,:) =1
rshft(:,-1)=-1
rshft(:,0)=0
rshft(:,1)=1
return
end subroutine setlat
```

```
subroutine col slcol(kc,ls,lc)
implicit none
integer,intent(in)::kc
integer,intent(out)::lc,ls
ls=int(kc/mbits)+1
lc=mod(kc,mbits)
return
end subroutine col-slcol

function energy(ic,ir) result(e)
implicit none
integer,intent(in)::ic,ir
real::e
real::sumnn,sumnnn,sumnnnc
if(envir(ic,ir,0,0) == 0) then
e=0.
return
else
sumnn=envir(ic,ir,0,-1)+envir(ic,ir,0,1)+envir(ic,ir,-
  1,0)+envir(ic,ir,1,0)
if(mod(ic+ir,2)==0) then
sumnnn= envir(ic,ir,-1,1)+envir(ic,ir,1,-1)
sumnnnc=envir(ic,ir,-1,-1)+envir(ic,ir,1,1)
else
sumnnnc= envir(ic,ir,-1,1)+envir(ic,ir,1,-1)
sumnnn = envir(ic,ir,-1,-1)+envir(ic,ir,1,1)
end if
e=vnn*sumnn+vnnn*sumnnn+vnnnc*sumnnnc
end if
return
end function energy
```

```
subroutine deltae(icl,irl,sx,sy,ic2,ir2,de)
implicit none
integer,intent(in)::icl,irl,sx,sy
integer,intent(out)::ic2,ir2
real,intent(out)::de
real::eold,enew
eold=energy(icl,irl)
ic2=mod(icl+ncol+sx,ncol)
ir2=mod(irl+nrow+sy,nrow)
call hop(icl,irl,ic2,ir2)
enew=energy(ic2,ir2)
de=enew-eold
call hop(ic2,ir2,icl,irl)
if(sx*sy == 0) return
if(mod(icl+irl,2) == 0 ) then
if( sx*sy == 1) then
      de=de+qnnnc
      else
          end
          else
        de=de+qnnn
    if( sx*sy == 1) then
        de=de+qnnn
        else
    de=de+qnnnc
    end if
    end if
    return
    end subroutine deltae

subroutine metrostep(icl,irl,sx,sy,ic2,ir2,accept)
implicit none
integer,intent(in)::icl,irl
integer,intent(out)::sx,sy,ic2,ir2
logical,intent(out)::accept(3)
```

```
integer::nvacant,tx,ty,tc2,tr2
real::r,rrand(2)
real::de
integer :: local(-1:1,-1:1)
integer,allocatable,dimension(:) :: cvac,rvac
integer::jump,rlocal,clocal
sx=0
sy=0
ic2=icl
ir2=irl
accept=.false.
if(envir(icl,irl,0,0) == 0) then
return
end if
accept(1)=.true.
nvacant=9-sum(envir(icl,irl,:,:))
if(nvacant == 0) then
 return
end if
accept(2)=.true.
allocate( cvac(nvacant)
local=envir(icl,irl,:,:)
cvac=pack( cshft , mask = local 0)
rvac=pack( rshft , mask = local 0)
call random number(r)
jump = int(nvacant*r)+1
tx=cvac(jump)
ty=rvac(jump)
call deltae(icl,irl,tx,ty,tc2,tr2,de)
if(de <= 0.) then
accept(3)=.true.
ic2=tc2
ir2=tr2
sx=tx
sy=ty
```

```
return
else
call random-number(r)
if (exp(-de/temper) > r) then
accept(3)=.true.
ic2=tc2
ir2=tr2
sx=tx
sy=ty
else
return
end if
end if
return
end subroutine metrostep

  subroutine hop(ic,ir,kc,kr)
  implicit none
  integer,intent(in)::ic,ir,kc,kr
  integer::js,jc,ls,lc
  integer::tc,tr,iic,iir
  call col slcol(ic,js,jc)
  if(.not. btest(blatt(js,ir),jc)) return
  call col slcol(kc,ls,lc)
  if(btest(blatt(ls,kr),lc)) return
  blatt(js,ir)=ibclr(blatt(js,ir),jc)
  blatt(ls,kr)=ibset(blatt(ls,kr),lc)
  do tc=-1,1
  do tr=-1,1
  iic=mod(ic+tc+ncol,ncol)
  iir=mod(ir+tr+nrow,nrow)
  envir(iic,iir,-tc,-tr)=0
  end do
  end do
  do tc=-1,1
  do tr=-1,1
```

```
iic=mod(kc+tc+ncol,ncol)
iir=mod(kr+tr+nrow,nrow)
envir(iic,iir,-tc,-tr)=1
end do
end do
return
end subroutine hop
```

C. THE RELATIONSHIP BETWEEN TRACER AND CHEMICAL DIFFUSION COEFFICIENTS

The tracer diffusion coefficient D* is defined by the following relations:

$$D^*=D_0^*\ e^{-E/kT} \qquad \text{(C-1)}$$

where D_0^* is the diffusion constant, E is the activation energy, k the Boltzmann constant and T the temperature [4,35].

$$D^*= 0.5\ a^2 p_v \omega f \qquad \text{(C-2)}$$

where p_v is the vacancy availability factor (the probability that a vacancy is next to a given atom), ω is the average jump probability , f is the tracer correlation factor and a is the jump distance [4,28].

The chemical diffusion coefficient D is given by

$$D=0.5\ a^2 \omega f_v\ [1+\ [\partial \ln\gamma/\partial \ln c] \qquad \text{(C-3)}$$

where $[1+\ [\partial \ln\gamma/\partial \ln c] = F$, f_v is the correlation factor for the diffusion of the vacancies, γ and c the activity coefficient and the concentration, respectively, of the oxygen ions.

For an isotropic system D* is related to the chemical diffusion coefficient by the Darken equation [35],

$$D = D^{*} F h$$

where F is the thermodynamic factor and h is the ratio $f_v : f$ (the Haven ratio)

$$F = (c/kT)[\partial\mu/\partial c]_T$$

where μ is the chemical potential of the particles.